Postgraduate Thesis

Molecular-level Modelling of Complex Liquid Interfaces.

Author:
Sean O'Connor

Supervisor:
Prof. Maxim Fedorov

A thesis submitted to the University of Strathclyde
in partial fulfilment of the requirements
for the degree of
MPhil Physics

Department of Physics
February 2015

Declaration of Authorship

I declare that, except where specifically indicated, this thesis titled, 'Molecular-level Modelling of Complex Liquid Interfaces.' and the work presented in it are my own and I am the sole author of all parts.

List of Publications

V. Ivaništšev, S. O'Connor, M.V. Fedorov. Poly(a)morphic portrait of the electrical double layer in ionic liquids. *Electrochemistry Communications*, **2014** (publication pending)

UNIVERSITY OF STRATHCLYDE

Abstract

Department of Physics

MPhil Physics

Molecular-level Modelling of Complex Liquid Interfaces.

by Sean O'Connor

In a world with ever-increasing energy demands, it is important that the oil industry continually adapts and innovates in order to ensure maximum possible yield of oil recovery. Enhanced Oil Recovery, **(EOR)**, is being increasingly applied to optimise oil recovery. One method of EOR is through the use of water injection.

Water injection involves flooding an oil reservoir with water. This helps maintain the pressure during the extraction of oil and can also be used to move the oil to a more favourable position in the reservoir. The competitive interaction between oil and water at the reservoir wall is better understood through analysis of several interfacial properties, such as partial density distribution, interfacial tension, adsorption energy and contact angle.

Researching these interfacial properties will allow prediction of the optimum characteristics of water injected into a reservoir based on its interaction with the hydrocarbon fluid and the sedimentary rock surface. At the same time it will be determined whether or not Molecular Dynamics is a useful tool to assist and improve EOR.

Molecular Dynamics simulations were employed to explore several interfacial properties of water and dodecane at the $\{10\bar{1}4\}$ surface of calcite. A series of different initial water configurations were investigated at two different temperatures.

Partial density analysis demonstrated a significant increase in the density distribution of water at the surface of calcite. It was found that the partial density distribution of water is lower for the simulations carried out at the higher temperature at the calcite surface.

An investigation into the interfacial tension between water and dodecane resulted in a value of 50.05 mN/m. This result was comparable to those found in both experimental and other computational studies.

Use of the Radial Distribution Function yielded adsorption free energy results of -33.4 kJ mol^{-1} and -39.4 kJ mol^{-1} for at 298K and 353K respectively. Potential of Mean Force analysis yielded an adsorption energy result of -44.0 kJ mol^{-1} for water at the $\{10\bar{1}4\}$ calcite surface. Several studies carried out in recent years have produced results comparable to this, though a portion of the scientific community believe this result to be too low. It has been shown that the value for adsorption energy is dependent on the $Ca - O_{water}$ distances for computational studies. However the results in this study do not follow this trend.

Contact angle analysis showed that the addition of dodecane inhibited the spreading of water on the $\{10\bar{1}4\}$ calcite surface, but not entirely. A new computational method was also developed for measuring the contact angle for GROMACS coordinate files which, whilst producing efficient results for uniform spreading, is generally than the more traditional method. However for non-uniform spreading it could be argued that the traditional method is less reliable.

Analysis of a water droplet system proved unequivocally that the $\{10\bar{1}4\}$ surface of calcite is water-wet.

Acknowledgements

I wish to thank Professor Maxim V. Fedorov for his extensive support and guidance over the last 2 years. I am extremely grateful to him for giving me the opportunity to work in his group and perform this research.

This work is part of a collaboration between the University of Strathclyde and Schlumberger Limited. I wish to thank my collaborator from Schlumberger, Mikhail Stukan, for his support and advice throughout this project.

I thank my colleagues Stephanie Crosthwaite, Vladislav Ivaništšev, Rosemary Orr, Anastasia Romanova, David Palmer and Kelly Thomson for many enjoyable and useful hours of conversation. I reserve particular thanks for Maksim Mišin as his input in the contact angle script was invaluable. His intelligence and enthusiasm for science is infectious and he is therefore capable of improving the understanding of all those around him.

This project would not have been feasible without the university's High-Performance-Computing facility, ARCHIE-WeSt. I would like to thank Karina Kubiak-Ossowska, Richard Martin and Paul Mulheran. I acknowledge the service they provide and their support during this project.

I want to thank Amy and my whole family for their patience, confidence and support.

Contents

List of Figures

Abbreviations

EOR	**E**nhanced **O**il **R**ecovery
OOIP	**O**riginal **O**il **I**n **P**lace
MD	**M**olecular **D**ynamics
AFM	**A**tomic **F**orce **M**odel
XR	**X**-ray **R**eflectivity
IFT	**I**nter**F**acial **T**ensions
GROMACS	**GRO**ningen **MA**chine for **C**hemical **S**imulations
NaRIBaS	**N**anomaterials **a**nd **R**oom Temperature **I**onic Liquids in **B**ulk **a**nd **S**lab
PME	**P**article **M**esh **E**wald
OPLS-AA	**O**ptimised **P**otential for **L**iquid **S**imulation **A**ll **A**tom
SCDR	**S**chlumberger **D**haran **C**arbonate **R**esearch **C**entre
TIP3P	**T**ransferable **I**ntermolecular **P**otential **3**-**P**oint
CW	**C**alcite **W**ater
CWD	**C**alcite **W**ater **D**odecane
LJ	**L**ennard **J**ones
VMD	**V**isual **M**olecular **D**ynamics
PMF	**P**otential **M**ean **F**orce
MATLAB	**MAT**rix **LAB**oratory
TIP4P	**T**ransferable **I**ntermolecular **P**otential **4**-**P**oint
TIP5P	**T**ransferable **I**ntermolecular **P**otential **5**-**P**oint
NPT	**N**umber of moles **P**ressure **T**emperature
NVT	**N**umber of moles **V**olume **T**emperature
RDF	**R**adial **D**istribution **F**unction
WHAM	**W**eighted **H**istogram **A**nalysis **M**ethod
HPC	**H**igh **P**erformance **C**omputing

Chapter 1

Introduction and Literature Review

Patience is bitter, but its fruit is sweet.

Aristotle

This chapter describes the background to the research, examining in detail each of the components studied. It pays particular attention to any substantive findings, alongside any experimental and theoretical contributions to the subject.

1.1 Oil Recovery from Carbonate Reservoirs

Petroleum is a naturally occurring liquid found trapped beneath the Earth's surface. It is refined into various types of fuels through a process known as **fractional distillation** [2]. The word *petroleum* has become synonymous with both the crude oil itself and its products. Crude oil is a mixture of liquid organic compounds, mainly hydrocarbons [2]. It is a finite resource and is formed when vast quantities of deceased organisms, generally algae and zooplankton, are trapped beneath sedimentary rock and undergo extremes of heat and pressure. The production of petroleum is vital to many industries, and is of paramount importance to help maintain modern civilisation. It is, therefore, a critical concern for many governments and commercial entities alike. Oil accounts for a large percentage of the world's energy consumption. It ranges from a low of almost 30% for Europe and Asia, to a high of greater than 50% for the Middle East [3]. However, with petroleum being a depleting resource it is important that the engineering processes involved in recovering it are as efficient and effective as possible. Therefore, companies will invest time and effort to explore new innovative methods of enhancing oil recovery. It is estimated that more than 60% of the world's oil reserves are held in carbonate reservoirs. For example, the Middle East has extensive oil-containing carbonate fields, with around 70% of oil reserves held within these reservoirs [4]. Carbonate reservoirs are often fractured and typically have low porosity. In addition to this, oil-to-mixed wet rock properties usually means that recovery from carbonate reservoirs is not very efficient. Enhanced Oil Recovery **(EOR)** strategies are typically employed. The focus of Enhanced Oil Recovery is to extract the trapped and discontinued collections of oil distributed along the apertures in the network of the rock. More often than not, these are liquid injection methods. This involves drilling *injection wells* into a reservoir and encouraging oil production by the introduction of water, chemicals or brine solutions. The injected water typically helps to increase depleted pressure within the reservoir. Morevover it also moves the oil into place where recovery will be more fruitful. However, in most cases 40 to 50% of the Original Oil In Place **(OOIP)** is not produced [5, 6]. It is therefore important that any possible improvement that can be made to the process, no matter how minor, should be investigated. Measurement and control of the interfacial properties will help optimise hydrocarbon recovery.

1.2 Calcium Carbonate

Calcium carbonate ($CaCO_3$) is one of the most abundant substances found in sedimentary rocks in all parts of the Earth. It is estimated that more than 4% of the Earth's crust is made up of the compound $CaCO_3$ [7, 8], often in the forms of limestone and chalk. These sedimentary rocks are mainly composed of the minerals *aragonite* and *calcite*. These are two of the most common crystal forms of calcium carbonate.

Calcuim carbonate has been the focal point of diverse and extensive research because of its useful applications in industrial, medical and environmental fields. It is used extensively in the ornamental tile industry [9] and as a pigment mixture in the paper industry [10]. It is also thought it could have a significant impact in the evolution and biogeography of coral [11]. It has been used in medicine in the process of dialysis [12]. $CaCO_3$ can also be used as a cheap dietary supplement or gastric supplement [13, 14].

There are three different polymorphs of $CaCO_3$ which are found in sediments and organisms. These are vaterite, aragonite and calcite. Due to the fact they are polymorphs, meaning they have different crystal structures and symmetry. Vaterite is hexagonal, aragonite is orthorhombic and calcite is trigonal-rhombohedral. Calcite is the most commonly occurring and ubiquitous form of the calcium carbonate polymorphs. It is the most stable polymorph at what can be considered *normal* conditions. With normal being temperatures and pressures encountered in the environment. Vaterite and aragonite will, given enough time, transform to calcite. Aragonite is also an abundant mineral, though not as common as calcite, whereas vaterite is rarely found in natural systems. It is always found under conditions where it is metastable with respect to calcite and aragonite [15].

1.2.1 Calcite

Calcite is the polymorph on which this study is focused. The lowest energy surface of calcite is the (1,0,4) plane of the calcite crystal that also characterises the rhombohedral morphology. This surface is the most stable and rhombohedral crystals are therefore also the most dominant morphology of calcite observed in the natural environment.

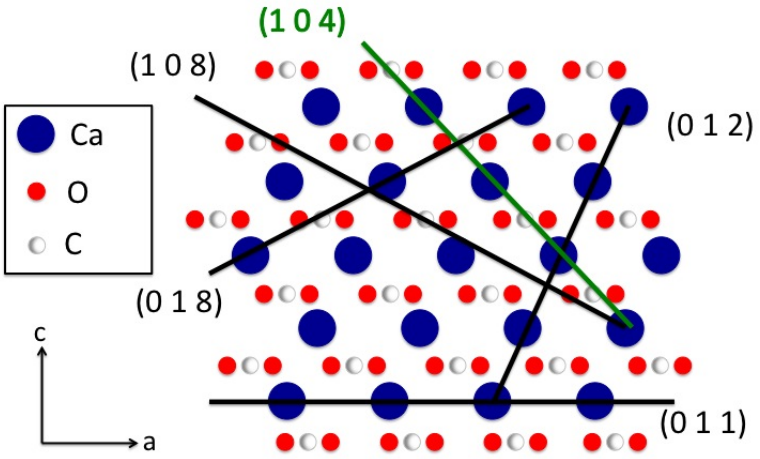

FIGURE 1.1: The various cleavages of calcite with the (1,0,4) cleavage shown in green.

Calcite is transparent to opaque and may occasionally show fluorescence. Calcite, like most carbonates, will dissolve in most forms of acidic solvent. Calcite can be either precipitated by or dissolved by water, depending on several factors including the temperature, dissolved ion concentrations and pH. Calcite exhibits an unusual characteristic called *retrograde solubility* [16]. This means that as the water temperature increases calcite becomes *less* soluble (See Figures 1.2 and 1.3 taken from [1]). When conditions are appropriate for precipitation, mineral coatings of calcite form that bind the existing rock grains together, alternatively it can fill fractures between rocks. When conditions are appropriate for dissolution, porosity and permeability of the rock can increase significantly by the removal of calcite. If this continues over a long period of time the result can be the formation of caves. On a larger scale, continued dissolution of calcite-rich rocks can lead to the eventual collapse of cave systems [17]. Calcite is a central component in the sedimentary rock limestone. Many oil reserves are located in so-called hydrocarbon *traps* in limestone rock formations.

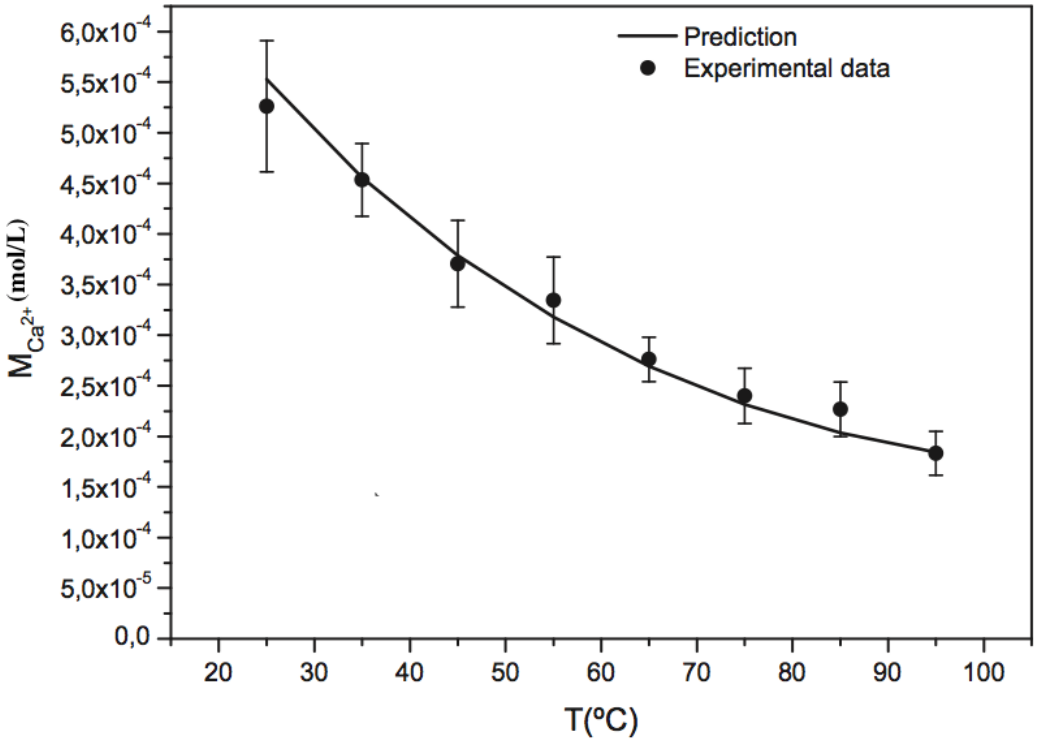

FIGURE 1.2: Influence of the temperature on the $CaCO_3$ solubility (P = 1 bar) [1].

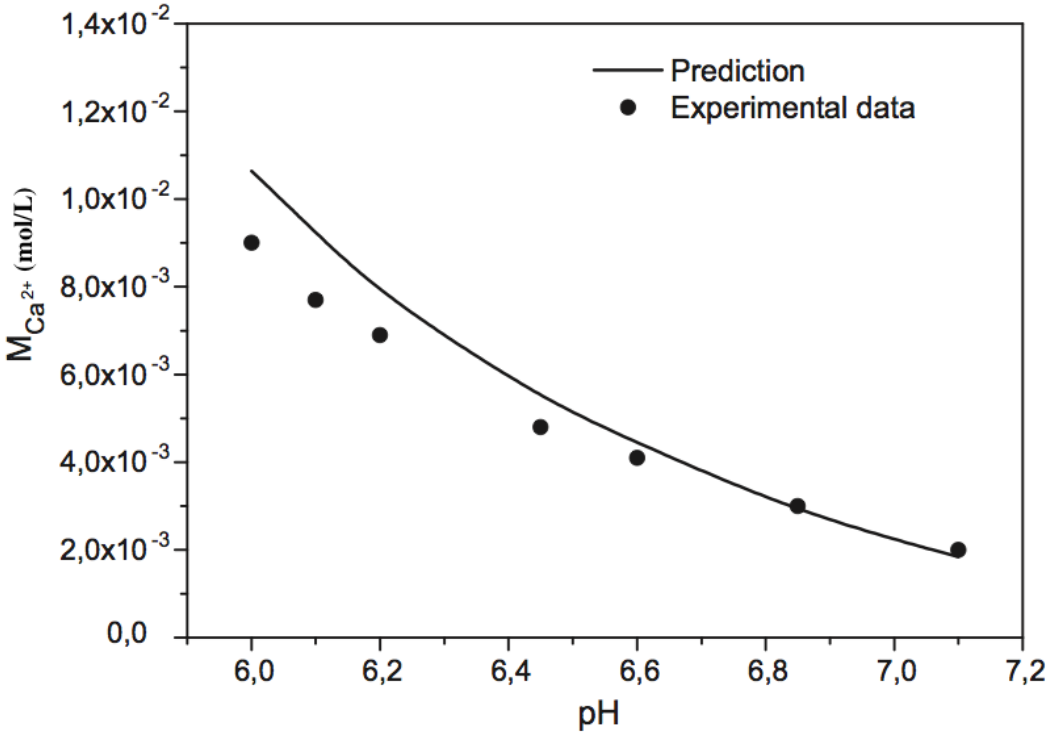

FIGURE 1.3: Effect of the pH on the $CaCO_3$ solubility at 25°C and 1 bar air pressure [1].

1.3 Molecular Dynamics

As described in my previous work [18]:

Molecular Dynamics **(MD)** is a computer simulation of the kinetics of atoms and molecules. These atoms and molecules are permitted to interact for a set period of time. Their movement is deciphered through solving Newton's equations of motion. The forces between the particles and their respective potential energy are defined by molecular mechanics *force fields*. This computational method is one of the principle tools in the theoretical study of biological molecules. These methods are now routinely used to investigate the structure, dynamics and thermodynamics of molecules and their complexes. Molecular Dynamics simulations require the definition of a potential function. These describe how particles in a simulation can interact. These are commonly referred to as force fields. They are usually based on molecular mechanics and modelled on classical particle-particle interactions [19]. In this research the force fields consist of the summation of bonded pairs (see Figure 1.4) associated with chemical bonds, angles, dihedrals and the non bonded forces associated (see Figure 1.5) with van der Waals and electrostatic interactions.

$$E = E_{bonded} + E_{non\ bonded} \tag{1.1}$$

$$E_{bonded} = E_{bond} + E_{angle} + E_{dihedral} \tag{1.2}$$

Bonded

$$E_{bond} = \sum k(b - b_0)^2 \tag{1.3}$$

$$E_{angle} = \sum k(\theta - \theta_0)^2 \tag{1.4}$$

$$E_{dihedral} = \sum k(1 - \cos(n\phi - \phi_0)) \tag{1.5}$$

where k is a spring constant, b is the bond length, b_0 is the equilibrium bond length, θ is the bond angle, θ_0 is the equilibrium bond angle, n is the integer constant, ϕ is angle between the planes for a quartet of atoms with ϕ_0 being the corresponding equilibrium angle.

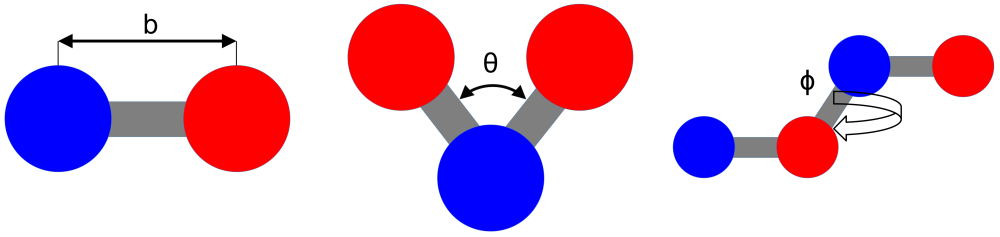

FIGURE 1.4: A schematic showing the bonds, angles and dihedrals.

Non bonded

$$E_{nonbonded} = E_{electrostatic} + E_{van\ der\ Waals} \tag{1.6}$$

The van der Waals interactions are frequently calculated based on the Lennard-Jones

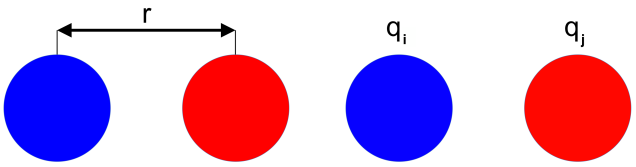

FIGURE 1.5: A schematic showing the distance of separation and the charge magnitudes.

potential:

$$V = 4\epsilon[(\sigma/r)^{12} - (\sigma/r)^{6})] \tag{1.7}$$

V is the intermolecular potential between the two atoms or molecules, ϵ is a measure of how strongly the two particles attract each other, σ is the distance at which the intermolecular potential between the two particles is zero and thus gives a measurement of how close two non bonding particles can get. It is referred to as the van der Waals radius. It is equal to one-half of the internuclear distance between non bonding particles. Finally, r is the distance of separation between both particles measured from the centre of one particle to the centre of the other particle. The electrostatic interactions between two molecules, or parts of the same molecule, are often calculated as a sum of interactions between pairs of point charges using Coulomb's law [19]:

$$\Psi = \sum_{i=1}^{N_A} \sum_{j=1}^{N_B} \frac{q_i q_j}{4\pi\epsilon_0 r_{ij}} \tag{1.8}$$

N_A and N_B are the numbers of point charges in the two molecules with q_i and q_j referring to the relevant magnitudes of each charge. As above r represents the distance of separation. Also ϵ_0 refers to the permittivity of the media.

Classical molecular dynamics simulations based on *force fields* are an attractive means to assess our understanding of interfaces and their properties because they can simulate systems with a large number of atoms for significant simulation times. The results can also be compared directly with experimental data [20, 21]. However, a general hurdle to overcome with regards to MD simulations is evaluating the associated uncertainties and determining the overall accuracy of the results. The parametrisation of the force field and the accuracy can be particularly difficult to determine. It is also a challenge to compare experimental and computational results directly. This is partly because experimentally derived structures are, more often than not, obtained with some explicit or implicit assumptions that may bias the overall interpretation of the results.

1.4 Previous Work

1.4.1 Calcite-Water Interface

Over the past decade the structures of fluids at solid interfaces has been more intensely researched and scrutinised. One reason for this has been the need to better understand the properties of various fluids, both simple and complex. In confined spaces, such as carbonate reservoirs, where the interfacial fluid properties might dominate, research has indicated that the properties of a fluid may differ near an interface, when compared with that of a fluid in the bulk [22–24]. One hypothesis is that this behaviour is due to changes in the structure of the fluid near interfaces [25–27]. Liang et al [28] used Atomic Force Microscopy **(AFM)** to conclude that there is a degree of relaxation on the calcite surface. Various experimental and computational methods have proven that calcite is a *hydrophilic*, water-loving, surface [29, 30]. Fenter et al [31, 32] have performed extensive analysis on the calcite-water interface. This analysis has been undertaken using results obtained from Molecular Dynamics simulations and high resolution X-ray reflectivity **(XR)** experiments. They have concluded that, whilst these techniques have provided further understanding of the calcite-water interface, further research must be undertaken as the interface is not fully understood. Research has shown that the structure of water at a calcite surface differs to that in the bulk. Specifically the water molecules tend to pack closer together nearer the surface. However, opinion is divided over whether a single *monolayer* is formed or several densely packed layers.

1.4.2 Oil-Water Interface

Interactions between oil and water have long interested humankind. The modern investigations focus on both environmental and industrial applications. The environmental applications primarily focus on the outcomes of major oil spills. The reason being that a better understanding of the oil-water interface could help in the prevention and more efficient cleaning up of environmental disasters as a result of oil spills [33]. The industrial applications focus on the use of water as a driving fluid to enhance oil recovery [5].
It is a well known fact that oil and water are immiscible fluids. A mixture of oil and water is naturally unstable. There are ways of stabilising the mixture. Some research has involved the use of *surfactants*. These molecules contain a polar group, which is of course soluble in water, and an aliphatic tail, meaning that it is soluble in oil. They will be positioned at the oil-water interface and can significantly decrease the interfacial energy [34].

1.5 Interfacial Properties

1.5.1 Interfacial Tension

Interfacial tension, **(IFT)**, is a property at the interface between two, usually immiscible, fluids. A technical definition would be that interfacial tension is the Gibbs free energy per unit area of interface at a fixed temperature and pressure. This is a so-called *energy definition* but it can also be defined in terms of force. This property occurs because a molecule near the interface of a fluid experiences different molecular interactions than an equivalent molecule within the bulk of the fluid. It is important for EOR as it defines how immiscible fluid will interact with each other. The interfacial tension is key when discussing the mechanisms of certain types of EOR. The mechanisms behind the behaviour of oil in a pore can be elegantly described by the capillary number. This dimensionless number is defined as:

$$N_{cap} = \frac{v\mu}{\sigma \cos(\theta_c)} \tag{1.9}$$

where v and μ are the velocity and viscosity of the oil respectively, σ is the surface tension and θ_c is the contact angle. It is the ratio of viscous and capillary forces. The higher this capillary number is the faster the flow-rate. Therefore lowering the interfacial tension, through use of surfactants, can increase oil production [35–38]. It is important to investigate how accurate IFT prediction is from MD simulations.

1.5.2 Wettability and Contact Angle

W.G. Anderson defined *wettability* as "the tendency of one fluid to spread on or adhere to a solid surface in the presence of other immiscible fluids" [39]. The calcite may be oil-wet, water-wet or neutral-wet if both of the fluids have similar affinities for the calcite surface. For smooth surfaces, wettability can be described by **contact angles**, which is dependent on the **interfacial tensions**. The contact angle θ_c depends on the oil-solid IFT, σ_{os}, water-solid IFT, σ_{ws}, and oil-water IFT, σ_{ow}. These are described by Young's equation,

$$\sigma_{os} = \sigma_{ws} + \sigma_{ow} \cos\theta_c \tag{1.10}$$

Rearranging gives you the equation for the contact angle,

$$\theta_c = \cos^{-1} \frac{\sigma_{os} - \sigma_{ws}}{\sigma_{ow}} \tag{1.11}$$

With water as the reference fluid, the surface is water-wet when $\theta_c < 90°$, oil-wet when $\theta_c > 90°$, and neutral-wet when $\theta_c = 90°$.

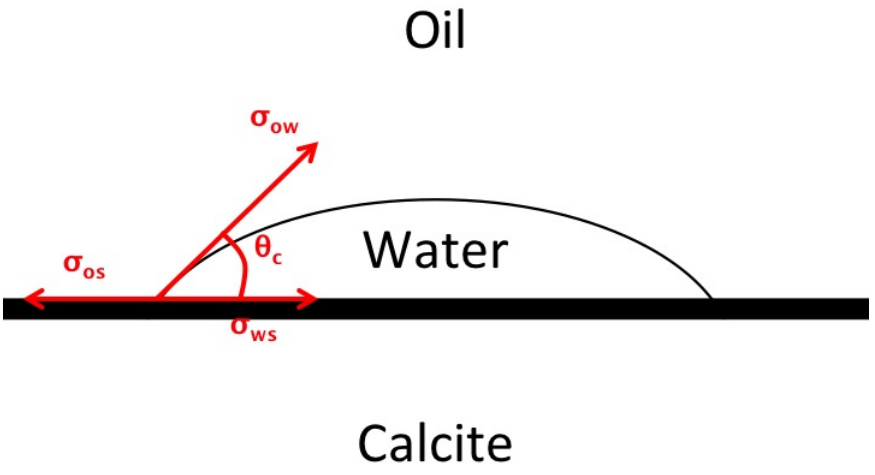

FIGURE 1.6: A water droplet on a flat calcite surface immersed in oil. The surface is water-wet

Understanding wettability is of paramount importance in the field of Enhanced Oil Recovery. If a reservoir is wrongly categorised as oil-wet or water-wet it can lead to irreversible damage to the reservoir [40].

1.5.3 Adsorption

Adsorption, a term first used by Heinrich Kayser [41] is described as the adhesion of atoms at a surface. It is characterised by an increase in the density of a fluid, gas or dissolved solid near a surface. It is an interfacial property in the sense that it occurs at the boundary between the surfaces of different materials. Like surface tension, it is the surface energy that leads to the phenomenon of adsorption. For the calcite surface the following equations were used to calculate the adsorption energy:

$$E_{water-adsorption} = E_{calcite-water} - (E_{calcite} + E_{water}) \tag{1.12}$$

where $E_{calcite-water}$, $E_{calcite}$ and E_{water} signify the single-point energies of the interfaces and components of the system. The binding energy is typically defined as the negative of the adsorption energy, such that $E_{binding} = -E_{adsorption}$. A more stable adsorption structure will have a larger binding energy. The binding energy of course describes the extent to which a molecule wants to be at a surface. It will help engineers to understand what it will take to displace a fluid from a surface and how varying conditions will affect this ease of displacement. It is therefore of great importance for understanding oil reservoirs and EOR.

1.6 Statistical Mechanics and Free Energy

Before going into details about statistical mechanics and free energy it is important to briefly summarise statistical physics. The primary goal of equilibrium statistical mechanics is to provide a connection between *macroscopic* properties of materials in thermodynamic equilibrium, and the *microscopic* description of a physical system. A **macrostate** is the description of a physical system that is enough to determine external parameters. These can include temperature, volume and mass. A **microstate** is the precise microscopic description of a physical system. Microstates can be understood as instantaneous snapshots of all particle positions and their corresponding momenta in the system. The microstate is typically unknowable and therefore must be dealt with in terms of probabilities.

In thermodynamics the *free energy* is the amount of work that a particular thermodynamic system can perform. The free energy is defined as the internal energy of the system minus the amount of energy that is unavailable to perform work. This unusable energy is equivalent to the entropy of the system multiplied by the temperature. In practice the absolute free energy of a single system is not of interest, rather the free energy differences between various states. There are two thermodynamic potentials which are regularly distinguished from each other: *Gibbs free energy* and *Helmholtz free energy.*

The equation for the change in Gibbs free energy is:

$$\Delta G = \Delta H - T\Delta S \tag{1.13}$$

where ΔH is the change in enthalpy of the system, T is the temperature in Kelvin and ΔS is the change in entropy. The change in enthalpy is defined as:

$$\Delta H = \Delta U + P\Delta V \tag{1.14}$$

where ΔU is the change in internal energy of the system, P is the pressure, and ΔV is the change in volume of the system. To calculate the Gibbs free energy a simulation in the isothermal-isobaric ensemble, (NPT), must be performed. In this ensemble the volume fluctuates. For the canonical ensemble, (NVT), the thermodynamic potential

that is minimised is Helmholtz free energy:

$$\Delta A = \Delta U - T\Delta S \tag{1.15}$$

However if the pressure imposed in the NPT ensemble results in its average volume being identical to the volume in the NVT ensemble, then the Gibbs free energy difference and the Helmholtz free energy difference will be the same [42].

For the canonical ensemble the Helmholtz free energy can be related to the partition function by the following equation:

$$F(N, V, T) = -k_B T \ln(Z) \tag{1.16}$$

where k_B is the Boltzmann constant and Z is the partition function:

$$Z = \sum_{i}^{states} e^{\frac{-e_{tot}i}{k_B T}} \tag{1.17}$$

with $-e_{tot}i$ being the states energy difference.

1.6.1 Potential of Mean Force

How the free energy changes as a function of reaction coordinates is useful to know when seeking to understand molecular interactions. The Potential of Mean Force, **(PMF)**, is the free energy as a function of separation between the solid surface and the centre of mass of, in the case of this study, water molecules. It is a free energy profile. It can be said that the PMF of a system is the potential that gives the average force over all the configurations of the system. It is, in effect, a convenient way to describe complex systems in a simple way. Potentials of Mean Force can be determined from both molecular simulations and experiments performed under equilibrium conditions by producing a histogram of values from the selected reaction coordinate, resulting in a probability distribution. They are commonly used to represent the energetics of various systems, such as: interactions between molecules (like the adsorption in this study), conformational changes within a molecule, organic reactions in fluids and permeation through membrane channels.

This study involves *force pulling*. This essentially means that a molecule is physically

manipulated away from a surface to determine the contribution of the intermolecular forces of attraction. This will result in a quantitative description of the adsoprtion free energy between a surface and a molecule.

1.6.2 Radial Distribution Function

The Radial Distribution Function **(RDF)**, $g(\mathbf{r})$, is a useful tool to describe a system's structure, particularly a liquid system. It describes how the atomic density varies as a function of the distance from a reference atom. A typical radial distribution function calculated from a molecular dynamics simulation is shown in Fifure 1.7. At lesser distances $g(\mathbf{r})$ is zero. This is caused by the strong repulsive forces at this distance. Peaks in a $g(\mathbf{r})$ graph show the likelihood that one defined atom or molecule will be found at this distance from another. Therefore, greater peaks mean there is a greater probability of finding two atoms/molecules at this separation. Thermodynamic properties can be studied by calculating the radial distribution function. It is defined for spherical particles in a homogeneous liquid in the following way [43]:

$$g(\mathbf{r}) = \frac{\langle \sum_{i,j} \delta(\mathbf{r} - \mathbf{r_{ij}}) \rangle}{\rho^2} \tag{1.18}$$

where δ stands for the Kronecker delta, $\mathbf{r_{ij}} = \mathbf{r_i} - \mathbf{r_j}$, $\langle ... \rangle$ stands for ensemble averaging (r_i and r_j are the cartesian position vectors of atoms i and j), ρ is the number density and the summation is performed over all the pairs of particles. A schematic for a basic radial distribution function is given in Figure 1.7. Essentially $g(\mathbf{r})$ describes the ratio of density between point $\mathbf{r}$ and in the bulk. Due to the fact that density is another way to describe probability, it is related to the PMF. In fact, we can generate the PMF from RDF using the equation:

$$U_{PMF}(r) = -RT \ln g(\mathbf{r}) \tag{1.19}$$

However, it is possible that a bias may be necessary to get an appropriate PMF value due to the occurence of low sampling. A slight change in the $g(\mathbf{r})$ can correspond with an order of magnitude change of PMF. It is widely agreed that the use of umbrella sampling and the WHAM algorithm [44] is one of the most accurate ways to measure the PMF from molecular dynamics simulations.

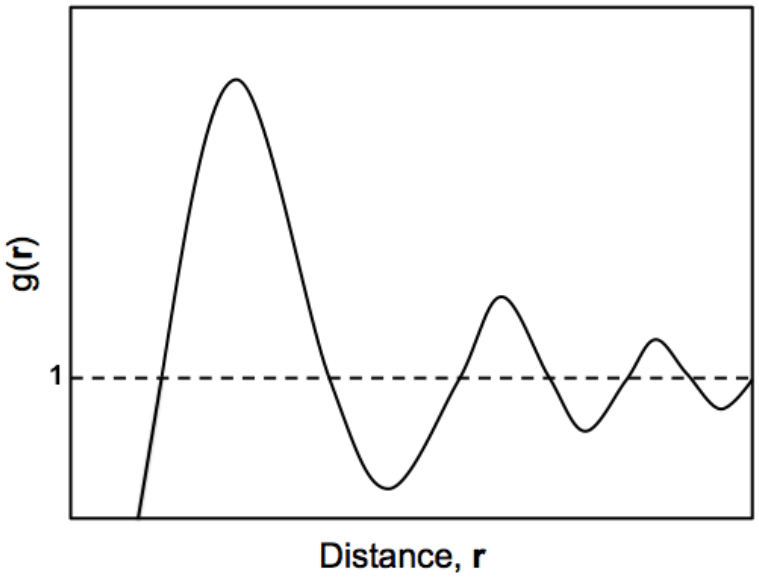

FIGURE 1.7: A simple radial distribution function graph.

1.6.3 WHAM Algorithm

The WHAM algorithm uses information obtained under different simulation conditions, such as all the intermediate positions in a 'pulling' simulation, to determine properties (e.g. averages or PMFs) of the system under a single condition. By analysing all the information at once the WHAM algorithm can greatly reduce the number of loops that need to be performed. The example in this work is the determination of a PMF to obtain accurate measurements of a free energy difference, in order to quantify adsorption free energy.

Chapter 2

Methodology

All the effects of Nature are only the mathematical consequences of a small number of immutable laws.

Pierre-Simon Laplace

This chapter describes the water and liquid alkane models and the Molecular Dynamics **(MD)** techniques used to simulate the behaviour of complex liquid interfaces. The choice of software and method used will be examined in detail and the advantages and disadvantages of each choice will be discussed accordingly. Explicit details are given referring to the implementation of the software and techniques used in this research.

2.1 System Preparation and Software Used

2.1.1 GROMACS

All molecular dynamics simulations were performed using the GROMACS program package, version 4.6.3 double-precision [45, 46]. Each system contained ≈ 23900 water molecules placed in a spherical droplet. In each system there were eight layers of calcite with the bottom two layers coupled to the V-rescaling thermostat [47]. For each production simulation the other components of each system remained uncoupled. The systems were simulated in an NVT environment. The van der Waals and Coulombic interactions were cut off at 1.0 nm, and the long-range Coulombic interactions were accounted for using the slab particle mesh Ewald **(PME)** method in 2d [48–50]. The simulations had periodic boundary conditions in 3-dimensions with a correction applied to force and potential in the z dimension which produced an artficial 2-dimensional summation [51]. For all simulations the OPLS-AA force field [52, 53] was used. This force field was modified by researchers at the Schlumberger Dharan Carbonate Research Center **(SDCR)** to replicate realistic interactions between water and calcite. This force field was then modified further to include parameters for dodecane.

The first step in building our system was generation of a stable flat surface. The (1,0,4) cleavage of calcite was chosen due to its stability and the fact that several successful molecular dynamics studies had been carried out on it. Our colleagues at the Schlumberger Dhahran Carbonate Research Center provided a stable model for calcite.

FIGURE 2.1: The (1,0,4) cleavage of calcite generated by our colleagues at SCDR.

The Transferable Intermolecular Potential 3-Point **(TIP3P)** water model was chosen for our simulations [54]. The team at the University of Strathclyde then designed a dodecane topology for use in conjunction with the calcite-water system. The topology had to reflect the physical behaviour between dodecane and water. Test simulations were performed on the dodecane system examining its physical properties to check they were consistent with experimental values.

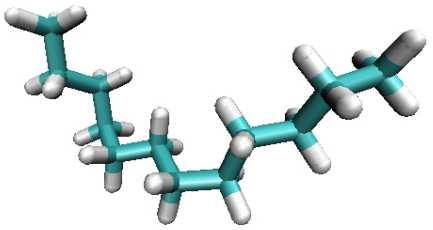

FIGURE 2.2: A dodecane molecule used in the topology created by the author at the University of Strathclyde.

System	**Number of Water Molecules**	**Number of Dodecane Molecules**	**x (nm)**	**y (nm)**	**z (nm)**
CW (flat water)	23891	-	29.72483	30.51994	20
CW (domed water)	23891	-	29.72483	30.51994	20
CWD (flat water)	23891	31080	29.72483	30.51994	22
CWD (domed water)	23891	30677	29.72483	30.51994	22
CWD (water droplet)	23891	28190	29.72483	30.51994	22

TABLE 2.1: Parameters for each system configuration with CW and CWD standing for Calcite-Water and Calcite-Water-Dodecane respectively.

2.1.2 VMD

Visual analysis is a useful tool in modern scientific research, especially in the field of computational simulations. According to Friendly [2008] it is "primarily concerned with the visualization of three-dimensional phenomena (architectural, meteorological, medical, biological, etc.), where the emphasis is on realistic renderings of volumes, surfaces, illumination sources, and so forth, perhaps with a dynamic (time) component" [55]. It allows creation of a broader spectrum of what is actually happening during the course of a simulation. Visual analysis was performed using the Visual Molecular Dynamics **(VMD)** [56] program developed by the Theoretical and Computational Biophysics group at the University of Illinois and the Beckman Institute. It is a program that allows users to display, animate, and perform qualitative analysis on large molecular systems using rendered 3-dimensional images of molecules. These images were rendered using this program and examples are present throughout this thesis. These are useful because they allow simple visualisation of the behaviour of the system during simulation. However, as useful a tool as VMD may be it cannot be the only analysis technique and should always be used in conjunction with more traditional quantitative analysis.

2.1.3 NaRIBaS

NaRIBaS [57] is a tool which provides a framework that allows the user to generate many simulation set-ups by defining set parameters. It eliminates the laborious process of opening new terminals and creating new input files for simulations which change 1 or more parameters but are relatively similar. NaRIBaS is not a substitute for a MD package like Gromacs, but instead allows iterative repetition of tasks whilst changing selected input parameters.

2.1.4 MATLAB

MATLAB [58] (matrix laboratory) numerical analysis software was used to analyse and plot graphs from the raw data generated by GROMACS.

2.2 Simulation

2.2.1 Calcite-Water System Set-Up

Before starting production simulations of calcite, water and dodecane preliminary simulations were performed on systems with only calcite and water. An issue arose early in the tests. This was believed, and later confirmed, to be the 'flying ice-cube' artifact [59]. This is an artifact that occurs visibly in molecular dynamics simulations, like those described in this work. All of the system's kinetic energy accrues as translational and rotational motion. This results in the system having essentially no energy associated with internal motion and behaving like an ice-cube flying through space. This problem was solved by allowing the droplet to be heated for 100ps of simulation time. This enabled it to form a domed shape on the surface of the calcite. A 'ceiling' of purely repulsive Lennard-Jones spheres was also designed and introduced. This prevented any water evaporating at any point in the simulation, travelling through the xy plane at z_{max} and spreading on the bottom layer of the calcite.

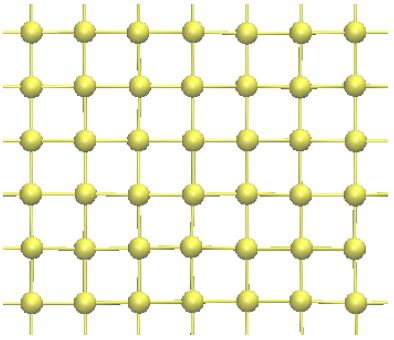

FIGURE 2.3: The mesh form of the repulsive Lennard-Jones spheres.

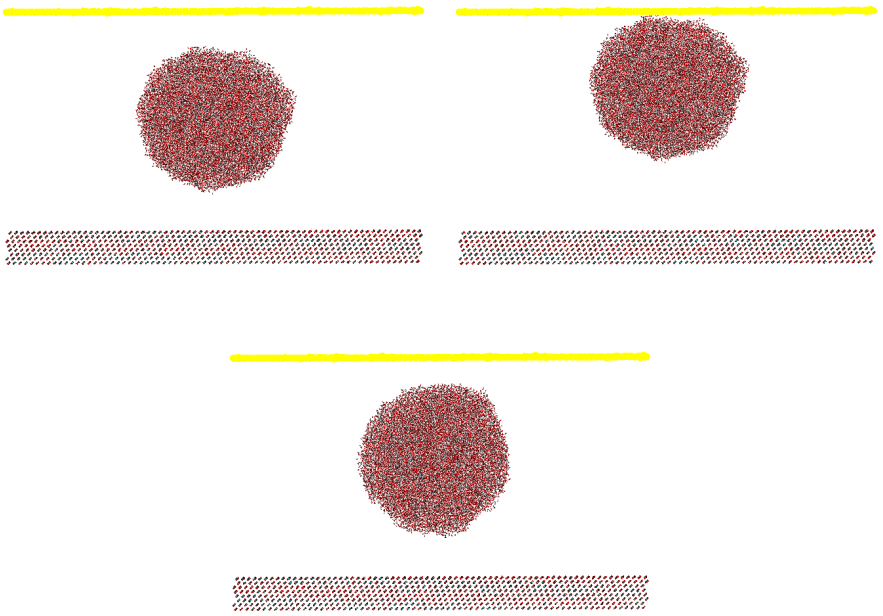

FIGURE 2.4: The 'flying ice-cube' artifact and the effect of the Lennard-Jones 'ceiling'.

There were two systems simulated with calcite and water. Several simulations were carried out on water after it formed a domed shape on the calcite surface, with a total simulation time of $\approx$ 20ns. This enabled analysis of the spreading of the calcite droplet on the surface. Simulations were also carried out for 10ns after the water had fully spread on the calcite surface. All of the simulations performed with the thermal calcite layers coupled at 298K in one instance and 353K in the other. These temperatures were chosen by our colleagues at Schlumberger to replicate both ambient temperature and a temperature approaching the boiling point of water.

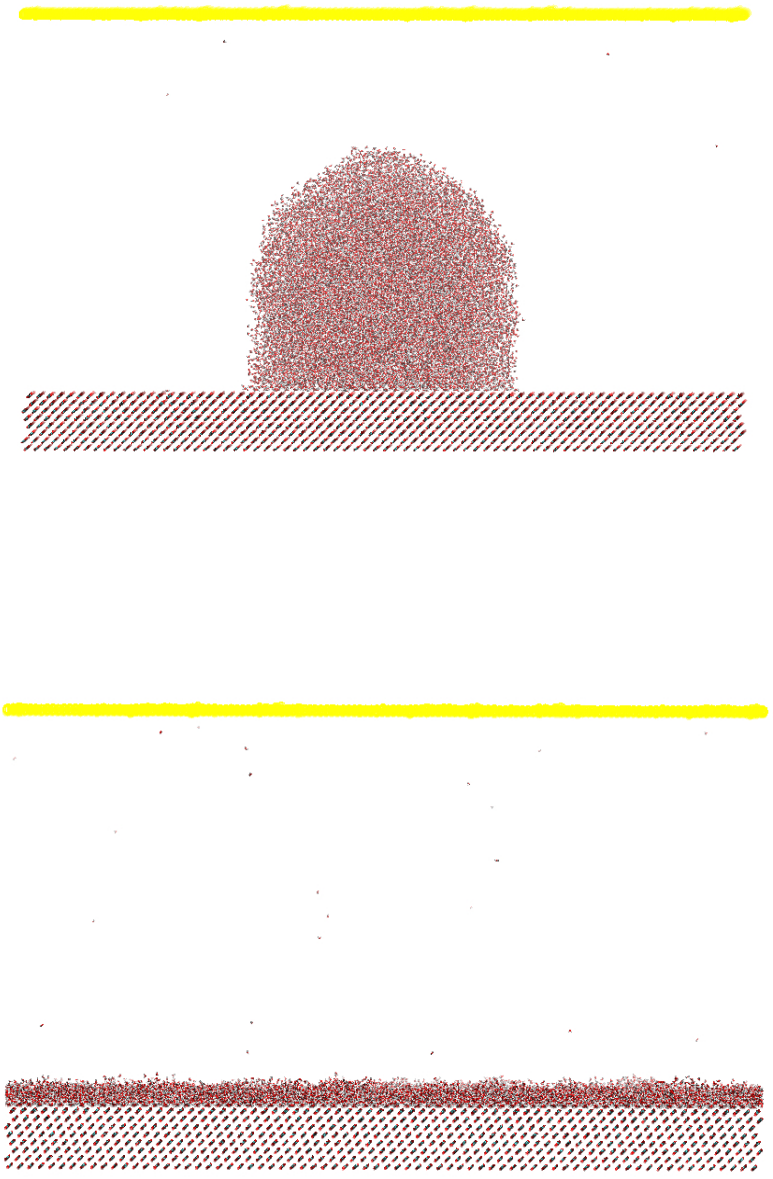

FIGURE 2.5: The two starting configurations in the calcite/water simulations

2.2.2 Calcite-Water-Dodecane System Set-Up

After the simulations of calcite and water, production simulations were performed with calcite, water and dodecane. This consisted of adding dodecane to the earlier initial configurations, and an additional configuration with a water droplet above the calcite surface. Energy minimisation was then performed. This is a process used in computaional chemistry to arrange a system in such a way that the net inter-atomic force on each atom is within a defined margin close to zero. The simulations were then carried out for 15ns each. This allowed comparison of the surface wetting with the simulations without dodecane.

The set-up was performed by moving every coordinate in the system down a set amount, such that the bottom layer of calcite was at $z = 0$. The z axis of the box was then reduced in size such that the Lennard-Jones surface was at z_{max}. This ensured that no dodecane was below the calcite surface or above the Lennard-Jones surface. Dodecane was then added to the system using the *genbox* command. This is a gromacs command which adds a defined solvent to a coordinate file. After this the system was moved back to its original position with the box dimensions changed accordingly. The Lennard-Jones surface was also raised to leave a layer of empty space between the dodecane and this surface.

2.2.3 ARCHIE-WeSt

The simulations were performed using GROMACS package on the ARCHIE-WeSt High Performance Computer (www.archie-west.ac.uk). EPSRC grant no. EP/K000586/1. The facility consists of almost 3500 cores that allow parallel computing providing almost 38 Teraflops peak performance, eight 512GB RAM large memory nodes, 8 GPU servers, two visualisation servers and 150TB of high performance LUSTRE storage.

FIGURE 2.6: The logo of the ARCHIE-WeSt High-Performance Computing **(HPC)** facility.

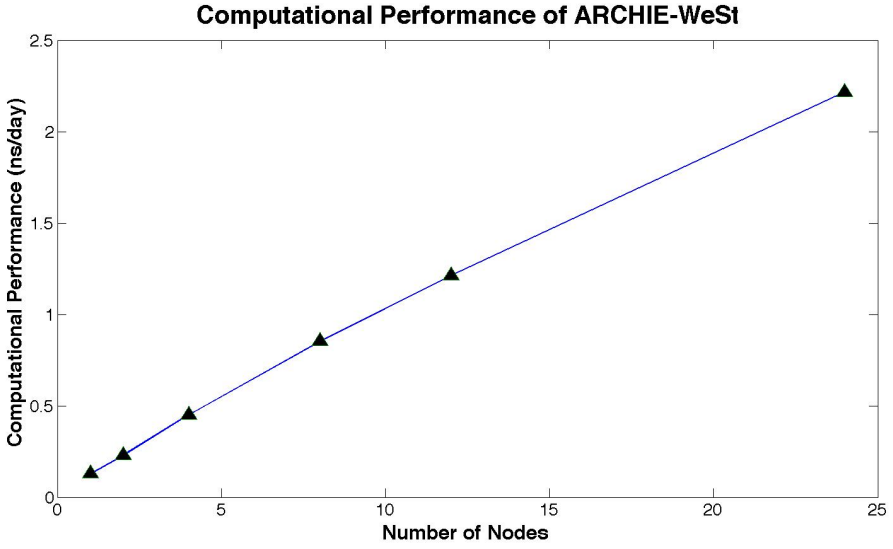

FIGURE 2.7: The performance of the ARCHIE-WeSt facility, relative to the amount of nodes used for the standard calcite-water simulation, containing 23891 water molecules.

2.3 Analysis Methodology

2.3.1 Density Analysis

Local density analysis was performed using the *g_density* program that is built into the GROMACS package. It computes the partial densities of a chosen component of the system as a function of box dimension. For the analysis in this thesis the partial densities were computed perpendicular to the calcite surface (xy plane).

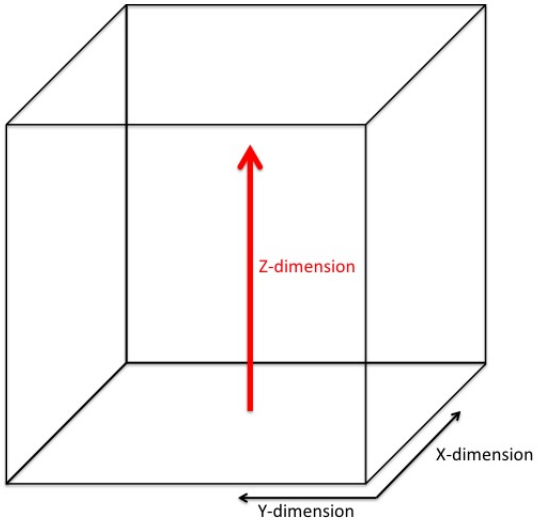

FIGURE 2.8: A diagram of the dimension along which the partial densities are computed. The partial density is measured along the z-dimension with a measurement being taken every 0.005nm.

2.3.2 Interfacial Tension

Interfacial tension analysis was performed by using the *rerun* option within GROMACS, which recalculates the forces and energies between defined molecule types for an input trajectory, and selecting dodecane and water as the reference energy groups.

2.3.3 Potential of Mean Force Analysis

The potential of mean force, (**PMF**) analysis was performed using a GROMACS *pull* simulation. A water molecule in contact with the surface of the calcite slabe was chosen. It was renamed and had the SETTLE [61] algorithm for rigid water molecules replaced by constraints. The settle algorithm is used to fix the length of bonds and angles after the integration of forces, such that they replicate water. These constraints replicated the behaviour of the SETTLE algorithm exactly. However, this change had to be made as GROMACS only allows one type of molecule to utilise the SETTLE algorithm and it was necessary for analysis purposes to change the name of the molecule. A dummy particle was placed with x and y coordinates corresponding to this molecule but placed 2nm below on the z axis. This particle's position was frozen in all three directions during the simulation. Using the particle as a reference point the water was 'pulled' away from it, back into the bulk and then eventually to the surface of the water layer. This trajectory was then used to create configurations. These initial configurations were taken along the z-direction from the calcite surface at increments of 0.1nm. Each of these configurations is then simulated further but no longer pulled. This is done because a free-energy landscape has several local minima. If these minima have free energy differences of the order of several k_BT they may all be of relevance. However, if they are separated by a high stationary point, that is not a local minima, in the free-energy landscape then the transition between minima could require a time scale which is out of reach for molecular dynamics. So performing a simulation using a biased free-energy landcsape will be free of a barrier. This potential acts as an 'umbrella' allowing easy transition from one minima to another. This is known as *Umbrella Sampling* and is used for the extraction of the potential of mean force. The WHAM algorithm [44] as described in Section 1.6.3 is then used to reconstruct a PMF curve. This process is well described in GROMACS tutorials found easily online (http://www.bevanlab.biochem.vt.edu/Pages/Personal/justin/gmx-tutorials/umbrella/index.html).

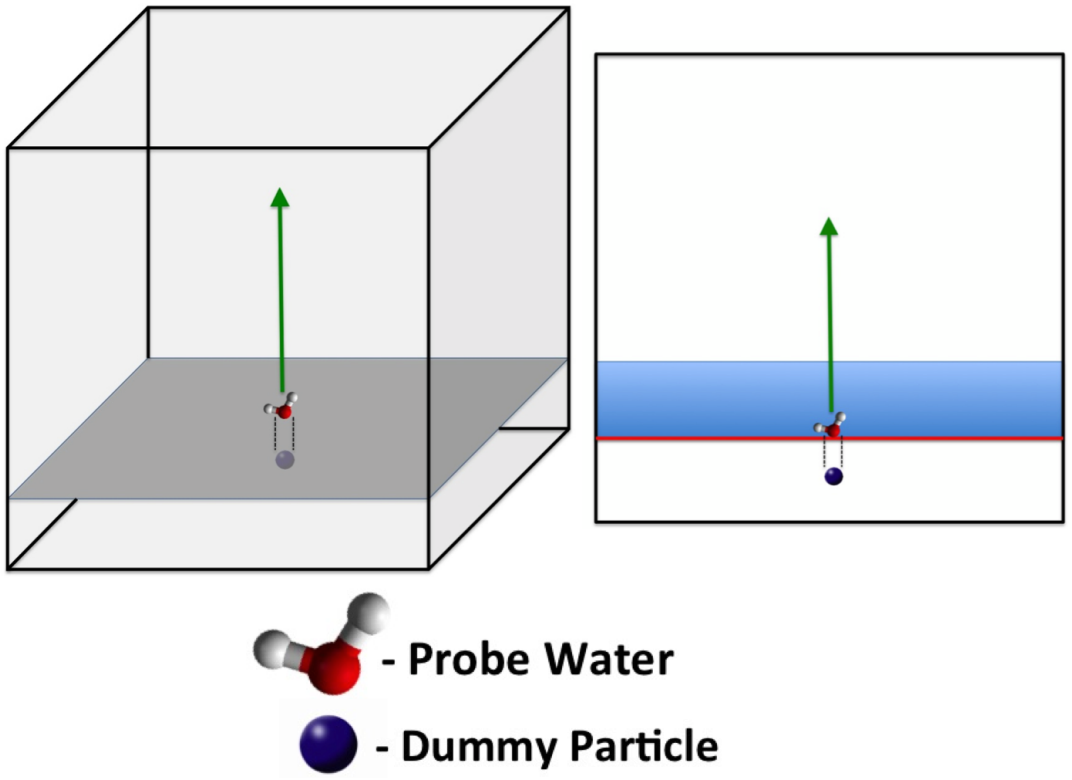

FIGURE 2.9: An oblique and sectional representation of the process of performing a *pulling* simulation to compute the Potential of Mean Force **(PMF)**.

2.3.4 Contact Angle Analysis

Manual Method

The contact angle was measured manually by first rendering images from the GROMACS trajectory using VMD. Snapshots were taken from four different projections and angles were measured accordingly. This meant that for each timestep eight different angles could be measured. The measuring was performed using a protractor and an average contact angle was produced. This may seem to be a rather *unscientific* method but it is the author's belief that this is the most effective method alternate for the measurement of droplet contact angles.

Computational Method

The script found in the appendices works as follows (See Figure 2.10):

1. Only the water molecules are extracted from a GROMACS coordinate file.
2. A mesh is placed onto the xy-plane of the new coordinate file.
3. Each water molecule is moved to the nearest of 60 grid points. The number of grid points could possibly be increased, which would in turn increase accuracy.
4. The molecule on each xy grid point with the second highest z coordinate is selected. The second highest is chosen as occasionally the highest molecule would be away from the bulk. This avoids the preservation of outliers.
5. A new origin is placed at the centre of the droplet and the selected coordinates are projected onto one dimension.
6. A simple linear regression is then plotted, and this is used to calculate the contact angle.

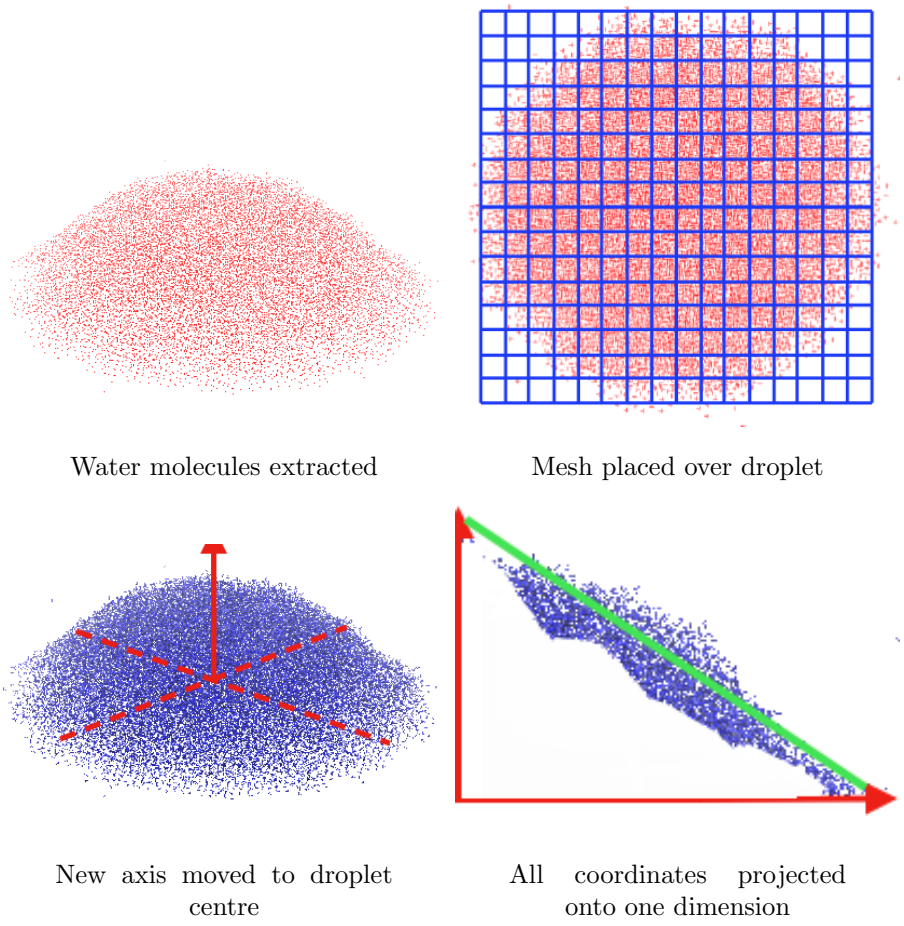

FIGURE 2.10: The evolution of the flat system in the simulation carried out with the thermal calcite layers coupled at 298K.

Chapter 3

Results and Analysis

Insanity: doing the same thing over and over again and expecting different results.

Albert Einstein

This chapter describes the various initial configurations used in the Molecular Dynamics (MD) simulations and the results yielded by each analysis technique for each respective initial configuration.

Summary

Systems Simulated and Analysis Performed				
System	**Partial Density Distribution**	**Interfacial Tension**	**Adsorption Free Energy**	**Contact Angle Analysis**
CW (flat water)	✓		✓	
CW (domed water)	✓			✓
CWD (flat water)	✓	✓		
CWD (domed water)	✓			
CWD (water droplet)				

TABLE 3.1: A summary of the systems simulated and the analysis performed on each system.

Table 3.1 contains a list of the different systems simulated in this study and the type of analysis performed on each. It is important to note that visual analysis was also performed on every system.

3.1 Calcite-Water Flat

There were two systems simulated with calcite and water. Simulations were also carried out for 10ns after the water had fully spread on the calcite surface. Several simulations were also carried out on water after it formed a domed shape on the calcite surface, with a total simulation time of $\approx$ 20ns. This enabled analysis of the spreading of the water droplet on the calcite surface. All of the simulations performed with the thermal calcite layers coupled at 298K in one instance and 353K in the other. The densities of water quoted are from the USGS Water Science school (http://water.usgs.gov/edu/density.html).

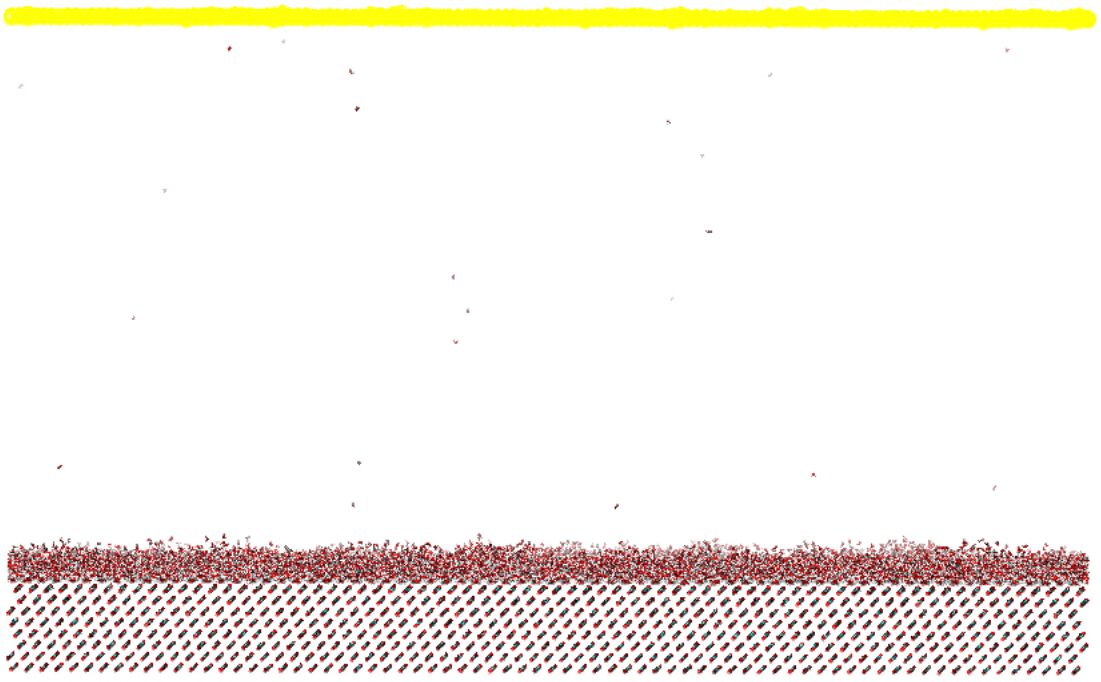

FIGURE 3.1: The starting configurations in the calcite/water flat simulations

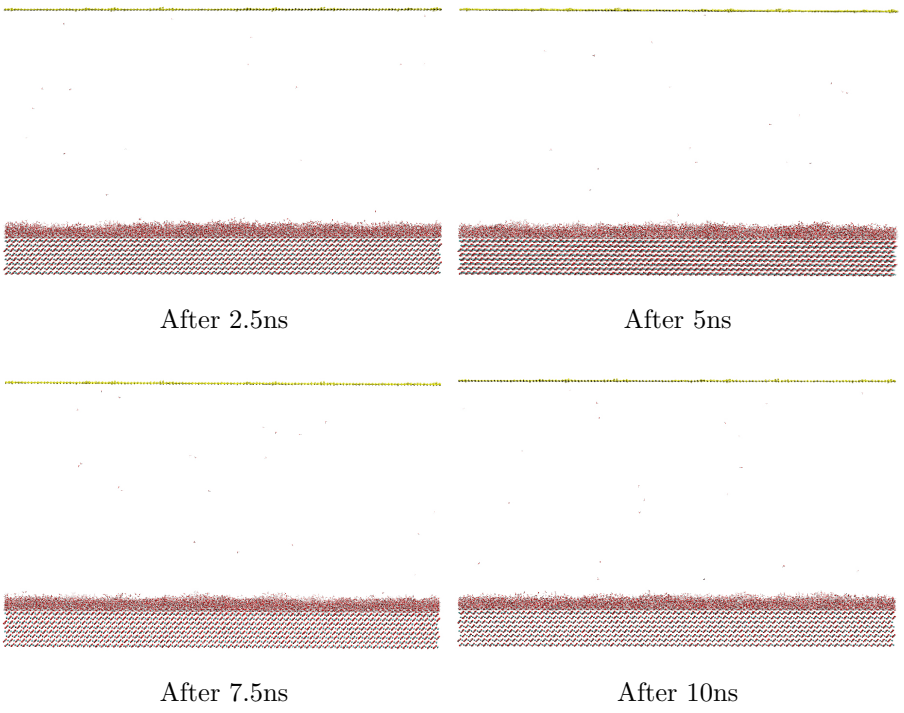

FIGURE 3.2: The evolution of the flat system in the simulation carried out with the thermal calcite layers coupled at 298K.

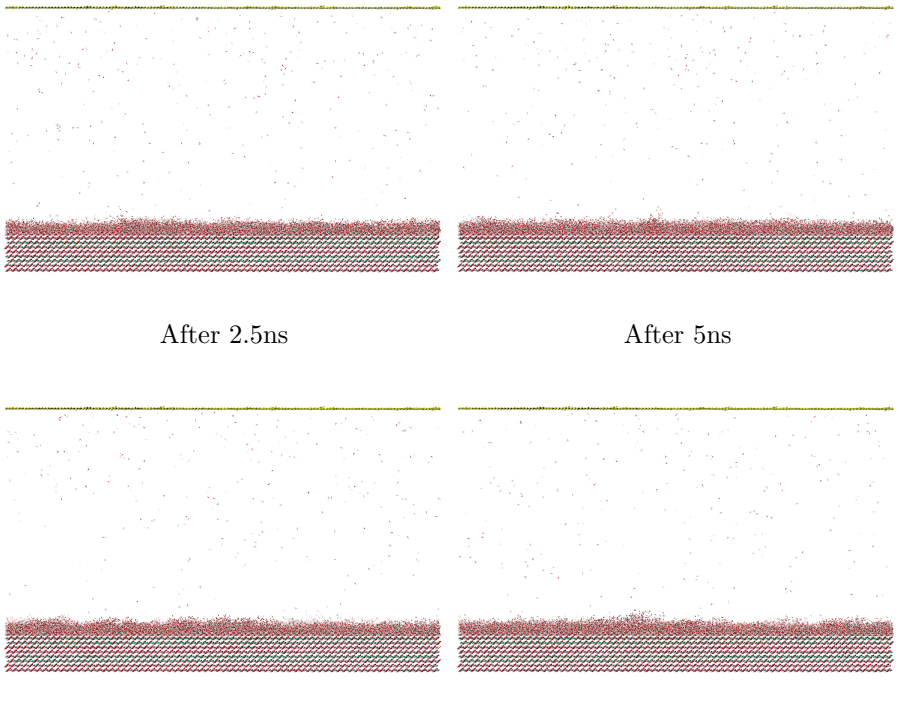

FIGURE 3.3: The evolution of the flat system in the simulation carried out with the thermal calcite layers coupled at 353K.

Figures 3.2 and 3.3 display the evolution of the calcite-water system with a flat initial configuration. Following energy minimisation the system relaxed, wetting the calcite until the surface of the water was relatively uniform. Note that Figure 3.3 shows a greater number of water molecules remain above the surface of the calcite.

3.1.1 Partial Density Distribution

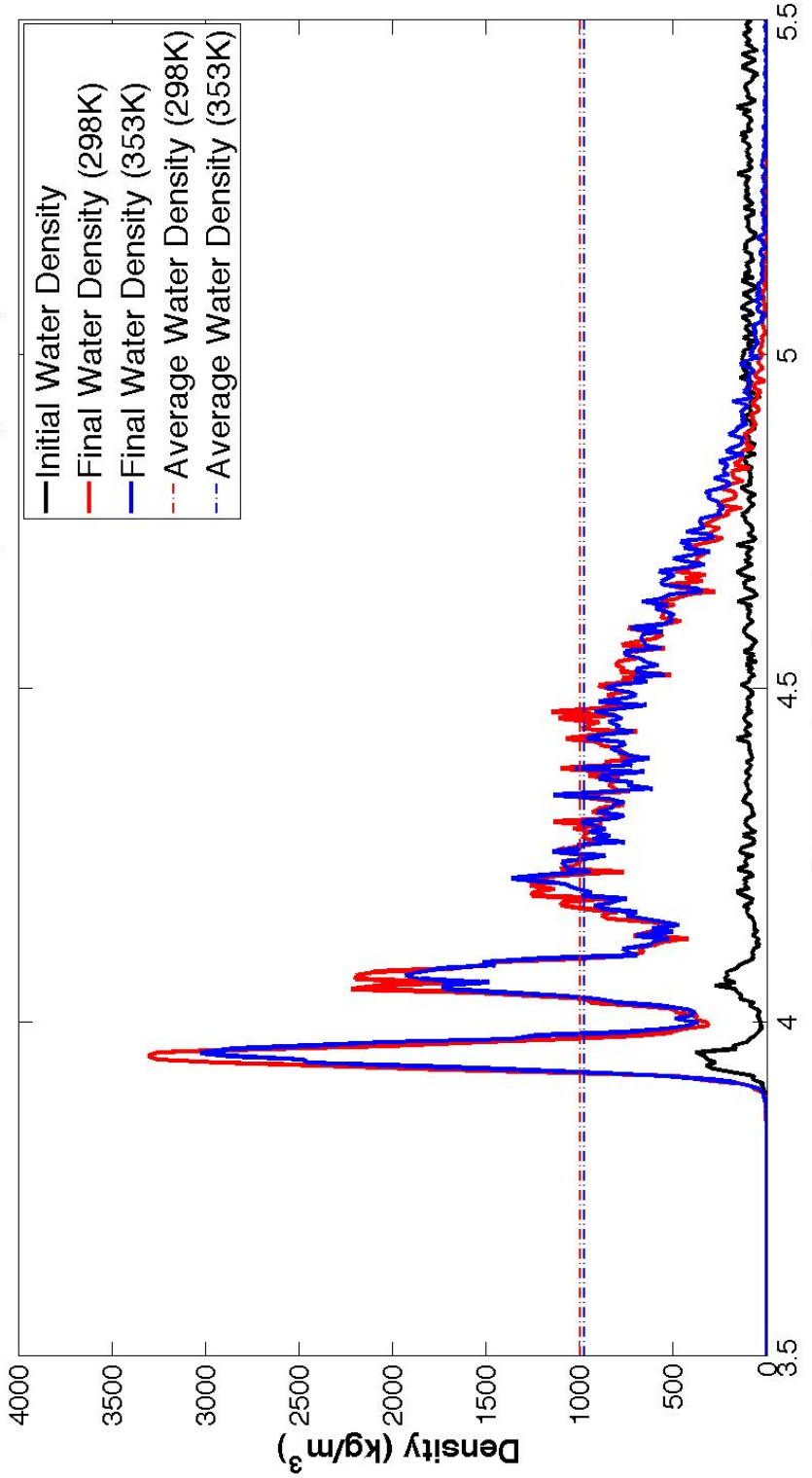

FIGURE 3.4: The partial density distribution of the flat water configuration perpendicular to the calcite surface.

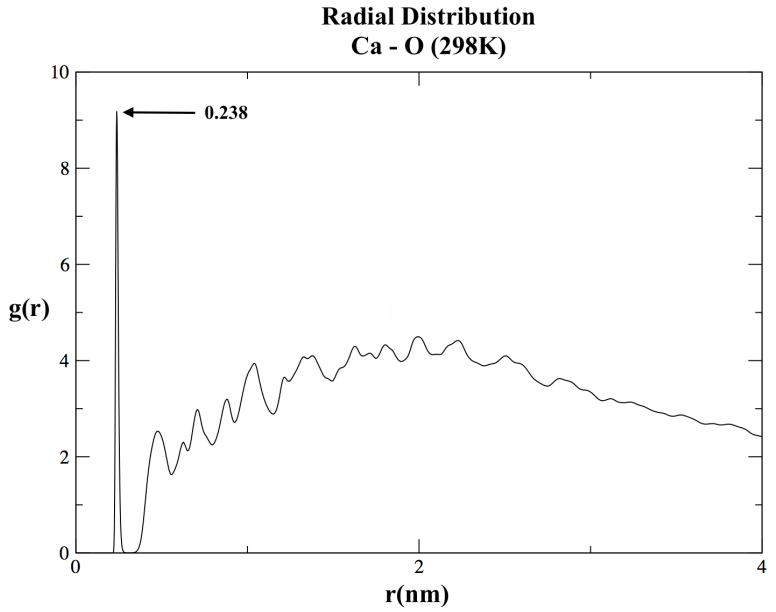

FIGURE 3.5: The radial distribution function for calcium ions and oxygen atoms for the simulation carried out at 298K.

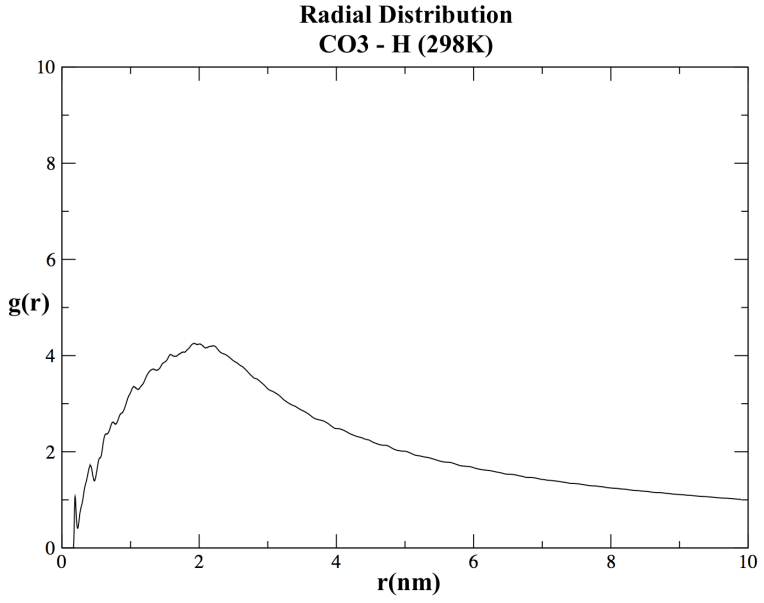

FIGURE 3.6: The radial distribution function for carbonate ions and hydrogen atoms for the simulation carried out at 298K.

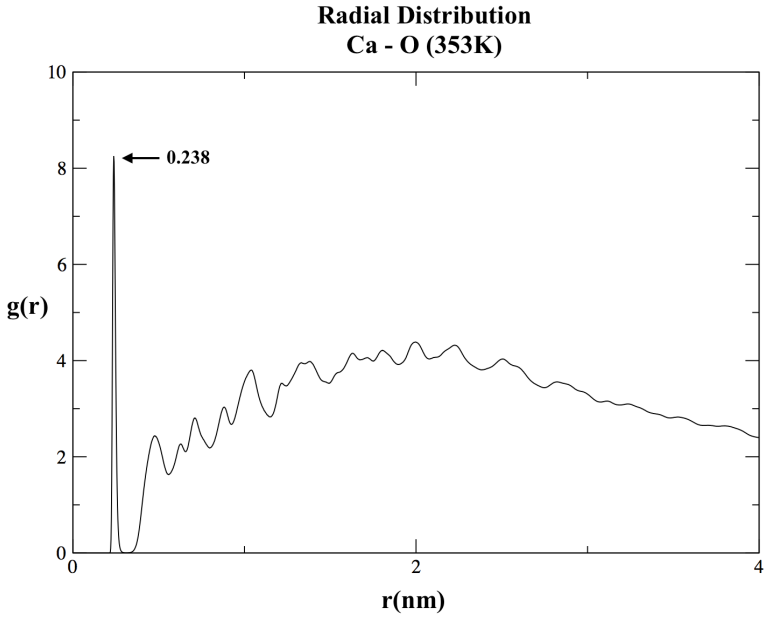

FIGURE 3.7: The radial distribution function for calcium ions and oxygen atoms for the simulation carried out at 353K.

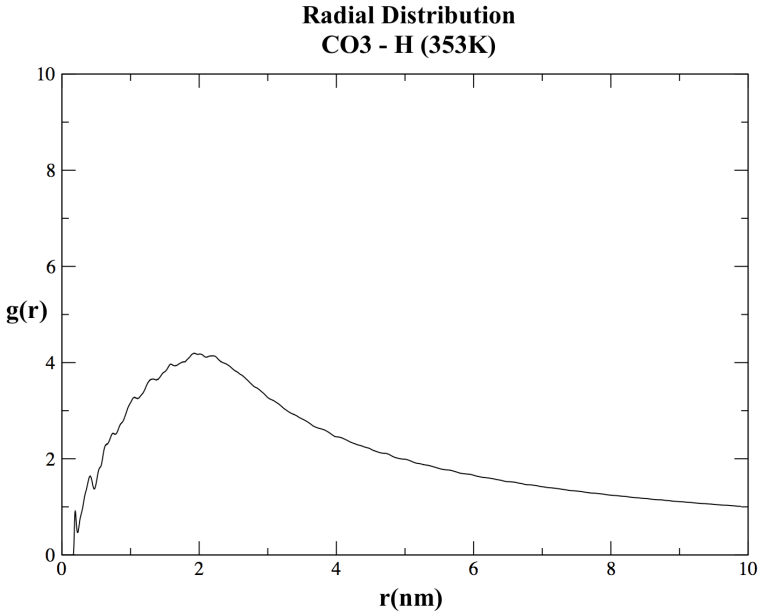

FIGURE 3.8: The radial distribution function for carbonate ions and hydrogen atoms for the simulation carried out at 353K.

Calcite-Water Flat Partial Density Distribution			
298K		**353K**	
1st Peak		1st Peak	
Z Dimension (nm)	Local Density (kg/m^3)	Z Dimension (nm)	Local Density (kg/m^3)
3.95	3304	3.955	3027.71
2nd Peak		2nd Peak	
Z Dimension (nm)	Local Density (kg/m^3)	Z Dimension (nm)	Local Density (kg/m^3)
4.065	2195.2	4.07	1929.71
3rd Peak		3rd Peak	
Z Dimension (nm)	Local Density (kg/m^3)	Z Dimension (nm)	Local Density (kg/m^3)
4.19	1254.21	4.215	1363.2

TABLE 3.2: The results for the partial density distribution calculations of the calcite-water flat configuration.

Figure 3.4 and Table 3.2 show a marked increase in density of water at the calcite surface between the start of the simulation and the end. In Figure 3.4 there is a distinct peak, followed by two smaller peaks, which are examined in Figure 3.2. It should be noted that the difference in the first and third peaks for 298K and 353K are 0.24nm and 0.26nm respectively. Examination of a TIP3P water molecule using equation 3.1 it was found that the distance between the centre of one hydrogen atom to the oxygen atom is 0.115nm. This corresponds approximately to the distance between each individual peak on the graph. Examination of the RDF graphs show that it is most probable for oxygen atoms to be found 0.238nm from the calcium ion, with a sharp peak of significant magnitude. Therefore, it can be reasonably assumed that, despite the three peaks, a densely packed monolayer of water molecules forms between the water and the calcite, driven by the electrostatic attraction between oxygen and calcium.

$$distance = \sqrt{(x_2 - x_1)^2 + (y_2 - y_1)^2 + (z_2 - z_1)^2} \tag{3.1}$$

3.2 Calcite-Water Domed

As discussed previously there were two systems simulated with calcite and water. Simulations were carried out for 10ns after the water had formed a domed structure on the calcite surface.

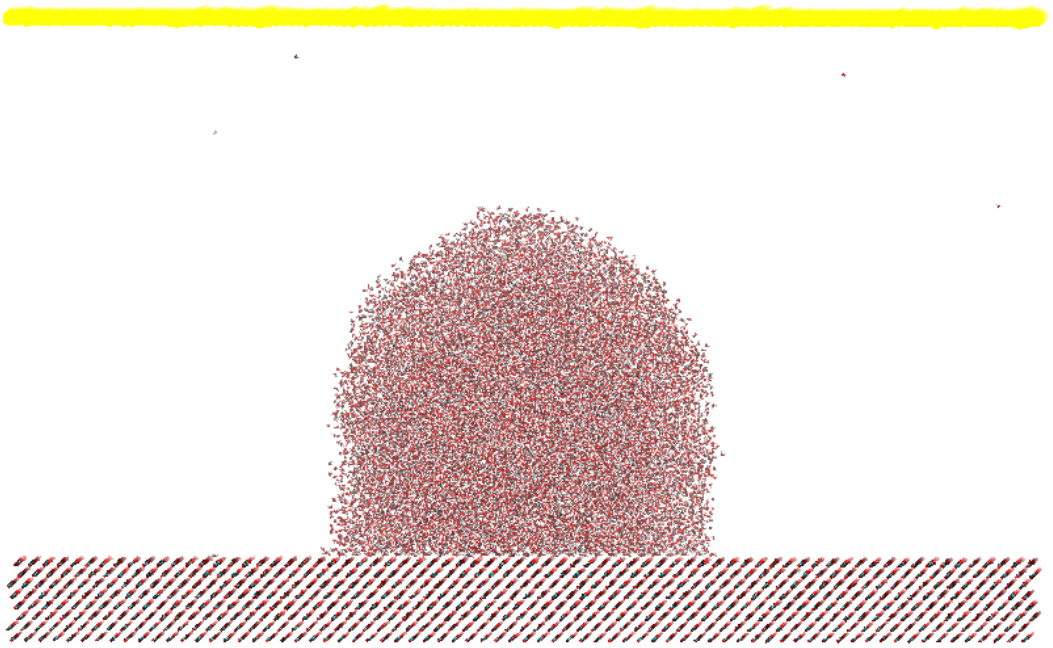

FIGURE 3.9: The starting configurations in the calcite/water domed simulations

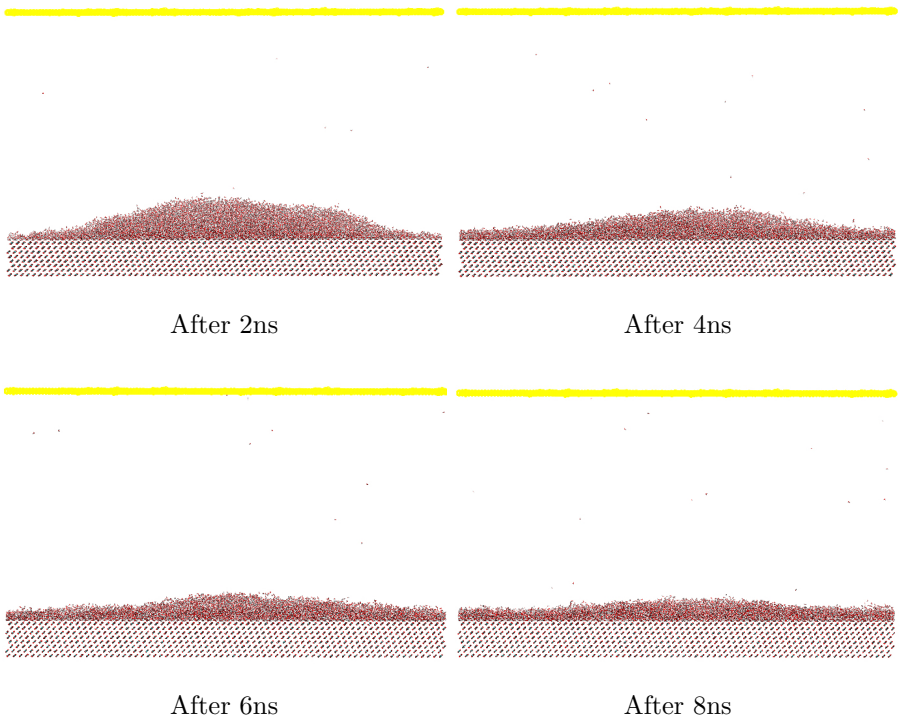

FIGURE 3.10: The evolution of the domed system in the simulation carried out with the thermal calcite layers coupled at 298K.

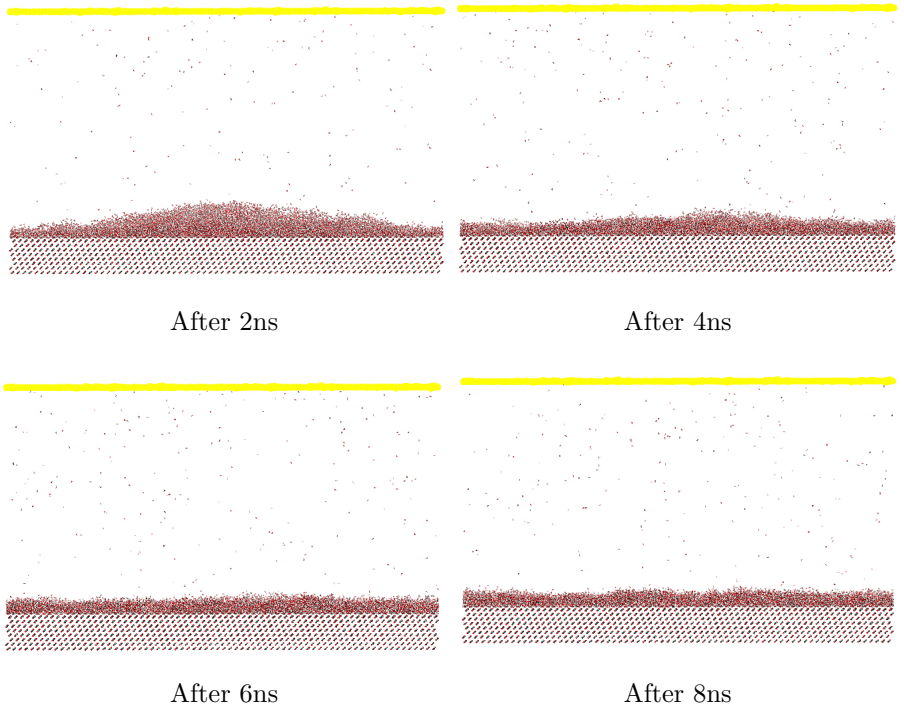

FIGURE 3.11: The evolution of the domed system in the simulation carried out with the thermal calcite layers coupled at 353K.

Figures 3.10 and 3.11 display the evolution of the Calcite-Water system with a domed initial configuration. Following energy minimisation the system relaxed, wetting the calcite surface. Note that Figure 3.11 shows a more efficient spreading and a greater number of water molecules remain above the surface of the calcite.

3.2.1 Partial Density Distribution

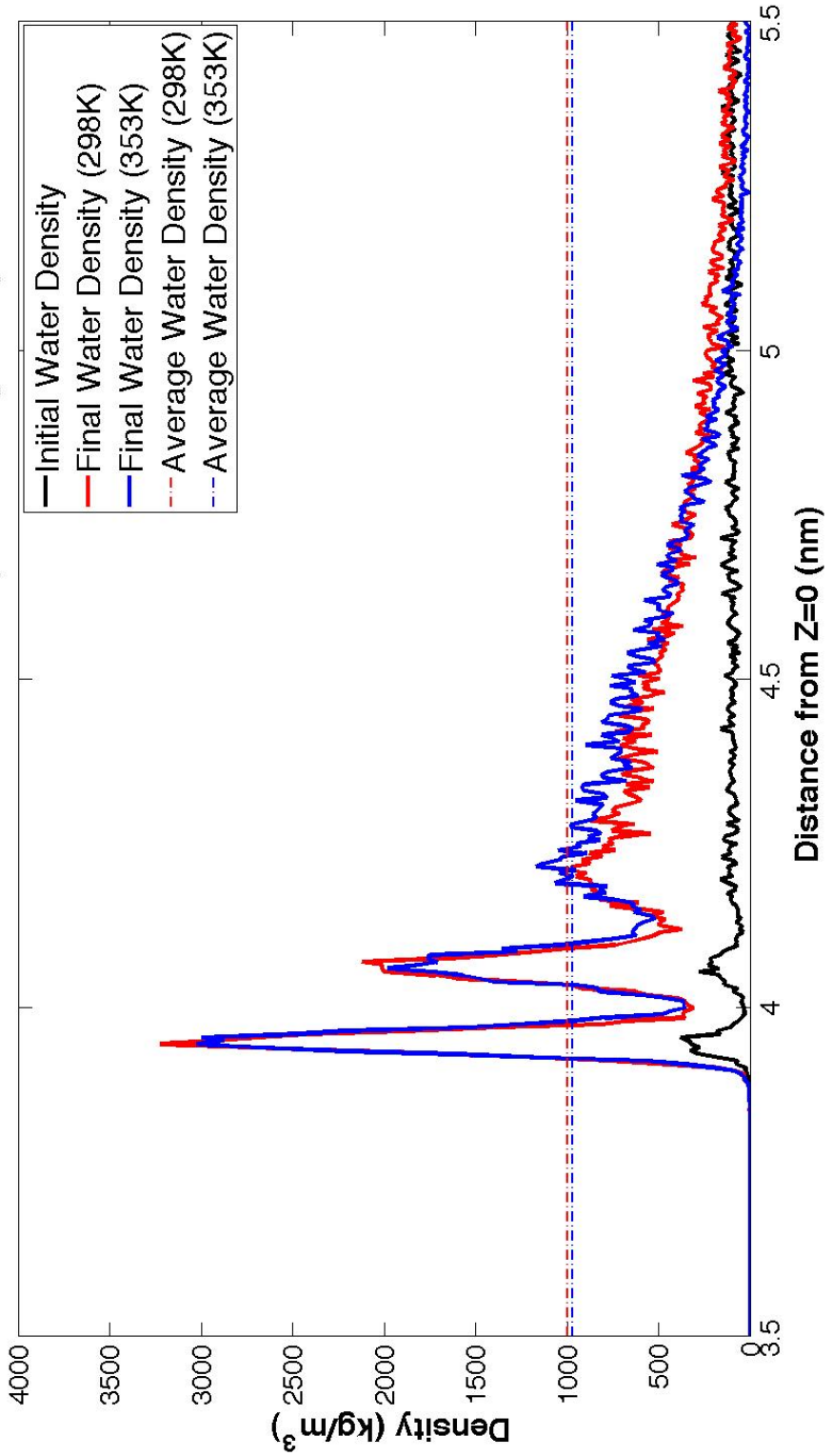

FIGURE 3.12: The partial density distribution of the domed water configuration perpendicular to the calcite surface.

Calcite-Water Domed Partial Density Distribution			
298K		**353K**	
1st Peak		1st Peak	
Z Dimension (nm)	Local Density (kg/m^3)	Z Dimension (nm)	Local Density (kg/m^3)
3.945	3222.56	3.945	3026
2nd Peak		2nd Peak	
Z Dimension (nm)	Local Density (kg/m^3)	Z Dimension (nm)	Local Density (kg/m^3)
4.06	2009.49	4.06	1981.13
3rd Peak		3rd Peak	
Z Dimension (nm)	Local Density (kg/m^3)	Z Dimension (nm)	Local Density (kg/m^3)
4.215	972.704	4.215	1167.24

TABLE 3.3: The results for the partial density distribution calculations of the calcite-water domed configuration.

Figure 3.12 and Table 3.3 show a marked increase in density of water at the calcite surface between the start of the simulation and the end. In Figure 3.12 there are three distinct peaks which are then examined in Figure 3.3. It should be noted that the difference in these peaks for 298K and 353K is 0.27nm. As discussed in the previous section the distance between the centre of one hydrogen atom to the oxygen atom is 0.115nm in the TIP3P water model. This corresponds approximately to the distance between the peaks on the graph. Therefore, it can be resonably assumed that a densely packed monolayer of water molecules forms between the water and the calcite.

3.3 Calcite-Water-Dodecane Flat

There were three systems simulated with calcite, water and dodecane. Dodecane was then inserted into the domed system, a system with a water droplet and a system in which the water had fully spread out on the calcite. Simulations were performed for 15ns with the thermal calcite layers coupled at both 298K and 353K respectively. This enabled analysis of the spreading of the droplet on the calcite surface as well as interactions between the water and dodecane.

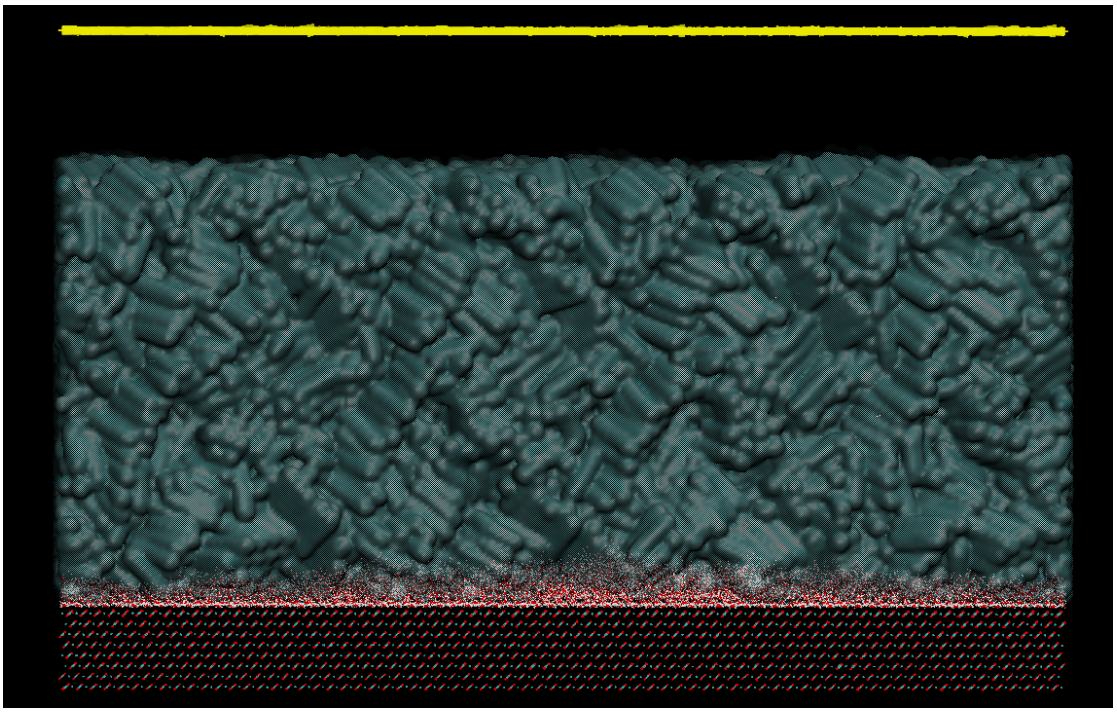

FIGURE 3.13: The starting configurations in the calcite/water/dodecane flat simulations

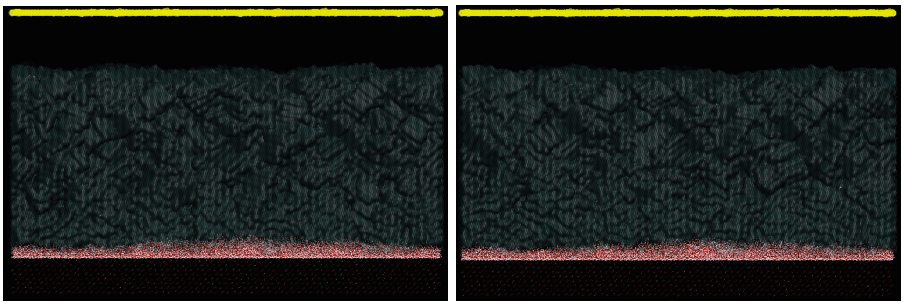

After 3.75ns After 7.5ns

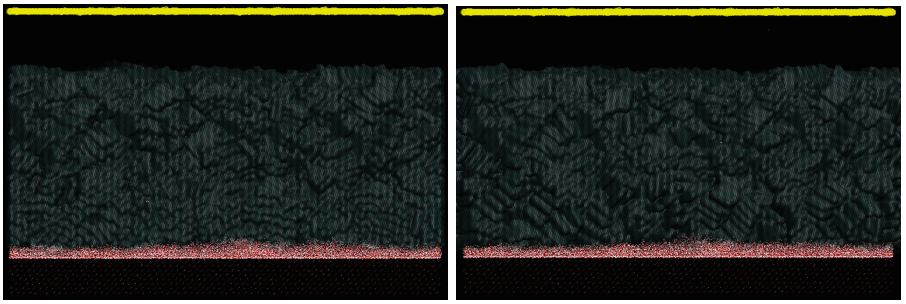

After 11.25ns After 15ns

FIGURE 3.14: The evolution of the flat system with dodecane in the simulation carried out with the thermal calcite layers coupled at 298K.

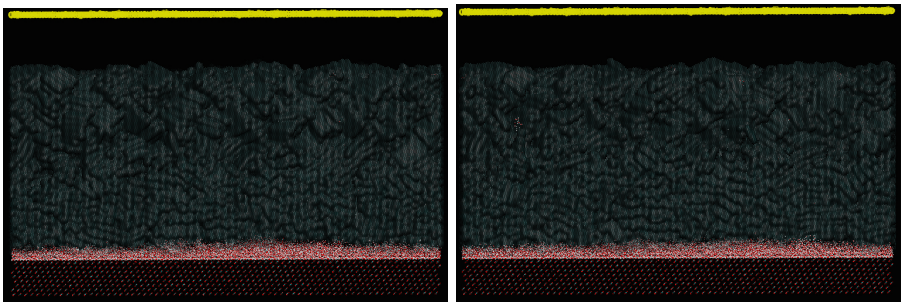

After 3.75ns After 7.5ns

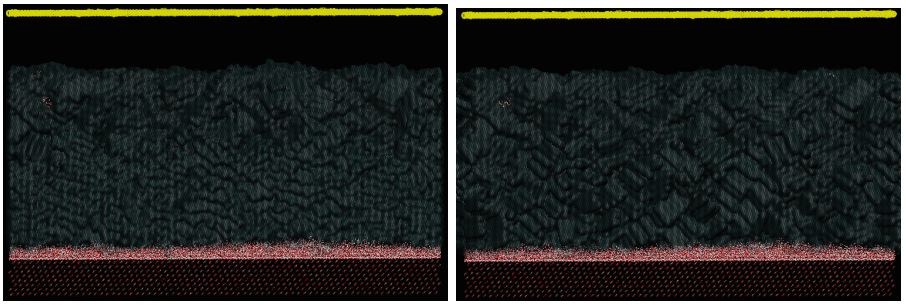

After 11.25ns After 15ns

FIGURE 3.15: The evolution of the flat system with dodecane in the simulation carried out with the thermal calcite layers coupled at 353K.

3.3.1 Partial Density Distribution

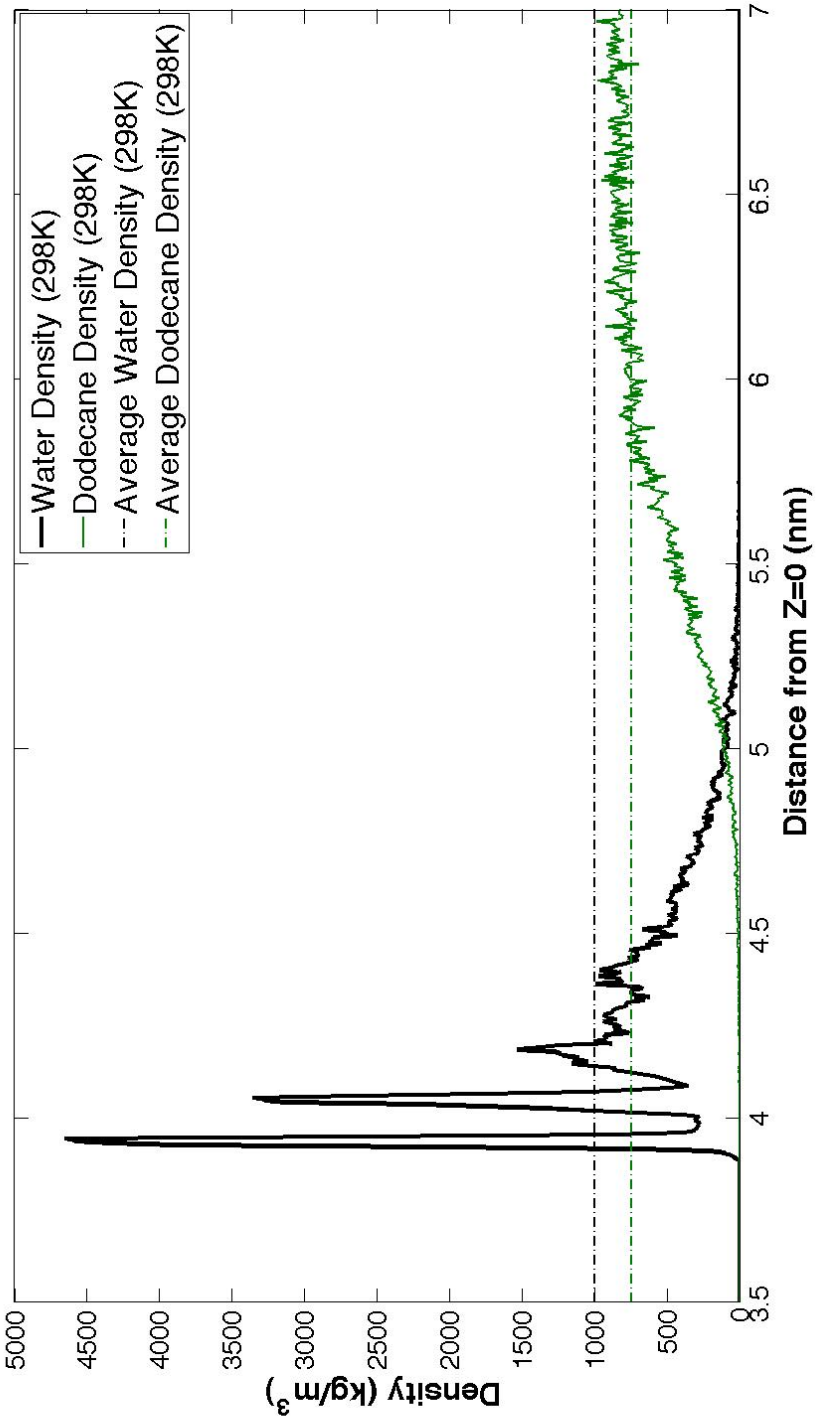

FIGURE 3.16: The partial density distribution of the flat water-dodecane configuration perpendicular to the calcite surface at the start of the simulation.

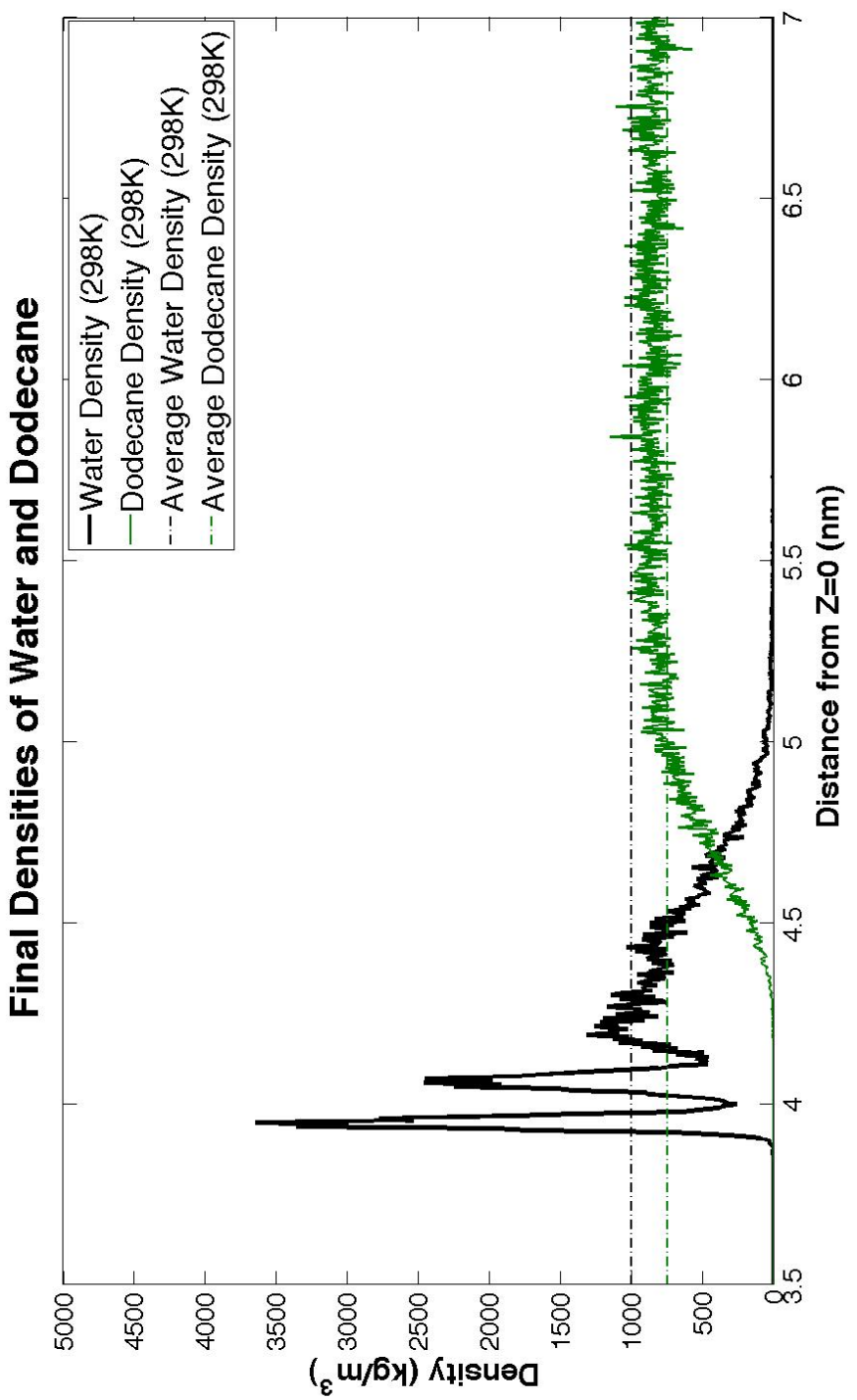

FIGURE 3.17: The partial density distribution of the flat water-dodecane configuration perpendicular to the calcite surface at the end of the simulation at 298K.

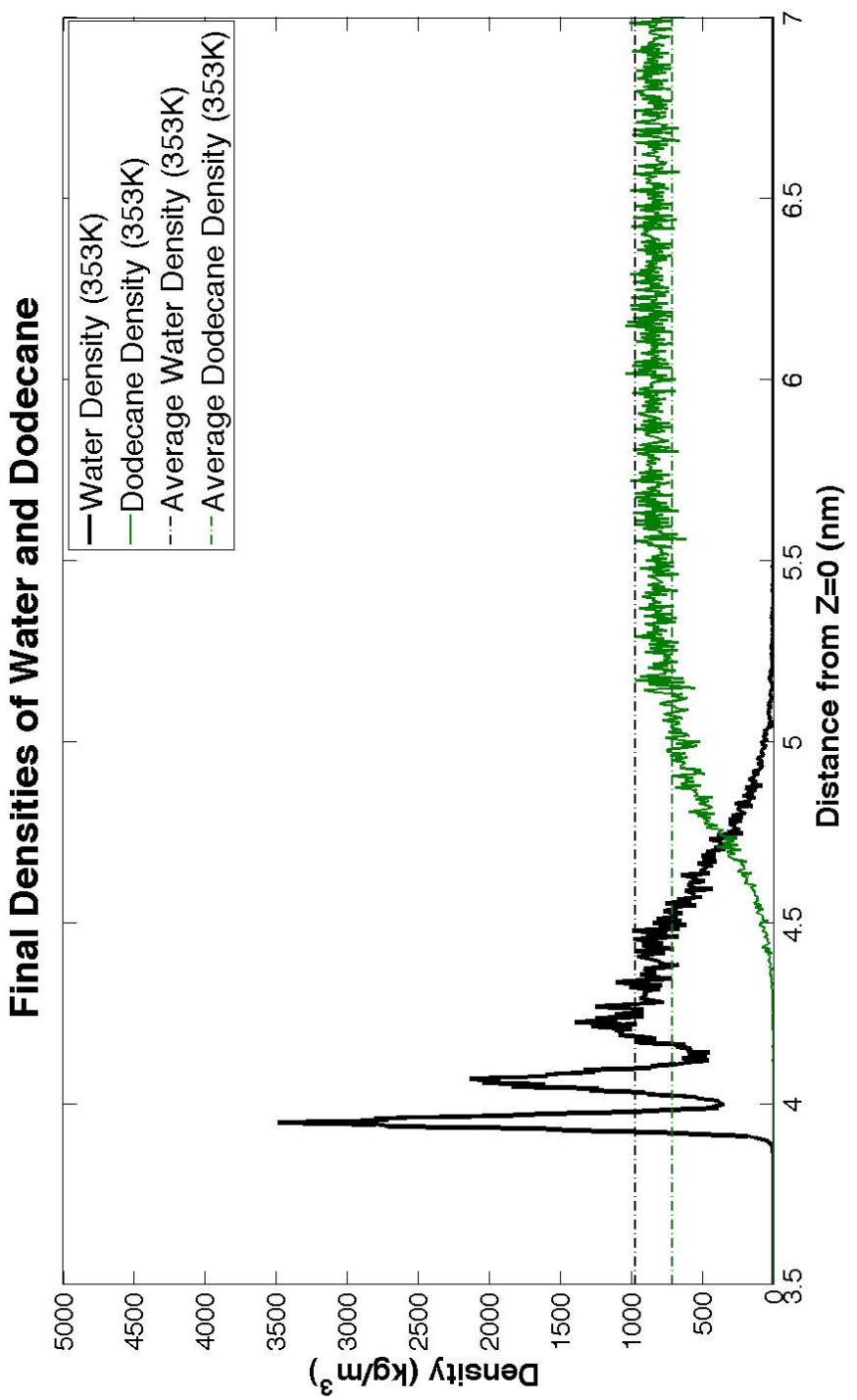

FIGURE 3.18: The partial density distribution of the flat water-dodecane configuration perpendicular to the calcite surface at the end of the simulation at 353K.

3.4 Calcite-Water-Dodecane Domed

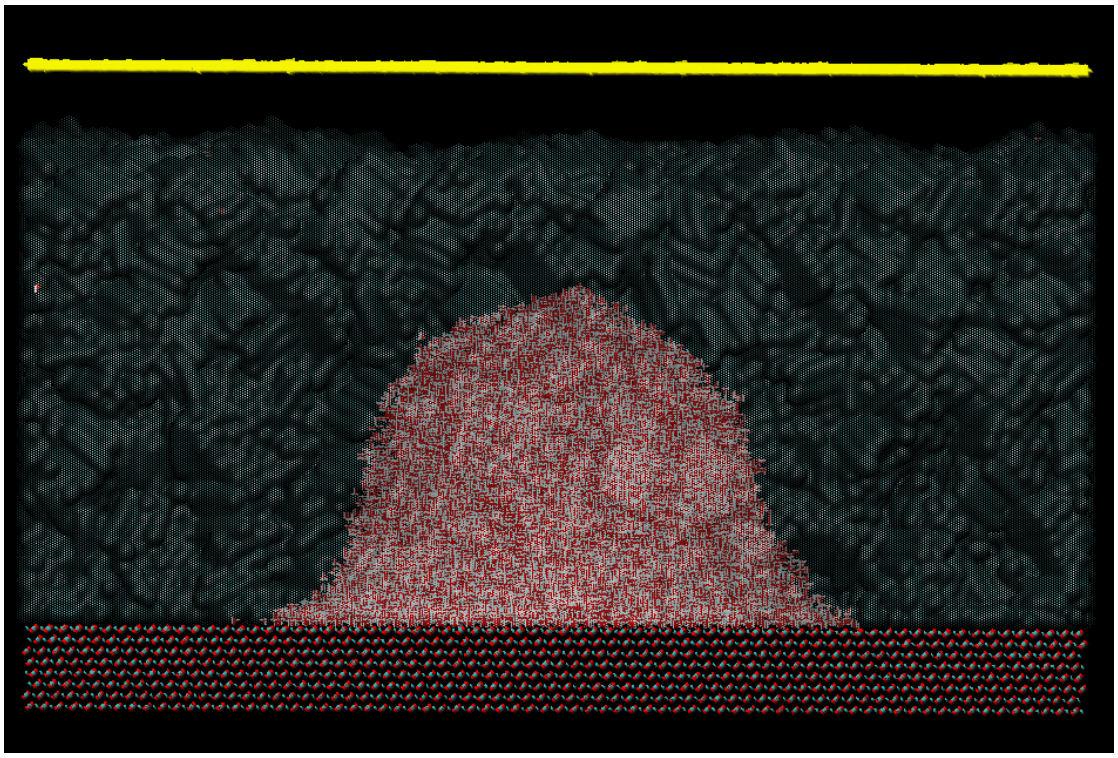

FIGURE 3.19: The starting configurations in the calcite/water/dodecane domed simulations

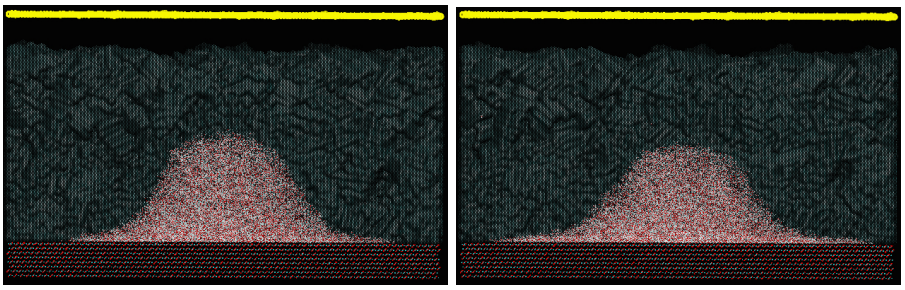

After 3.75ns After 7.5ns

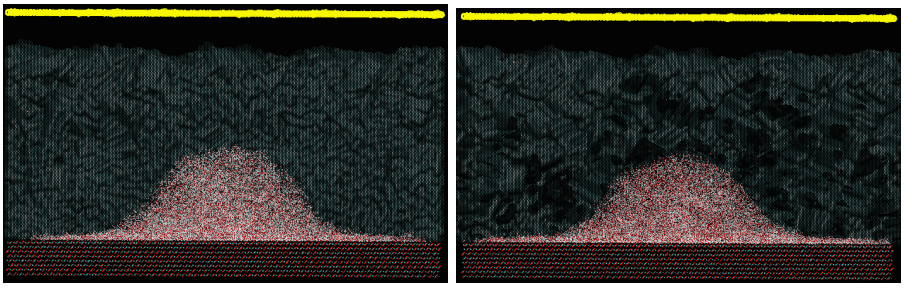

After 11.25ns After 15ns

FIGURE 3.20: The evolution of the domed system with dodecane in the simulation carried out with the thermal calcite layers coupled at 298K.

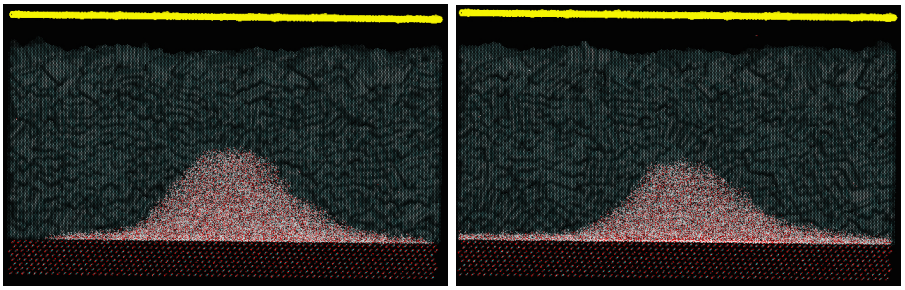

After 3.75ns After 7.5ns

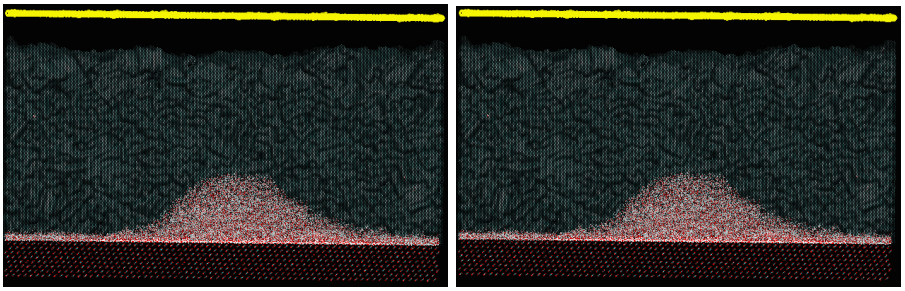

After 11.25ns After 15ns

FIGURE 3.21: The evolution of the domed system with dodecane in the simulation carried out with the thermal calcite layers coupled at 353K.

After 15ns of simulation at 298K (Figure 3.20) the water has differed only slightly from the initial domed structure, with the layers in contact with the calcite surface wetting. The spreading does appear relatively uniform as the spreading is equivalent both sides. Very few water molecules move away from the bulk water and are found in the dodecane layer above. This differs greatly from the simulations with no dodecane as almost complete wetting occurred in less than 10ns. Figure 3.21 demonstrates that after 15ns of simulation at this higher temperature, the water differs from the initial domed structure, with the layers in contact with the calcite surface wetting and a reduction in height of the dome. The spreading does not appear relatively uniform as the dome appears asymmetrical. This may be because of capillary waves. A capillary wave being a travelling wave across a phase boundary, whose dynamics are dominated by the effects of surface tension. Very few water molecules move away from the bulk water and are found in the dodecane layer above. This differs greatly from the simulations with no dodecane as almost complete wetting occurred in less than 10ns.

3.4.1 Partial Densities

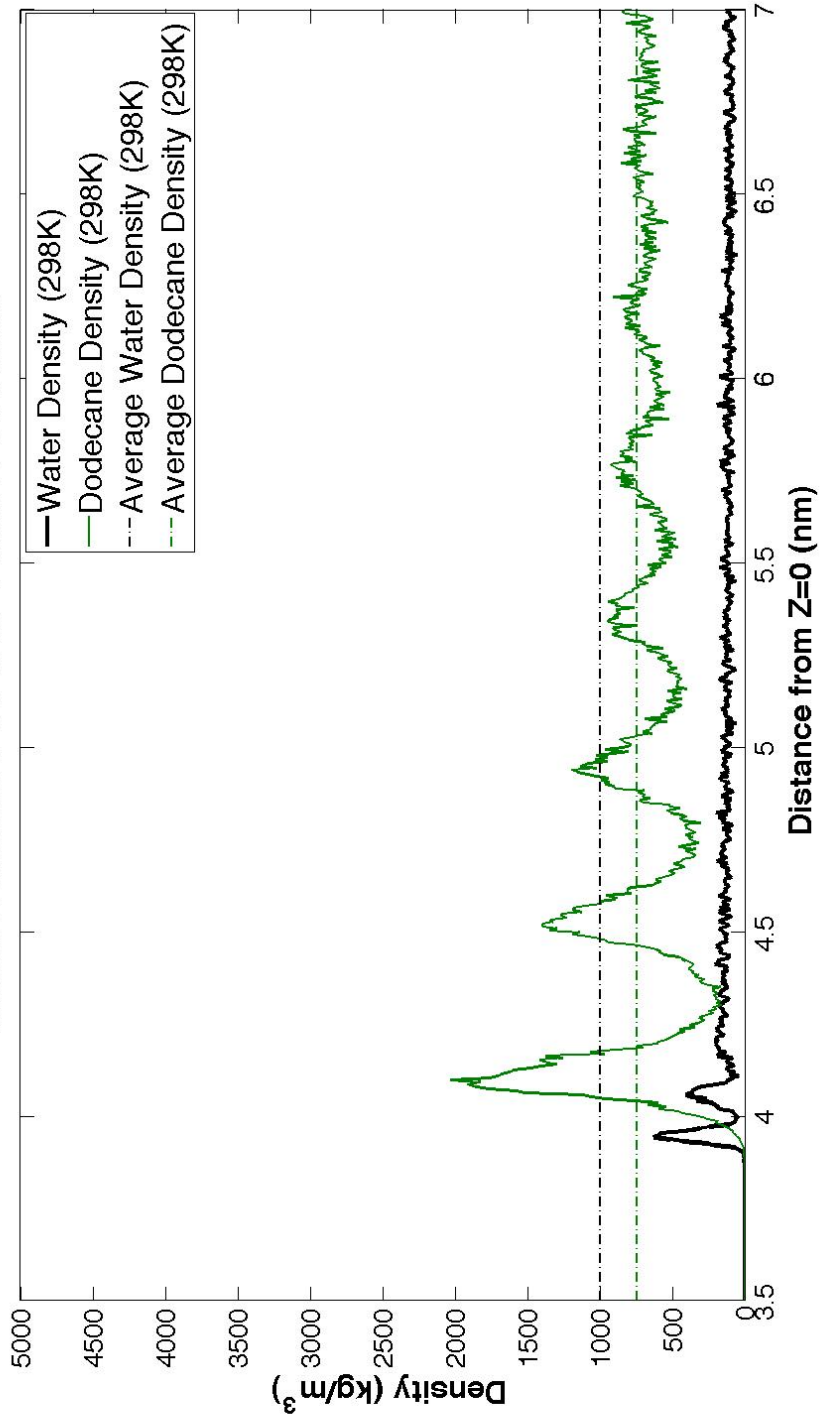

FIGURE 3.22: The partial density distribution of the domed water-dodecane configuration perpendicular to the calcite surface at the start of the simulation.

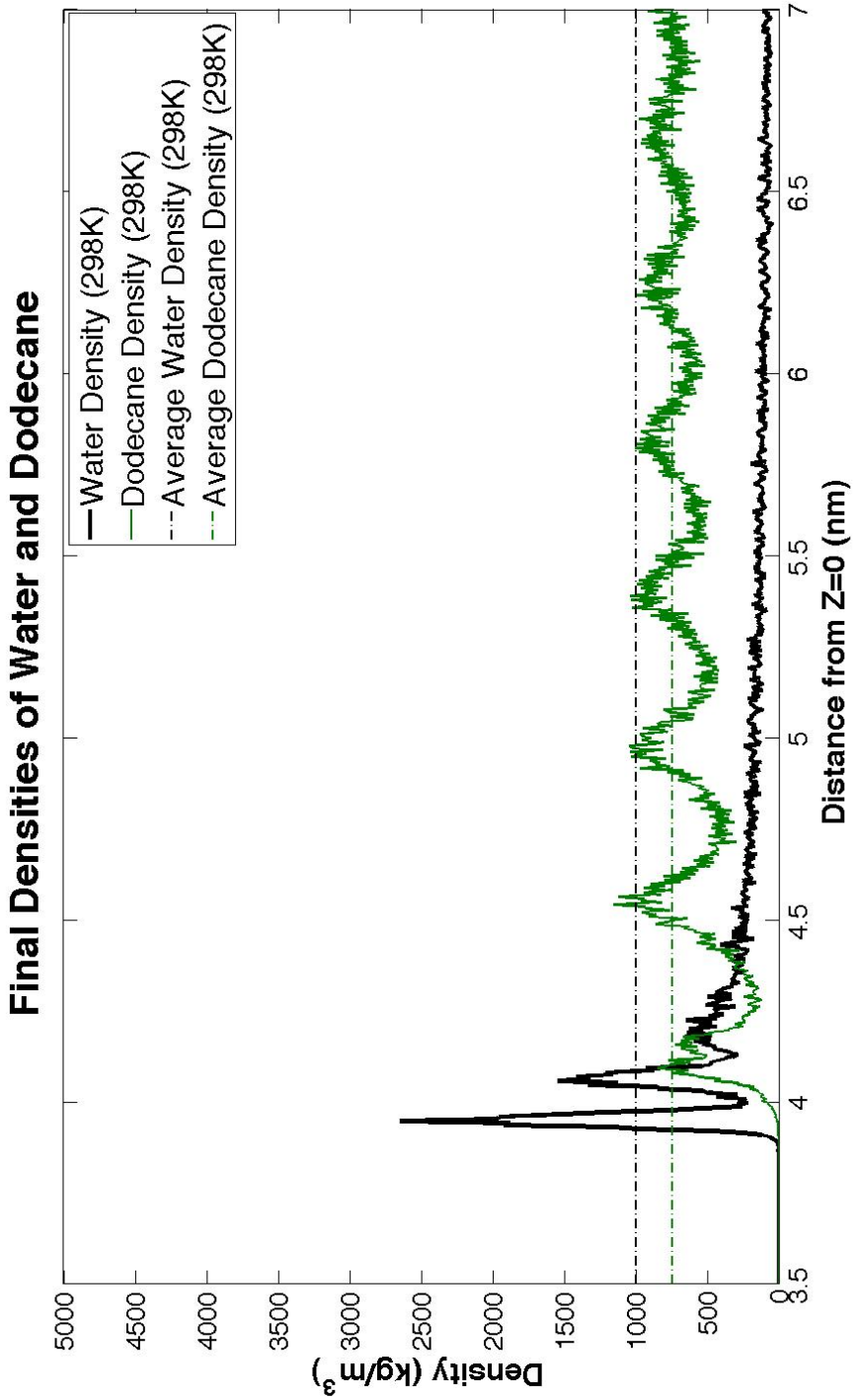

FIGURE 3.23: The partial density distribution of the domed water-dodecane configuration perpendicular to the calcite surface at the end of the simulation at 298K.

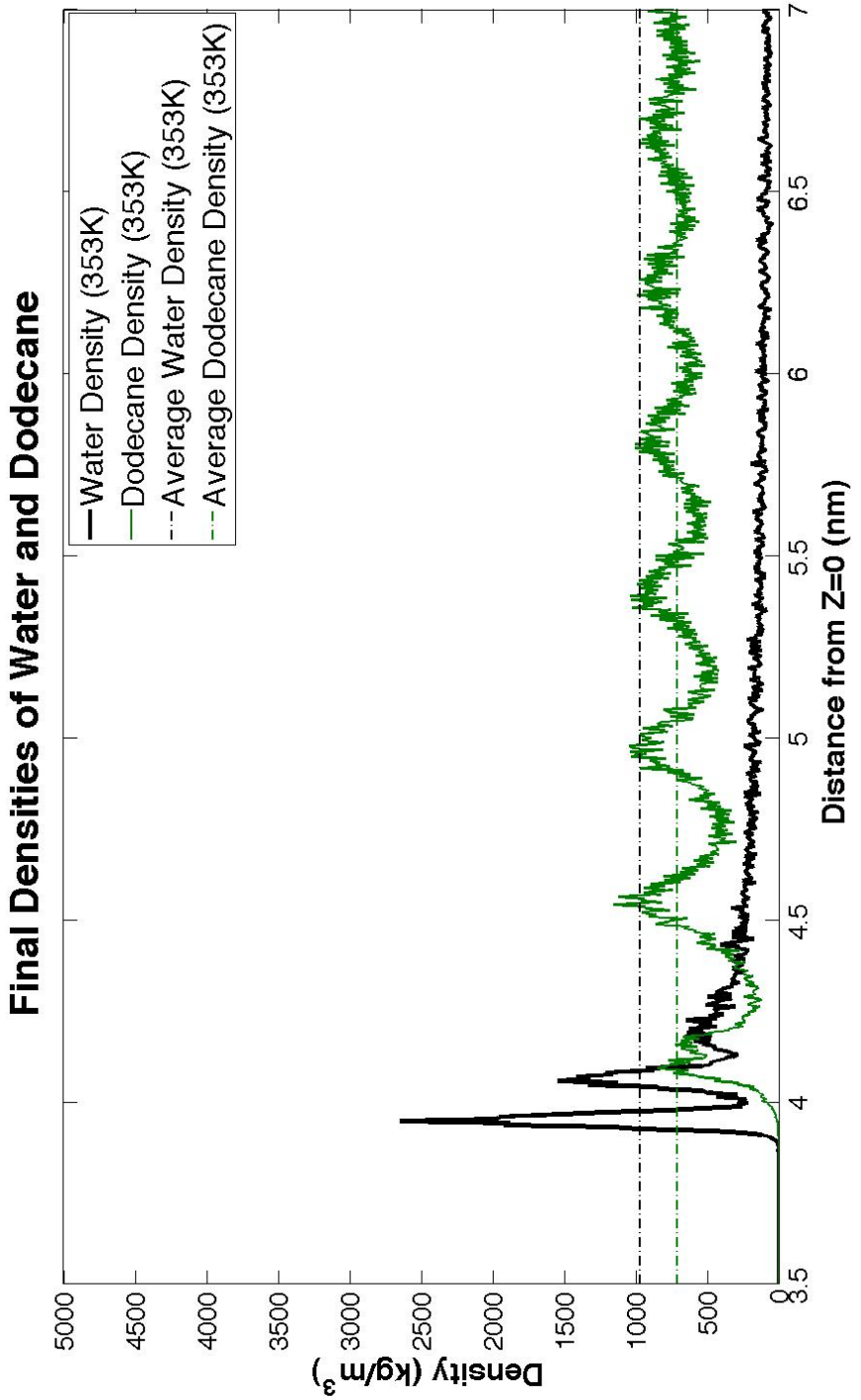

FIGURE 3.24: The partial density distribution of the domed water-dodecane configuration perpendicular to the calcite surface at the end of the simulation at 353K.

3.5 Calcite-Water-Dodecane Droplet

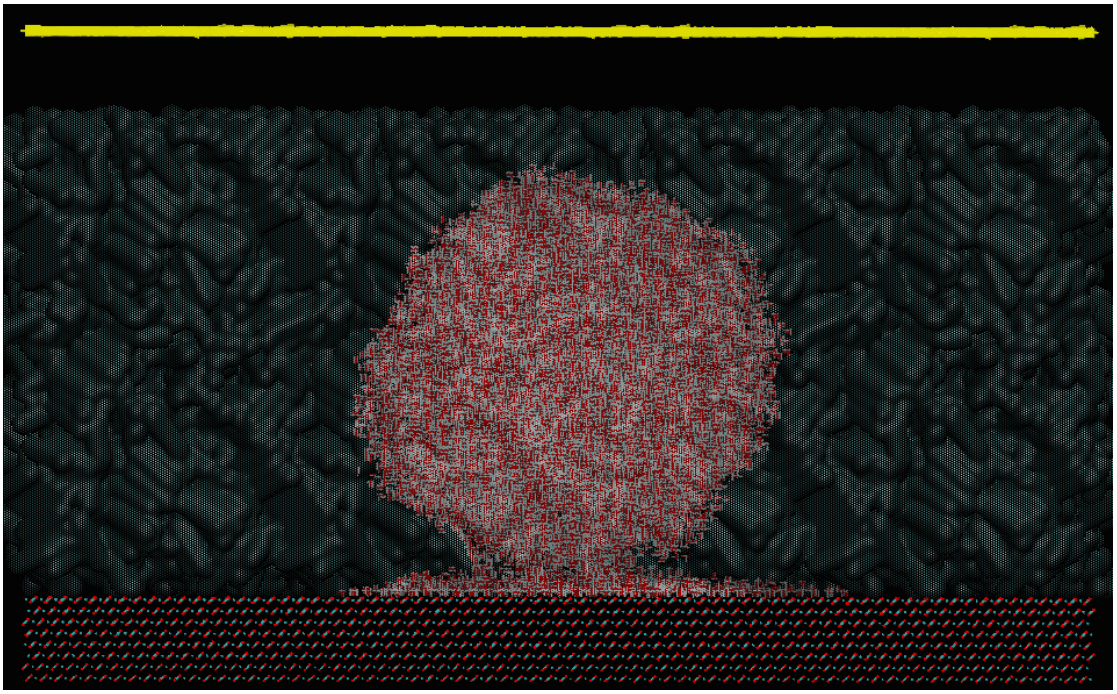

FIGURE 3.25: The starting configurations in the calcite/water/dodecane droplet simulations

Figure 3.25 demonstrates the initial conformation of the droplet configuration with dodecane. The dodecane and water were equilibrated separately by freezing everything else except the target for equilibration, be it water or dodecane. This is the reason that the water has started to partially spread on the calcite surface. The simulations were then performed for 10ns.

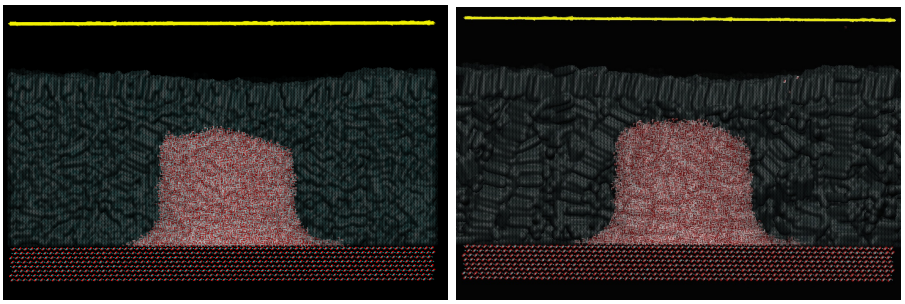

After 2.5ns After 5ns

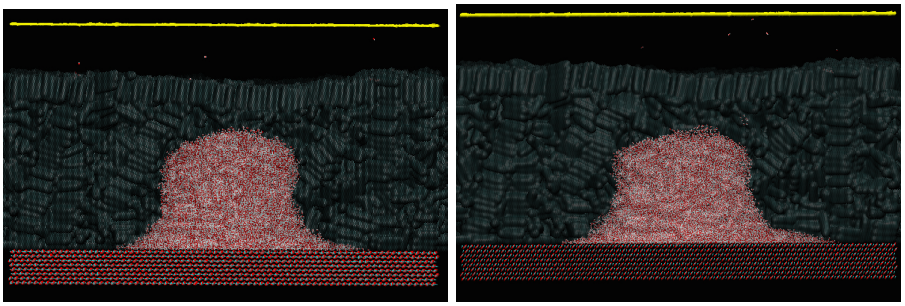

After 7.5ns After 10ns

FIGURE 3.26: The evolution of the droplet system with dodecane in the simulation carried out with the thermal calcite layers coupled at 298K.

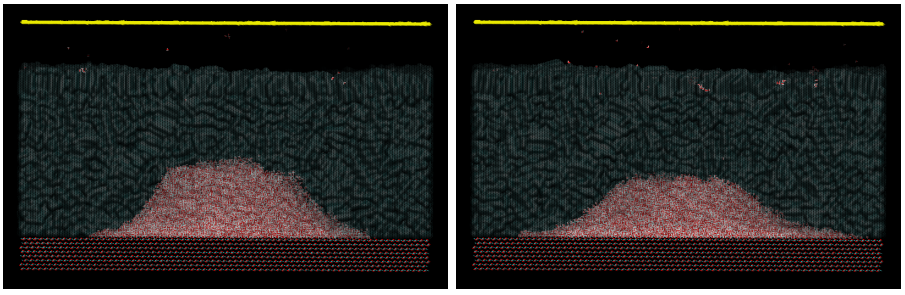

After 2.5ns After 5ns

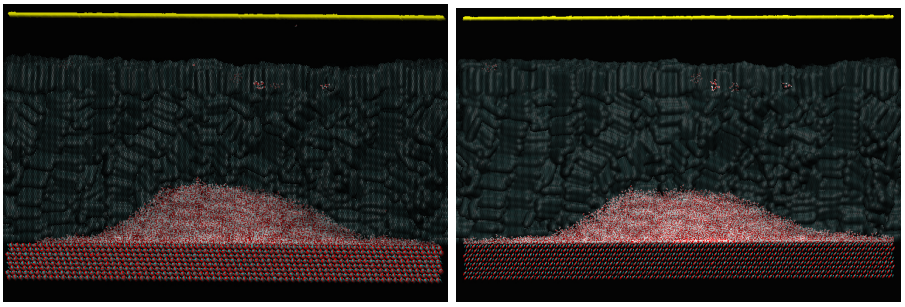

After 7.5ns After 10ns

FIGURE 3.27: The evolution of the droplet system with dodecane in the simulation carried out with the thermal calcite layers coupled at 353K.

3.6 Interfacial Tension

Using the *#Surf*SurfTen* option within the *g_energy* functionin gromacs, the average interfacial tension between dodecane and water was found to be 44.1 mN/m (*g_energy* is a program within GROMACS that extracts information from trajectories specifically related to energy). However, the standard deviation and variance, as with all pressure-related properties, was found to be very large. A basic understanding of statistical analysis states that, for a data set such as this, a median would be a much more appropriate measure for the *average* interfacial tension. Using the median the result obtained was 50.1 mN/m.

3.7 Adsorption and Free Energy

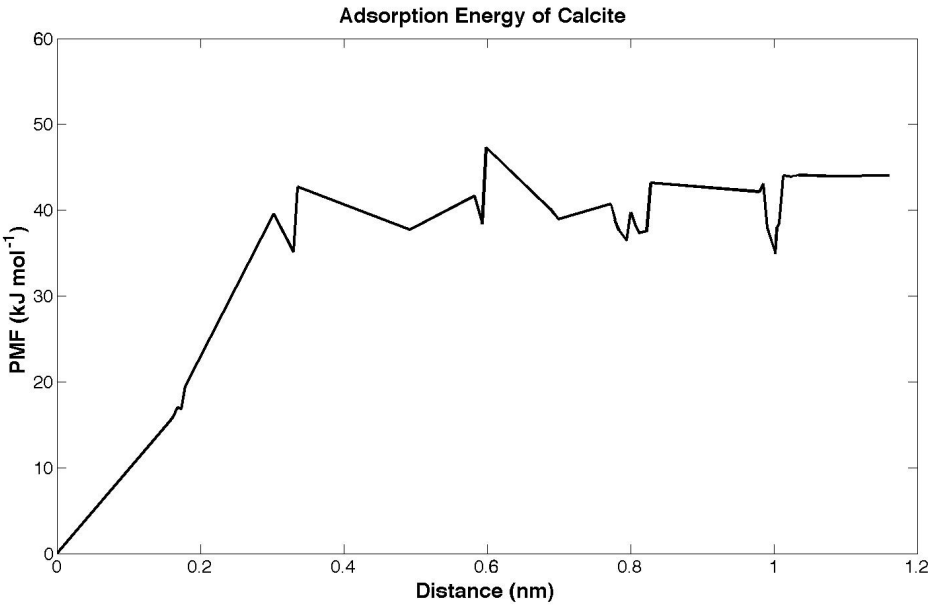

FIGURE 3.28: The PMF curve showing a value of ≈44 kJ mol^{-1} for ΔG of adsorption. This is calculated as the difference between the plateau region of the PMF curve and the energy minimum of the curve.

Figure 3.29 shows the radial distribution function, **(RDF)**, of O_{water} with respect to the calcium atoms of calcite. In layman's terms the RDF is a measure of the probability of finding an oxygen atom at a given distance **r** away from the reference calcium particle, relative to that for an ideal gas. Figure 3.29 shows that the most probable distance is

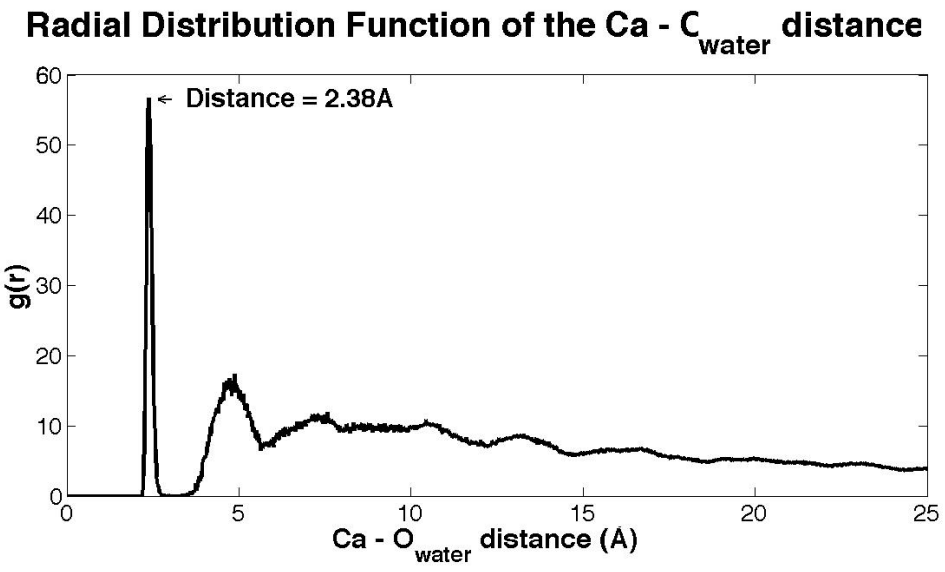

FIGURE 3.29: Radial distribution function for O_{water} with respect to Ca.

2.38 $\mathring{A}$, which is therefore the $Ca - O_{water}$ length.

Another pair of simulations were then performed with a single water molecule on the surface at 298K and 353K. The molecule was not pulled. The RDF was calculated between the oxygen atom of this water molecule and the corresponding calcium ion. Using the RDF values shown in Figures 3.30 and 3.31 alongside Equation 1.19 produced adsorption free energy results of -33.4 kJ mol^{-1} and -39.4 kJ mol^{-1} for the simulations at 298K and 353K respectively. These results are comparable to both previous experimental and computational works and the results produced in this study from the PMF analysis.

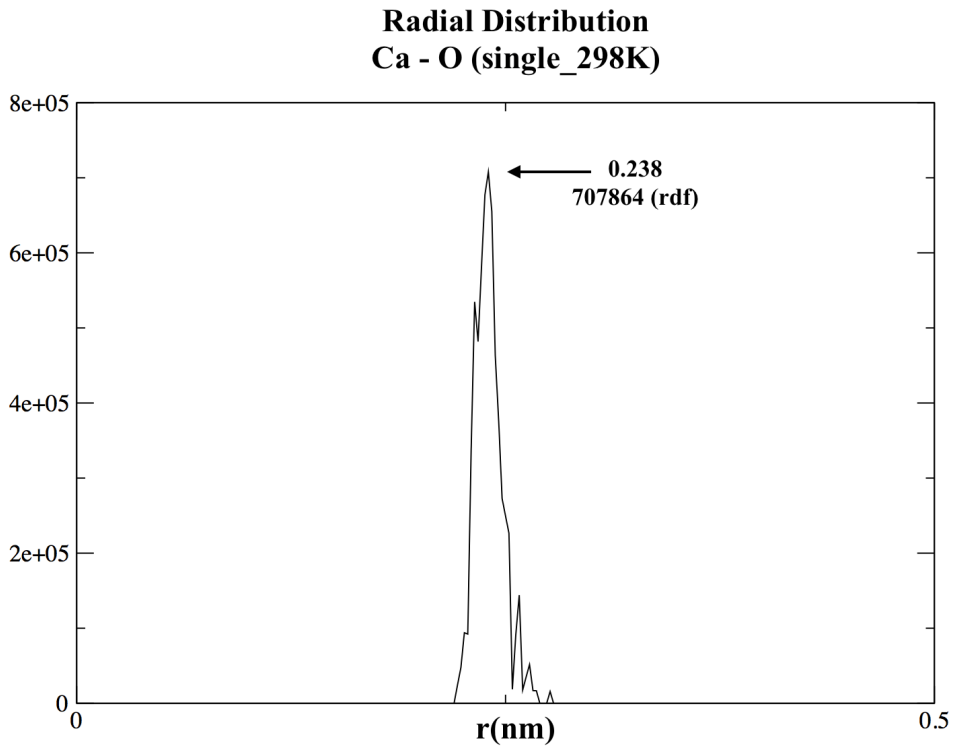

FIGURE 3.30: Radial distribution function for the O_{water} with respect to its corresponding Ca ion for the simulation at 298K.

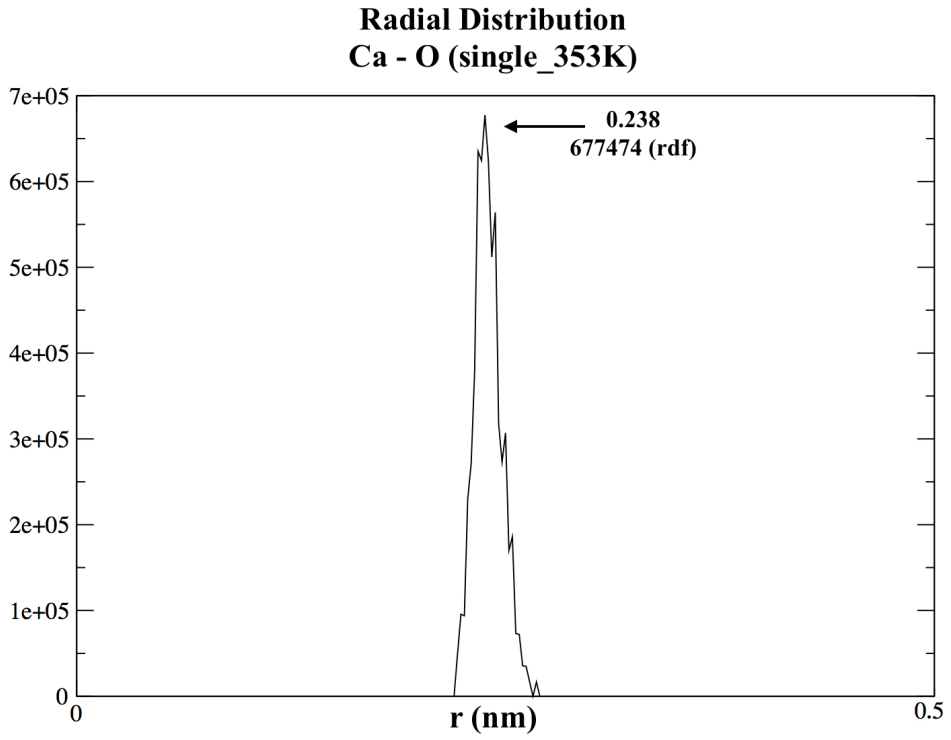

FIGURE 3.31: Radial distribution function for the O_{water} with respect to its corresponding Ca ion for the simulation at 353K.

3.8 Contact Angles

3.8.1 Computational Results

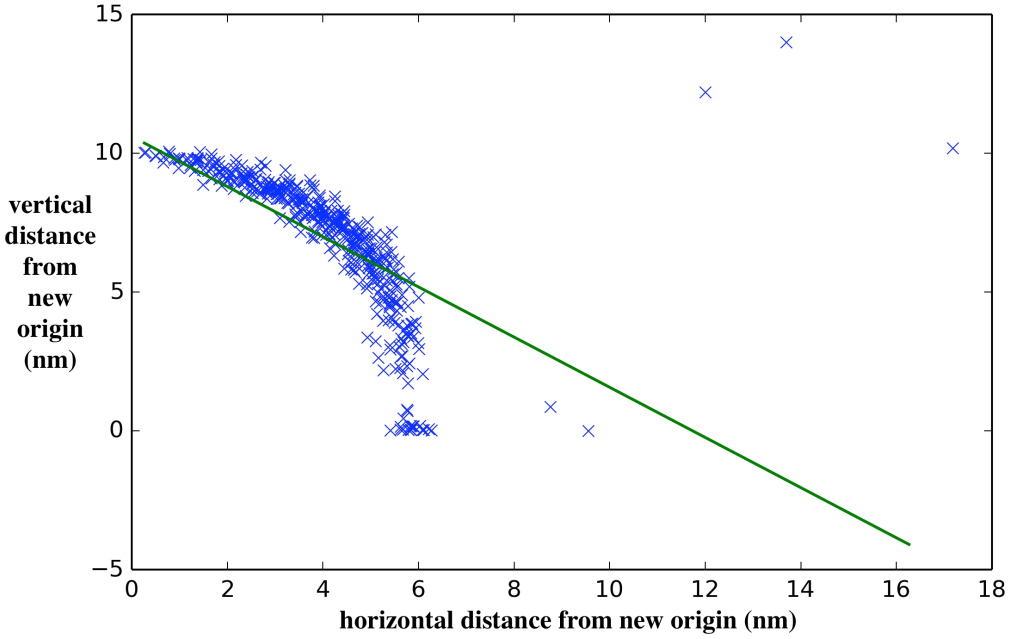

FIGURE 3.32: The coordinates of water molecules at 0ps projected onto one dimension.

Figure 3.32 shows the 1-dimensional projection of water at 0ps. The green line shows the linear regression. This demonstrates the case in which the contact angle script (see Section 2.3.4) fails. An artifact occurs showing that a linear regression of this droplet is not appropriate for this example, the script returns an angle of 42.10°, which vastly underestimates the actual contact angle of the droplet shown in Figures 3.9 and 3.32. This only seems to occur when the droplet spreading is non-uniform and approaches 90° (see Figure 3.33).

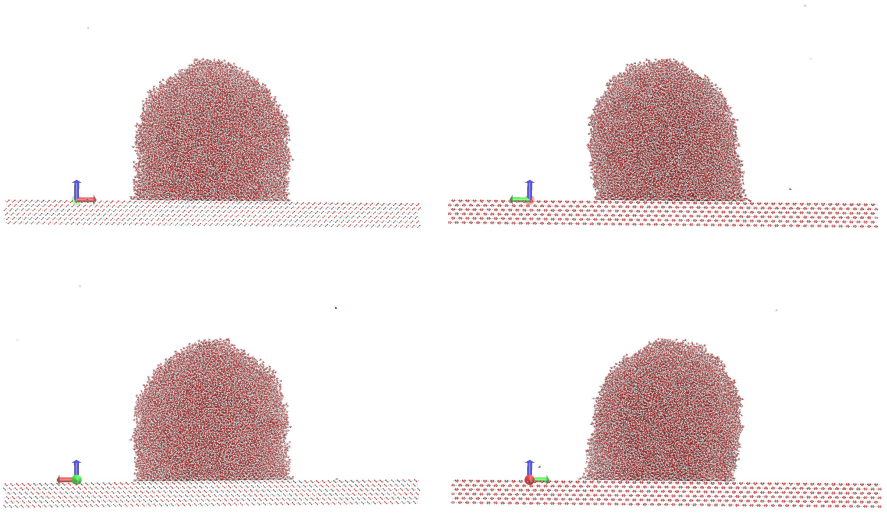

FIGURE 3.33: The droplet at 0ps from 4 different perspectives, demonstrating non-uniform spreading.

298K Results

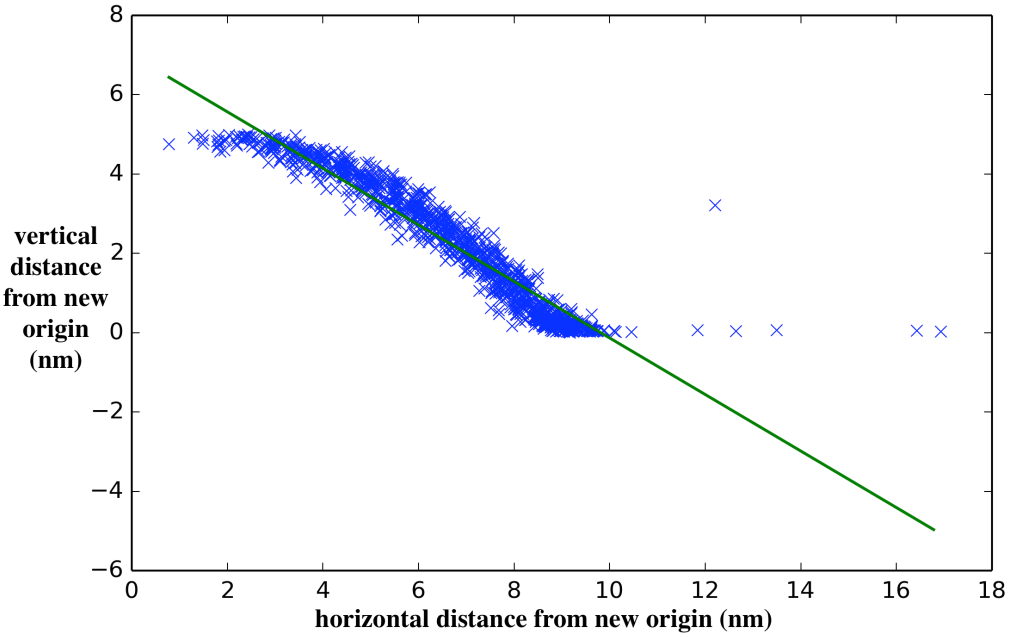

FIGURE 3.34: The coordinates of water molecules at 250ps projected onto one dimension with the linear regression line shown in green.

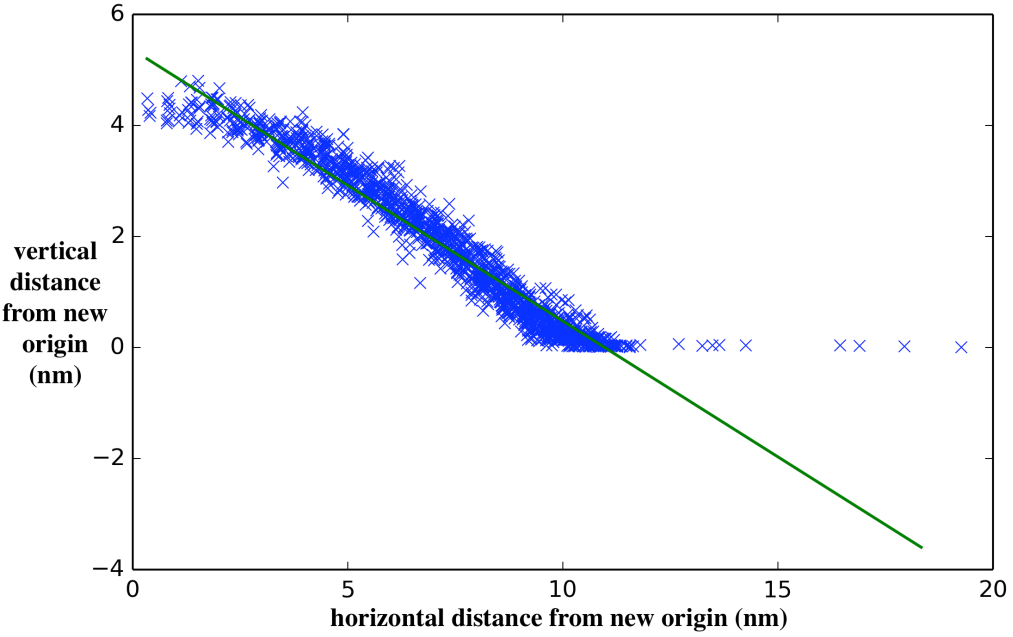

FIGURE 3.35: The coordinates of water molecules at 500ps projected onto one dimension with the linear regression line shown in green.

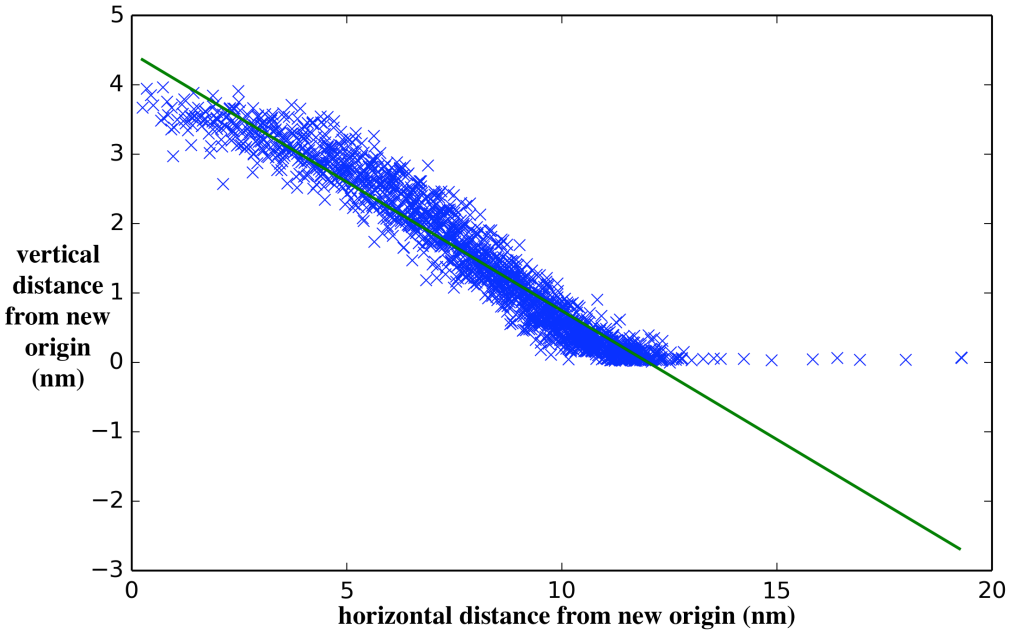

FIGURE 3.36: The coordinates of water molecules at 750ps projected onto one dimension with the linear regression line shown in green.

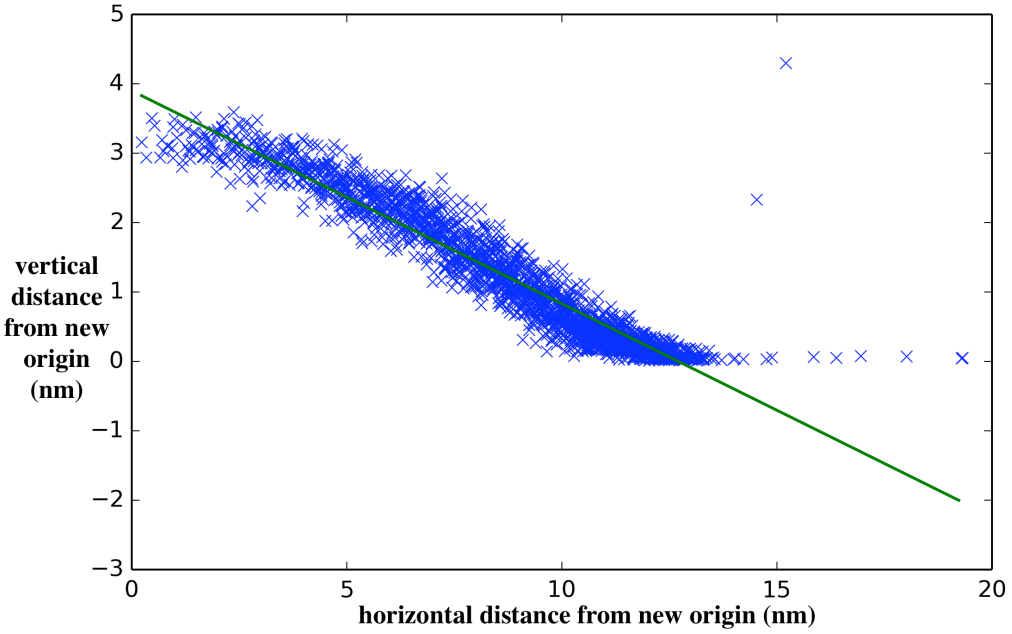

FIGURE 3.37: The coordinates of water molecules at 1000ps projected onto one dimension with the linear regression line shown in green.

353K Results

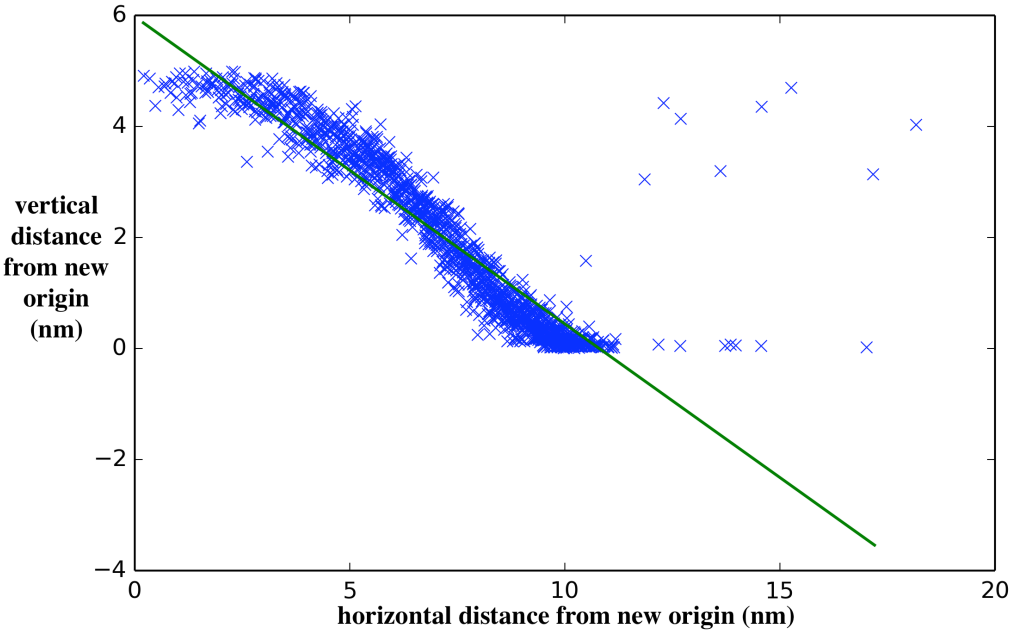

FIGURE 3.38: The coordinates of water molecules at 250ps projected onto one dimension with the linear regression line shown in green.

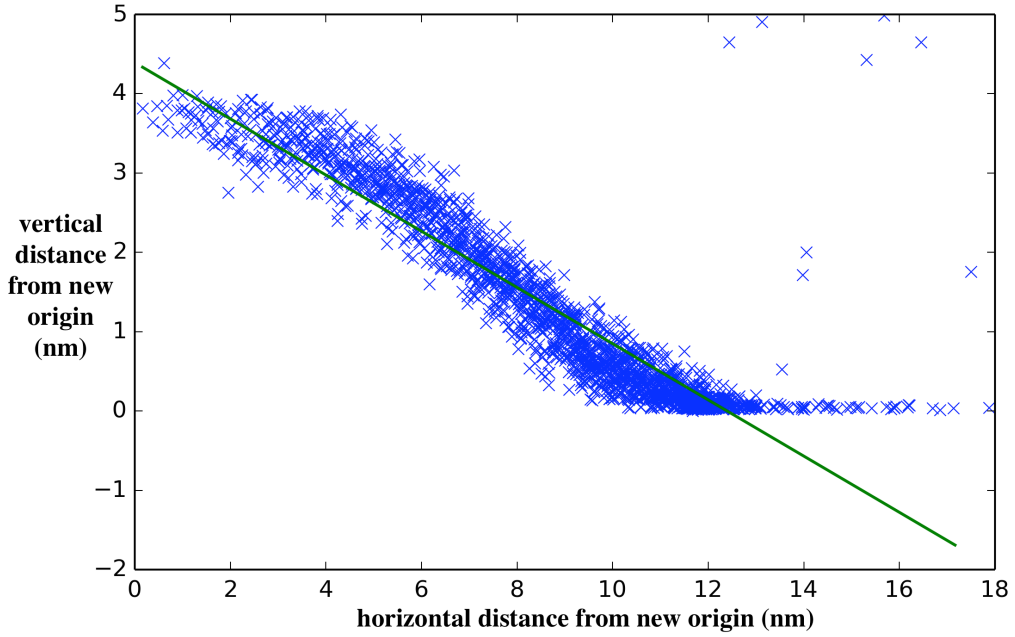

FIGURE 3.39: The coordinates of water molecules at 500ps projected onto one dimension with the linear regression line shown in green.

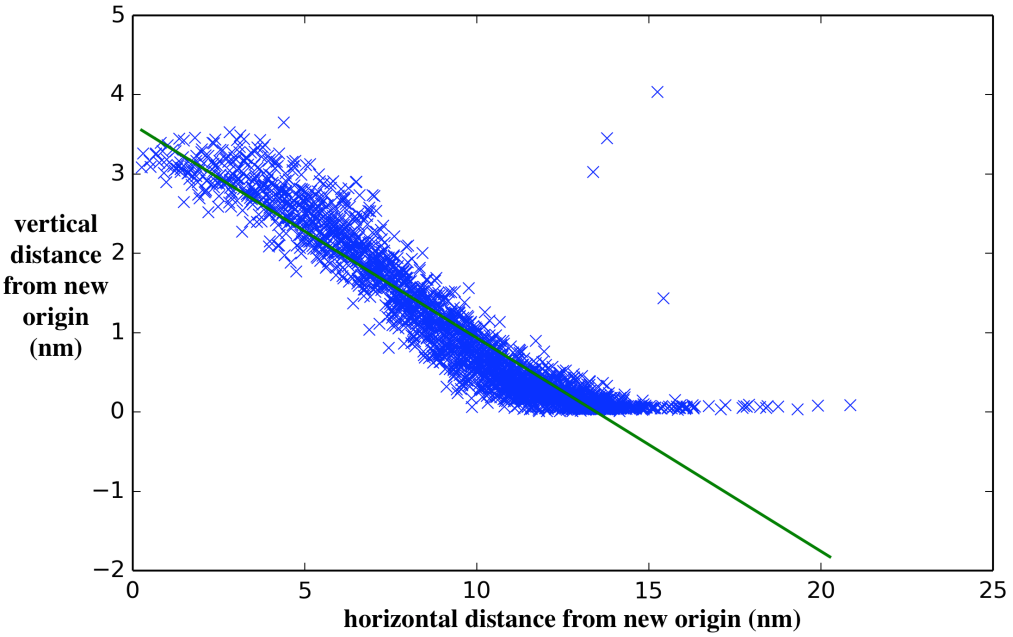

FIGURE 3.40: The coordinates of water molecules at 750ps projected onto one dimension with the linear regression line shown in green.

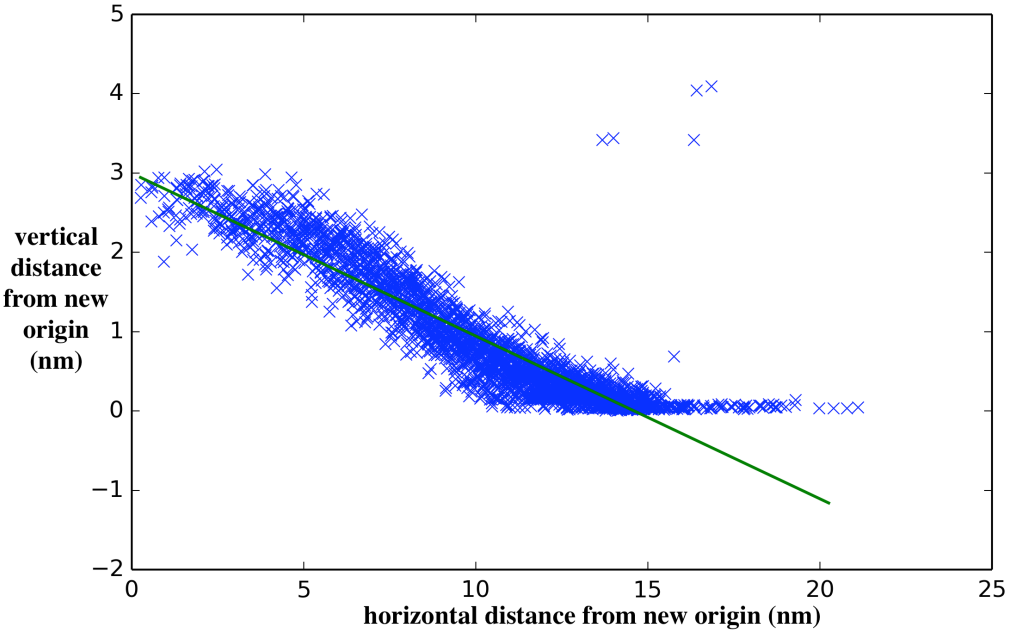

FIGURE 3.41: The coordinates of water molecules at 1000ps projected onto one dimension with the linear regression line shown in green.

Contact Angle of the Calcite/Water System (298K)		
Time (ps)	**Manual Measurement**	**Script Measurement**
0	$90 \pm 0.5°$	42.10°
250	$43.25 \pm 0.5°$	35.48°
500	$30.75 \pm 0.5°$	26.05°
750	$26 \pm 0.5°$	20.36°
1000	$18.375 \pm 0.5°$	17.06°

TABLE 3.4: The results for the contact angle of water on the calcite surface at 298K measured manually and using the designed computational script.

Contact Angle of the Calcite/Water System (353K)		
Time (ps)	**Manual Measurement**	**Script Measurement**
0	$90 \pm 0.5°$	42.10°
250	$36.875 \pm 0.5°$	28.96°
500	$23.125 \pm 0.5°$	19.52°
750	$16.125 \pm 0.5°$	15.05°
1000	$0 \pm 0.5°$[1]	11.60°

TABLE 3.5: The results for the contact angle of water on the calcite surface at 353K measured manually and using the designed computational script.

As shown in Tables 3.4 and 3.5 the contact angle script produces a result that is perenially lower than the contact angle recorded from manual measurement. This is because the script uses a linear regression method. This means that a *line of best fit* is plotted through n points in the graph. Simple visual assessment of Figure 3.32 and Figures 3.34 - 3.40 demonstrate why the script gives a value less than that of manual measurement. A person will measure the angle from the point of contact with the surface along the extremes (See Figure 3.42) For droplet simulations in MD the spreading is almost invariably non-uniform. This means that instantly a line of best fit will not reflect the *visual* contact angle. However, one could also argue that the visual contact angle is less realistic as the human eye will be unable to see the indentations in a droplet using visual analysis of a sectional view (see Figure 3.43).

[1]The water has reached the edge of the simulation box and, while there may still be a slight dome, the contact angle is 0° due to the occurence of complete wetting.

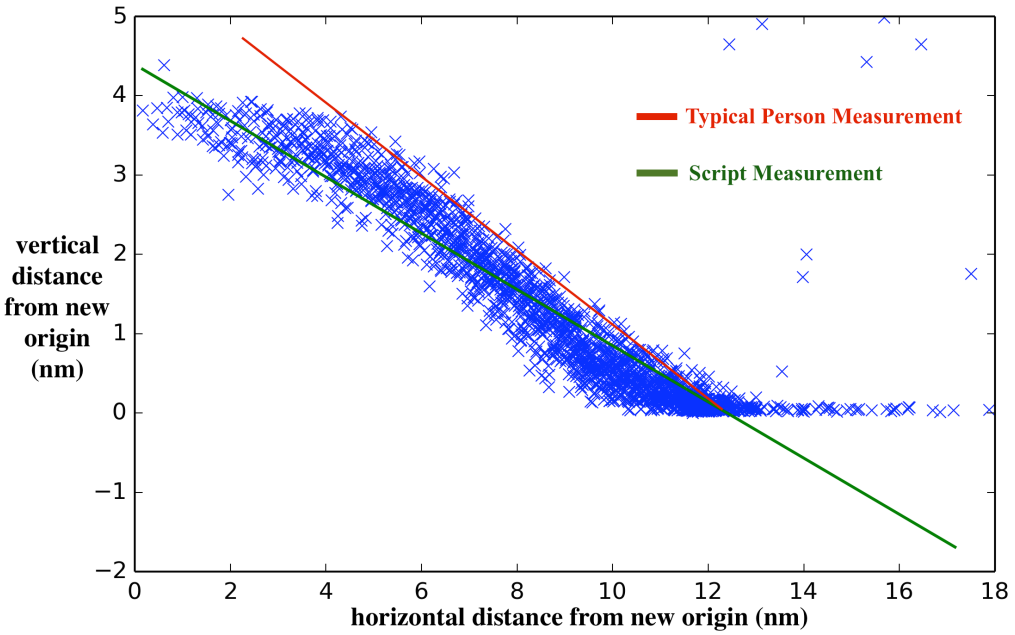

FIGURE 3.42: A schematic of the difference between the linear regression and what a person would measure contact angle from visually.

There is also typically a plateau region at the highest points in any droplet. The linear regression will therefore have a lesser gradient (see Figure 3.41) and therefore result in a lower contact angle than a person manually measuring it with a protractor.

A combination of both the aforementioned reasons is why the manual measurement of contact angle is typically higher than the result produced by the script.

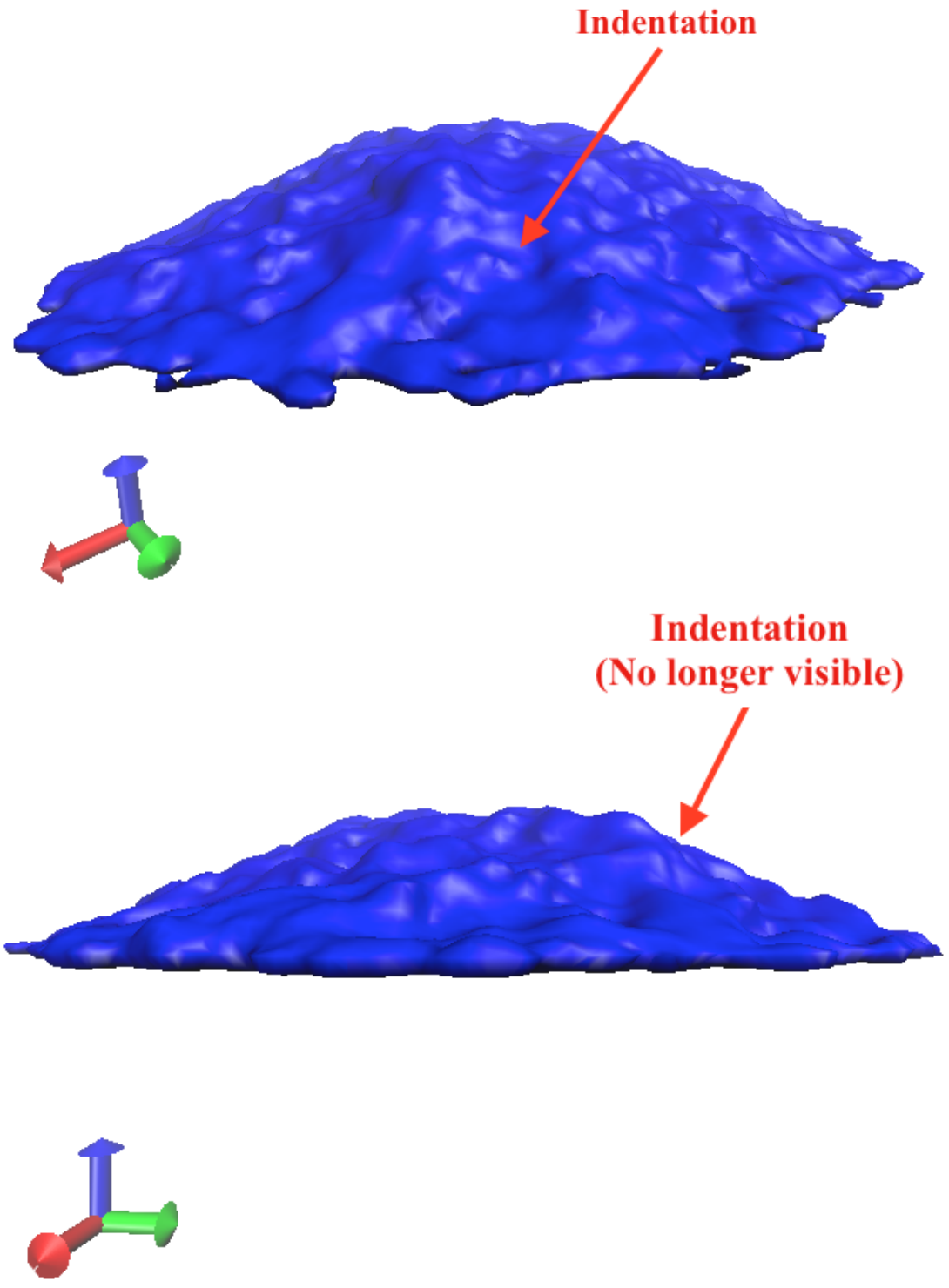

FIGURE 3.43: A schematic of why a visual measurement of contact angle from a sectional view may be unreliable for non-uniform spreading.

Chapter 4

Discussion

> *I think that in the discussion of natural problems we ought to begin not with the Scriptures, but with experiments, and demonstrations.*
>
> **Galileo Galilei**

This chapter compares the various results generated in this work, both with each other and experimental results. This will allow conclusions to be reached about the results, and therefore the accuracy of the methods undertaken.

4.1 Partial Density Distribution

On examining of Figure 3.4 and Table 3.2 it is apparent that upon simulation there is a marked increase in density distribution of water at the interface with calcite. For the simulations carried out with the temperature heated by the thermostat at 353K, the density distribution value is lower for each of the first two distinct peaks but higher for the third. As mentioned previously the distance between each of these three distinct peaks is rougly equivalent to the distance between the centre of one hydrogen atom to the oxygen atom in the TIP3P water model. Examination of the RDF graphs in Figures 3.5 - 3.8 show that it is most probable for oxygen atoms to be found 0.238nm from the calcium ion, with a sharp peak of significant magnitude. Therefore, it can be reasonably assumed that, despite the three peaks in the partial density distributions, a densely packed monolayer of water molecules forms between the water and the calcite, driven by the electrostatic attraction between oxygen and calcium. This is also the case with the simulations of domed water (See Figure 3.12 and Table 3.3). Again the density distribution value is lower for the first two peaks at the higher temperature, but higher for the third.

Examination of the systems composed of calcite, water and dodecane (See Figures 3.16, 3.17, 3.18, 3.22, 3.23 and 3.24) show that the addition of dodecane decreases the magnitudes of each density distribution of water at the calcite/water interface. The water spreading occurs less quickly in the systems with added dodecane when compared with those without.

4.2 Interfacial Tension

The analysis performed in this study resulted in a value of 50.05 mN/m for the interfacial tension between dodecane and water. This corresponds well to other studies of this property. Zeppieri et al. [62] found this value to be 52.55 mN/m using the oil-drop method. Goebel et al. [63] used the ring method an yielded a result of 53.7 mN/m. Finally Xiao et al. [64] used the same methods as those discussed in this work to produce a result of 57.23 mN/m. In conclusion, the methods used in this study produce results comparable to experiments, provided that the simuations are long enough to

alleviate statistical anomalies produced by the substantial fluctuations associated with pressure-related properties.

4.3 Adsorption and Free Energy

The PMF analysis carried out in this study yielded a result of -44 kJ mol^{-1} for water at the (1,0,4) calcite interface. The analysis from the RDF produced a results of -33.4 kJ mol^{-1} and -39.406 kJ mol^{-1} for 298K and 353K simulations respectively.

Several studies carried out in recent years have been in agreement with this result. Calirometer analysis carried out by Forbes et al. [65] produced an adsorption energy per molecule of -42.29 kJ mol^{-1} for water at the (1,0,4) interface. Van Cuong et al. [66] carried out MD studies and found an adsorption energy per molecule of -30 kJ mol^{-1}. Bridgeman and Skipper [26] performed Monte Carlo simulations that resulted in a calculation of -37.8 kJ mol^{-1}. Okhrimenko et al. [67] performed both DFT andMD studies yielding results of -58 kJ mol^{-1} and -65 kJ mol^{-1} respectively. Cooper and de Leeuw [68] performed MD yielding a result of -54 kJ mol^{-1}. Wright et al. [69] performed classical calculations and found a water adsorption energy of -53.9 kJ mol^{-1}. Rahaman et al. [70] performed Molecular Dynamics situations and found, using the exact method in this thesis, the water adsorption at the perfect $\{10\bar{1}4\}$ calcite surface to be -44.3504 kJ mol^{-1}. The study by Rahaman et al. differed from that discussed in this thesis because they used a polarisable water model, but produced comparable results. All of these afformentioned results are relatively consistent with the results found in this study. However, there is another school of thought within the scientific community. The results found by other groups differ from those above by a factor of 2. Molecular Dynamics simulations performed by Lardge, Kerisit, de Leeuw and Parker [60, 71–73] yielded results of -92.3 kJ mol^{-1}, -88 kJ mol^{-1} and -79.1 kJ mol^{-1}. These differed greatly from those found in the afformentioned studies.

On further reading of the literature it was suggested that the result for adsorption energy depended greatly on the result for $Ca - O_{water}$ distances for computational studies.

Dependancy of result on $Ca - O_{water}$ Distance			
First Author	**Type of Study**	**Result** (kJ mol^{-1})	$Ca - O_{water}$ ($\AA$)
Van Cuong	MD	-30	2.75
Bridgeman & Skipper	Monte Carlo	-37.8	2.85
Wright	Classical	-53.9	2.55
de Leeuw and Parker	MD	-79.1	2.4
Kerisit	MD	-88	2.26 - 2.51
Lardge	MD	-92.3	2.37
Rahaman	MD	-44.3504	2.2 $\pm$ 0.1
O'Connor	MD	-44	2.38

TABLE 4.1: The results for the partial density distribution calculations of the calcite-water flat configuration.

As shown in Table 4.1 there is, to a certain extent, a pattern between the $Ca - O_{water}$ distance and the adsorption energy. However the results presented in this thesis and those of Rahaman et al. seem to break free of this trend. The main differences between the two groups of molecular dynamics studies are twofold, one: various forcefields are used, all of which produce differing results and two: the analysis methods used to produce the results differ greatly.

For example, the work of Rahaman alongside the results presented in this thesis were obtained using the *potential of mean force* method whilst Lardge, de Leeuw, Parker and Kerisit use theoretical methods, most of which are a variation of Equation 1.12.

Rahaman investigated this further and used a theoretical method to produce an adsorption energy using his results. He found that using his trajectory and energies and inserting them into Equation 1.12 resulted in an adsorption energy of -89.1 kJ mol^{-1}. This coincides with the results of the aforementioned studies. He concluded that the differences in the results were due to the potential and the forcefield.

This may be true as the partial charges for Ca and O_{water} in the work in this thesis were 1.668 and -0.834 respectively. These are lower in magnitude than those used in the work of Kerisit [71]. The partial charges for Ca and O_{water} in that work were 2 and -1.250 respectively.

It is easy to conclude that the work in this study is more accurate and therefore a better

methodology because the results are in agreement with with experimental results. However it may just be a *happy accident*, as many Gromacs experts and developers, including Mark Abraham, expressed scepticism as to whether or not the OPLS-AA forcefield was parameterised to produce accurate values for adsorption energy. Therefore further work is certainly needed.

4.4 Droplet System

As demonstrated in Section 3.5 water will displace dodecane at the calcite interface and eventually fully wet the surface. This proves unequivocally that the $\{10\bar{1}4\}$ surface of calcite is strongly water-wet. This has been demonstrated in other studies [40, 74] and the Molecular Dynamics work in this study reflects this behaviour, and these results. However in reality no calcite reservoir will be a perfectly flat crystal with no fissures. Additionally crude oil is a very complex liquid made up of many components. Therefore most reservoirs will have areas which exhibit some mixed-wet characteristics.

4.5 Contact Angles

A new method was developed to measure the contact angle of water on the calcite surface directly from Molecular Dynamics coordinate files. It proved to be accurate for uniformly spreading droplets and a good alternative to the traditional, more simple, use of a protractor. However it is by no means flawless and does require further work. This is because the method does reshape the droplet to an extent, resulting in an unrealistic contact angle, even for a uniformly spreading droplet. It is the opinion of the author, which is in agreement the majority of researchers in the field, that use of snapshots and an angle measure is the most effective way of measuring contact angle.

4.6 Optimum Configuration for EOR

The most efficient configuration for oil recovery varies depending on the situation. Examination of sections 3.3 and 3.4 indicate that at the higher temperature spreading occurs more quickly, however it appears less uniform. This means that in practice *fingering* may occur. It is apparent from section 3.5 that as long as the water is in close proximity to the calcite surface it will eventually fully wet it, displacing the dodecane. However for optimum spreading it's probably best that the water is injected directly onto the calcite surface.

The future work aimed at optimising Enhanced Oil Recovery should investigate the addition of surfactants to the system. It would be useful to investigate whether or not Molecular Dynamics simulations accurately replicate the lowering of interfacial tension.

FIGURE 4.1: An example of stable and unstable water displacement, showing *fingering*.

This will allow us to investigate mixed liquid *washing* alongside the water driven displacement investigated in this thesis.

Chapter 5

Conclusions

And the end of all our exploring
Will be to arrive where we started
And know the place for the first time.

T.S. Eliot

This chapter concludes the work undertaken in this study and underlines the main ideas the reader should take from it.

The work in this thesis has investigated the interfacial properties and interactions between water, dodecane and the $\{10\bar{1}4\}$ calcite surface through the use of Molecular Dynamics simulations. The motive was to investigate the effectiveness of employing Molecular Dynamics for these properties and decipher whether or not it could be used as a useful tool for improving Enhanced Oil Recovery.

The density distribution of water increased significantly at the surface of calcite indicating adhesion at the interface between water and calcite. This meant that water can displace dodecane at a calcite wall and is a potential injection fluid for successful EOR.

The result for the interfacial tension between water and dodecane was comparable to other experimental and computational studies. This showed that Molecular Dynamics simulations are appropriate for an efficient and effective prediction of alkane/water interfacial tension. However the simulations should be long enough to alleviate the significant fluctuations associated with pressure-related properties. Accurate prediction of IFT by Molecular Dynamics means that it can be a useful tool for future EOR investigations, particularly those that may use surfactants.

The adsorption energy between water and calcite was found to be comparable to several studies, however there is a degree of disagreement among different portions of the scientific community as to how accurate this result is. Therefore, further research should be carried out in this area.

Contact angle analysis showed that the addition of dodecane does affect the efficiency of water spreading on the calcite surface. It was also shown that the perfect $\{10\bar{1}4\}$ calcite surface is strongly water-wet. A new technique was also developed for quick measurement of the contact angle of a fluid on a surface in a GROMACS coordinate file. This means that in future EOR research, particularly those using surfactants, there is a quick method for measuring contact angles from simulations.

The ideal configuration for Enhanced Oil Recovery will vary depending on exactly how the hydrocarbons should be displaced. This study has provided a good discussion of the advantages and disadvantages of several configurations in the previous chapter.

In conclusion, the work in this thesis has provided a good first step into Molecular Dynamics studies of water/alkane systems in carbonate reservoirs. Future work should include the studying of mixed-alkane fluid interactions with water at an imperfect calcite

surface. The following work would replicate the systems found in nature more accurately. In the future consideration should also be made as to which forcefield should be used. This could include the use of the OPLS-AA forcefield modified by Siu et al. [75] to produce what they describe as *more refined* behaviour with systems containing long chain hydrocarbons. Overall Molecular Dynamics is a useful tool in the investigation of Enhanced Oil Recovery.

Appendix A

Water Testing

A.1 Objective

To investigate the properties of three water models and determine whether or not they differ depending on which version of the Gromacs Molecular Dynamics (MD) package is used to perform the simulation.

A.1.1 Methodology

All simulations were performed using the GROMACS[45, 46, 76–78] Molecular Dynamics (MD) package.
The simulations were performed on the following GROMACS versions:
3.3.4
3.3.4 (double-precision)
4.5.5
4.5.5 (double-precision)
4.6.0
4.6.3
4.6.3 (double-precision)
5.0-beta1
5.0-beta1 (double-precision)
The water models tested were TIP3P[54], TIP4P[54], TIP5P[79] and the polarizeable SW10e[80].

A.1.2 Simulation Overview

All simulations were assembled using the Gromacs version which was being tested at the time. A cubic box was generated with axis dimensions of 5nm. The box was then filled with 4142 mols of the respective water model. The system was then energy minimised and equilibrated before being simulated for 8ns in an NPT environment. The simulations were performed at 298K using the v-rescale[47] thermostat where possible and the Berendsen[81] thermostat for the earlier versions, *where the former was not featured in the package*. The Berendsen barostat was used for pressure coupling.

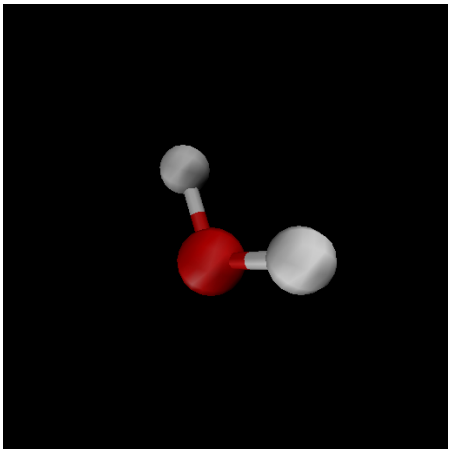

FIGURE A.1: 3-point

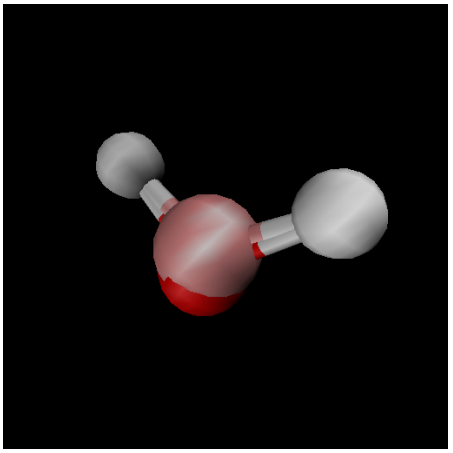

FIGURE A.2: 4-point

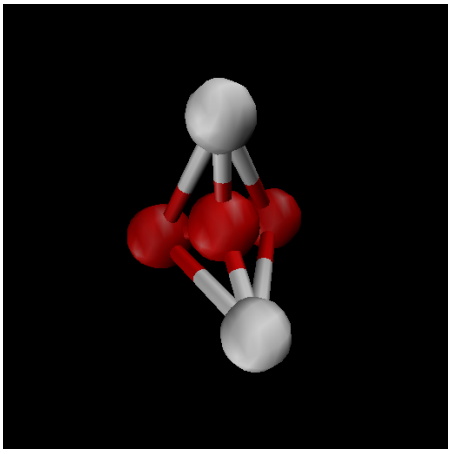

FIGURE A.3: 5-point

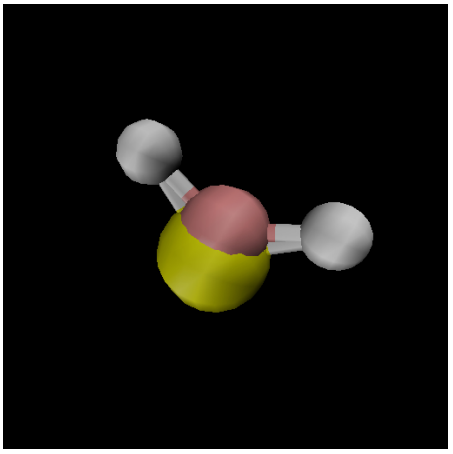

FIGURE A.4: SW10e

FIGURE A.5: Different water models

A.2 Results

GROMACS Version	**TIP3P Average Density (kg/m^3)**	**TIP4P Average Density (kg/m^3)**	**TIP5P Average Density (kg/m^3)**
3.3.4	975.37	984.013	973.195
3.3.4 double-precision	975.43	984.085	973.124
4.5.5	967.8222379	984.174	972.974
4.5.5 double-precision	967.8424245	983.986	973.093
4.6.0	975.4314389	984.115	973.842
4.6.3	975.4054165	984.047	973.883
4.6.3 double-precision	975.4199663	984.082	973.951
5.0-beta1	975.372	983.975	973.791
5.0-beta1 double-precision	975.383	984.047	973.824

The SW10e was only tested using versions 5.0-beta1 and 5.0-beta1 double-precision. The resultant average densities were 984.998 kg/m^3 and 984.222 kg/m^3 respectively.

A.3 Discussion

The density of water found by all Gromacs versions is consistent, with the exception of simulations performed in a box with the TIP3P[54] water model using version 4.5.5 and its *double-precision* counterpart. However these results were obtained with *ewald_geometry = 3dc*. After this was changed to *ewald_geometry = 3d* the results for 4.5.5 and 4.5.5 double-precision were 975.70256 and 975.34622 kg/m^3 respectively.

A.4 Conclusion

ewald_geometry = 3dc should only be used for simulations without periodicity in the z direction. Otherwise you might get serious artifacts which will affect the overall results of the simulation.

Appendix B

GROMACS Files

This chapter contains the necessary files to replicate the simulations described previously using the GROMACS simulation package.

B.1 Essential Files

Dodecane Molecule

```
DODEC
38
    1AEG     C2    1   1.766   5.553   6.258
    1AEG     H4    2   1.808   5.593   6.351
    1AEG     H5    3   1.659   5.536   6.276
    1AEG     C1    4   1.782   5.657   6.147
    1AEG     H1    5   1.888   5.676   6.123
    1AEG     H2    6   1.732   5.625   6.054
    1AEG     H3    7   1.738   5.753   6.177
    1AEG     C3    8   1.834   5.418   6.228
    1AEG     H6    9   1.808   5.386   6.126
    1AEG     H7   10   1.943   5.433   6.229
    1AEG     C4   11   1.795   5.306   6.326
    1AEG     H8   12   1.799   5.345   6.429
    1AEG     H9   13   1.690   5.279   6.308
    1AEG     C5   14   1.885   5.180   6.316
    1AEG    H10   15   1.899   5.153   6.210
    1AEG    H11   16   1.985   5.206   6.353
    1AEG     C6   17   1.833   5.058   6.393
    1AEG    H12   18   1.916   4.988   6.406
    1AEG    H13   19   1.802   5.087   6.494
    1AEG     C7   20   1.717   4.983   6.323
    1AEG    H14   21   1.628   5.048   6.319
    1AEG    H15   22   1.745   4.964   6.219
    1AEG     C8   23   1.680   4.849   6.389
    1AEG    H16   24   1.771   4.787   6.394
    1AEG    H17   25   1.650   4.865   6.493
    1AEG     C9   26   1.572   4.768   6.314
    1AEG    H18   27   1.603   4.755   6.209
    1AEG    H19   28   1.567   4.666   6.355
    1AEG    C10   29   1.430   4.828   6.316
    1AEG    H20   30   1.432   4.931   6.278
    1AEG    H21   31   1.367   4.772   6.244
    1AEG    C11   32   1.361   4.824   6.453
    1AEG    H22   33   1.352   4.719   6.486
    1AEG    H23   34   1.423   4.874   6.528
    1AEG    C12   35   1.222   4.888   6.454
    1AEG    H24   36   1.226   4.994   6.426
    1AEG    H25   37   1.155   4.838   6.383
    1AEG    H26   38   1.176   4.882   6.554
   7.40778   7.40778   7.40778
```

FIGURE B.1: The coordinate file of a single dodecane molecule.

Topology File

```
;       This is your topology file
;       Calcite/Water/Dodecane
;

#include "arapro.itp"

#include "LJ.itp"

#include "CA_CAP.itp"

#include "CO3_COP.itp"

#include "tip3p.itp"

#include "DODEC.itp"

[ system ]
; Name
calcium carbonate-water-protein in water

[ molecules ]
; Compound        #mols
;1 set
Srl1 18904
CAT  8640
CO3T 8640
CA   8640
CO3  8640
CA   8640
CO3  8640
CA   8640
CO3  8640
SOL  23891
AEG  28190
```

FIGURE B.2: The topology file for the calcite/water/dodecane system.

Files within the Topology

arapro.itp

```
;       arapro.itp
;       This is your topology file for aragonite-water-protein atomic interaction

#define _FF_OPLS
#define _FF_OPLSAA

[ defaults ]
; nbfunc        comb-rule       gen-pairs       fudgeLJ    fudgeQQ     N
     1          1                  no         0.5        0.5      12

#include "ffoplsaanb_c6c12.itp"

[ atomtypes ]
;name                      mass     charge      ptype        C6           C12
; Added by shijun for aragonite and aragonite-water-protein
Srl1          120.1100      0.000       A    0.0000000e+00     9.6145100e-08
Srr1          120.1100      0.000       A   -2.2000000e-01     1.8698000e+00
OW             9.95140     -0.834       A    2.4897080e-03     2.4350980e-06
HW1            4.03200      0.417       A    0.0000000e+00     0.0000000e+00
HW2            4.03200      0.417       A    0.0000000e+00     0.0000000e+00
CA     20     40.08000      1.668       A    1.6068353e-03     3.2116959e-07
CCO3   6      12.01100      0.999       A    4.6145469e-03     1.4363352e-05
OCO3   8      15.99940     -0.889       A    2.0264632e-03     1.7749711e-06
C2     6        12.011    0.10800       A    2.0305040e-03     3.7320000e-06
H4     1         1.008    0.00000       A    1.2257800e-04     2.9000000e-08
H5     1         1.008    0.00000       A    1.2257800e-04     2.9000000e-08
C1     6        12.011   -0.30300       A    2.0305040e-03     3.7320000e-06
H1     1         1.008    0.06500       A    1.2257800e-04     2.9000000e-08
H2     1         1.008    0.06500       A    1.2257800e-04     2.9000000e-08
H3     1         1.008    0.06500       A    1.2257800e-04     2.9000000e-08
C3     6        12.011   -0.00200       A    2.0305040e-03     3.7320000e-06
H6     1         1.008    0.00100       A    1.2257800e-04     2.9000000e-08
H7     1         1.008    0.00100       A    1.2257800e-04     2.9000000e-08
C4     6        12.011   -0.00200       A    2.0305040e-03     3.7320000e-06
H8     1         1.008    0.00100       A    1.2257800e-04     2.9000000e-08
H9     1         1.008    0.00100       A    1.2257800e-04     2.9000000e-08
C5     6        12.011   -0.00200       A    2.0305040e-03     3.7320000e-06
H10    1         1.008    0.00100       A    1.2257800e-04     2.9000000e-08
H11    1         1.008    0.00100       A    1.2257800e-04     2.9000000e-08
C6     6        12.011   -0.00200       A    2.0305040e-03     3.7320000e-06
H12    1         1.008    0.00100       A    1.2257800e-04     2.9000000e-08
H13    1         1.008    0.00100       A    1.2257800e-04     2.9000000e-08
C7     6        12.011   -0.00200       A    2.0305040e-03     3.7320000e-06
H14    1         1.008    0.00100       A    1.2257800e-04     2.9000000e-08
H15    1         1.008    0.00100       A    1.2257800e-04     2.9000000e-08
C8     6        12.011   -0.00200       A    2.0305040e-03     3.7320000e-06
H16    1         1.008    0.00100       A    1.2257800e-04     2.9000000e-08
H17    1         1.008    0.00100       A    1.2257800e-04     2.9000000e-08
C9     6        12.011   -0.00200       A    2.0305040e-03     3.7320000e-06
H18    1         1.008    0.00100       A    1.2257800e-04     2.9000000e-08
H19    1         1.008    0.00100       A    1.2257800e-04     2.9000000e-08
C10    6        12.011   -0.00200       A    2.0305040e-03     3.7320000e-06
H20    1         1.008    0.00100       A    1.2257800e-04     2.9000000e-08
H21    1         1.008    0.00100       A    1.2257800e-04     2.9000000e-08
C11    6        12.011    0.10800       A    2.0305040e-03     3.7320000e-06
H22    1         1.008    0.00000       A    1.2257800e-04     2.9000000e-08
H23    1         1.008    0.00000       A    1.2257800e-04     2.9000000e-08
C12    6        12.011   -0.30300       A    2.0305040e-03     3.7320000e-06
H24    1         1.008    0.06500       A    1.2257800e-04     2.9000000e-08
H25    1         1.008    0.06500       A    1.2257800e-04     2.9000000e-08
H26    1         1.008    0.06500       A    1.2257800e-04     2.9000000e-08
```

```
[ nonbond_params ]
;   i     j   f.tp     C6    C12
;parameters for aragonite
 Srl1  Srl1       1      0.0000000e+00          0.0000000e+00
 Srl1    OW       1      0.0000000e+00          4.0960000e-08
 Srl1   HW1       1       0.0000000e+00          4.0960000e-08
 Srl1   HW2       1       0.0000000e+00          4.0960000e-08
 Srl1    C2       1       0.0000000e+00          4.0960000e-08
 Srl1    C1       1       0.0000000e+00          4.0960000e-08
 Srl1    C3       1       0.0000000e+00          4.0960000e-08
 Srl1    C4       1       0.0000000e+00          4.0960000e-08
 Srl1    C5       1       0.0000000e+00          4.0960000e-08
 Srl1    C6       1       0.0000000e+00          4.0960000e-08
 Srl1    C7       1       0.0000000e+00          4.0960000e-08
 Srl1    C8       1       0.0000000e+00          4.0960000e-08
 Srl1    C9       1       0.0000000e+00          4.0960000e-08
 Srl1   C10       1       0.0000000e+00          4.0960000e-08
 Srl1   C11       1       0.0000000e+00          4.0960000e-08
 Srl1   C12       1       0.0000000e+00          4.0960000e-08
 Srl1    H1       1       0.0000000e+00          4.0960000e-08
 Srl1    H2       1       0.0000000e+00          4.0960000e-08
 Srl1    H3       1       0.0000000e+00          4.0960000e-08
 Srl1    H4       1       0.0000000e+00          4.0960000e-08
 Srl1    H5       1       0.0000000e+00          4.0960000e-08
 Srl1    H6       1       0.0000000e+00          4.0960000e-08
 Srl1    H7       1       0.0000000e+00          4.0960000e-08
 Srl1    H8       1       0.0000000e+00          4.0960000e-08
 Srl1    H9       1       0.0000000e+00          4.0960000e-08
 Srl1   H10       1       0.0000000e+00          4.0960000e-08
 Srl1   H11       1       0.0000000e+00          4.0960000e-08
 Srl1   H12       1       0.0000000e+00          4.0960000e-08
 Srl1   H13       1       0.0000000e+00          4.0960000e-08
 Srl1   H14       1       0.0000000e+00          4.0960000e-08
 Srl1   H15       1       0.0000000e+00          4.0960000e-08
 Srl1   H16       1       0.0000000e+00          4.0960000e-08
 Srl1   H17       1       0.0000000e+00          4.0960000e-08
 Srl1   H18       1       0.0000000e+00          4.0960000e-08
 Srl1   H19       1       0.0000000e+00          4.0960000e-08
 Srl1   H20       1       0.0000000e+00          4.0960000e-08
 Srl1   H21       1       0.0000000e+00          4.0960000e-08
 Srl1   H22       1       0.0000000e+00          4.0960000e-08
 Srl1   H23       1       0.0000000e+00          4.0960000e-08
 Srl1   H24       1       0.0000000e+00          4.0960000e-08
 Srl1   H25       1       0.0000000e+00          4.0960000e-08
 Srl1   H26       1       0.0000000e+00          4.0960000e-08
```

```
 CA    CCO3       1      0.0000000e-00          3.5000000e-06 ; stable block
 CA    OCO3       1      0.0000000e-00          9.4903220e-07
 CCO3  CCO3       1      1.4330917e-02          4.6063820e-06
 CCO3  OCO3       1      3.0778715e-04          9.0406445e-10
 OCO3  OCO3       1      5.2101900e-05          5.9403113e-07
 CA    CCO3       1      0.0000000e-00          3.5000000e-06 ; stable block
 CA    OCO3       1      0.0000000e-00          9.4903220e-07
 CCO3  CCO3       1      1.4330917e-02          4.6063820e-06
 CCO3  OCO3       1      3.0778715e-04          9.0406445e-10
 OCO3  OCO3       1      5.2101900e-05          5.9403113e-07
 C2    C2         1      2.0305040e-03          3.7320000e-06
 H4    H4         1      1.2257800e-04          2.9000000e-08
 H5    H5         1      1.2257800e-04          2.9000000e-08
 C1    C1         1      2.0305040e-03          3.7320000e-06
 H1    H1         1      1.2257800e-04          2.9000000e-08
 H2    H2         1      1.2257800e-04          2.9000000e-08
 H3    H3         1      1.2257800e-04          2.9000000e-08
 C3    C3         1      2.0305040e-03          3.7320000e-06
 H6    H6         1      1.2257800e-04          2.9000000e-08
 H7    H7         1      1.2257800e-04          2.9000000e-08
 C4    C4         1      2.0305040e-03          3.7320000e-06
 H8    H8         1      1.2257800e-04          2.9000000e-08
 H9    H9         1      1.2257800e-04          2.9000000e-08
 C5    C5         1      2.0305040e-03          3.7320000e-06
 H10   H10        1      1.2257800e-04          2.9000000e-08
 H11   H11        1      1.2257800e-04          2.9000000e-08
 C6    C6         1      2.0305040e-03          3.7320000e-06
 H12   H12        1      1.2257800e-04          2.9000000e-08
 H13   H13        1      1.2257800e-04          2.9000000e-08
 C7    C7         1      2.0305040e-03          3.7320000e-06
 H14   H14        1      1.2257800e-04          2.9000000e-08
 H15   H15        1      1.2257800e-04          2.9000000e-08
 C8    C8         1      2.0305040e-03          3.7320000e-06
 H16   H16        1      1.2257800e-04          2.9000000e-08
 H17   H17        1      1.2257800e-04          2.9000000e-08
 C9    C9         1      2.0305040e-03          3.7320000e-06
 H18   H18        1      1.2257800e-04          2.9000000e-08
 H19   H19        1      1.2257800e-04          2.9000000e-08
 C10   C10        1      2.0305040e-03          3.7320000e-06
 H20   H20        1      1.2257800e-04          2.9000000e-08
 H21   H21        1      1.2257800e-04          2.9000000e-08
 C11   C11        1      2.0305040e-03          3.7320000e-06
 H22   H22        1      1.2257800e-04          2.9000000e-08
 H23   H23        1      1.2257800e-04          2.9000000e-08
 C12   C12        1      2.0305040e-03          3.7320000e-06
 H24   H24        1      1.2257800e-04          2.9000000e-08
 H25   H25        1      1.2257800e-04          2.9000000e-08
 H26   H26        1      1.2257800e-04          2.9000000e-08
;parameters for aragonite-water
 OCO3  opls_112   1    9.6485000e-07          7.9812392e-09

#include "ffoplsaabon.itp"
```

FIGURE B.3: The arapro.itp file

LJ.itp

```
;       This is your topology file for definition of the LJ

;#########################################LJ#################################################
;#############################################################################################

[ moleculetype ]
; Name            nrexcl
Srl1               3

[ atoms ]
;  nr  type    resnr   residu  atom    cgnr
 1   Srl1  1      Srl1   Srl1      1     0.000

; Include Position restraint file
[ position_restraints ]
; atom  type      fx      fy      fz
   1     1   100000   100000   100000
```

FIGURE B.4: The file defining the Lennard-Jones spheres.

CA_CAP.itp

```
;
;       This is your topology file for definition of the Calcium

;#########################################CA#################################################
;#############################################################################################

[ moleculetype ]
;  name    exclu
  CA   0

[ atoms ]
;  nr  type    resnr   residu  atom    cgnr
 1   CA    1        CA     CA      1     1.668

; Include Position restraint file
[ position_restraints ]
; atom  type      fx      fy      fz
   1     1    100    100    100

[ moleculetype ]
;  name    exclu
  CAT   0

[ atoms ]
;  nr  type    resnr   residu  atom    cgnr
 1   CA    1        CAT     CA      1     1.668

; Include Position restraint file
[ position_restraints ]
; atom  type      fx      fy      fz
   1     1    10000    10000    10000
```

FIGURE B.5: The file defining Calcium.

CO3_COP.itp

```
;
;       This is your topology file for definition of the Carbonate

;#############################################CO3#################################################
;#################################################################################################
[ moleculetype ]
; name  nrexcl
CO3  0

[ atoms ]
;   nr  type    resnr   residu  atom    cgnr  charge     mass
1     CCO3     1       CO3    C        1     0.999
2     OCO3     1       CO3    O1       1    -0.889
3     OCO3     1       CO3    O2       1    -0.889
4     OCO3     1       CO3    O3       1    -0.889

[ angles ]
;  ai    aj    ak     funct    theta0      k_theta
   2     1     3       1       120.0       1852
   2     1     4       1       120.0       1852
   3     1     4       1       120.0       1852


[ dihedrals ]
;  ai    aj    ak    al   funct       phi_s           k_phi            n
   2    1     3     4      1          180             28.9          2

; Include Position restraint file
[ position_restraints ]
; atom  type      fx      fy      fz
   1     1    100  100  100
   2     1    100  100  100
   3     1    100  100  100
   4     1    100  100  100

[ moleculetype ]
; name  nrexcl
CO3T  0

[ atoms ]
;   nr  type    resnr   residu  atom    cgnr  charge     mass
1     CCO3     1       CO3T    C        1     0.999
2     OCO3     1       CO3T    O1       1    -0.889
3     OCO3     1       CO3T    O2       1    -0.889
4     OCO3     1       CO3T    O3       1    -0.889

[ angles ]
;  ai    aj    ak     funct    theta0      k_theta
   2     1     3       1       120.0       1852
   2     1     4       1       120.0       1852
   3     1     4       1       120.0       1852


[ dihedrals ]
;  ai    aj    ak    al   funct       phi_s           k_phi            n
   2    1     3     4      1          180             28.9          2

; Include Position restraint file
[ position_restraints ]
; atom  type      fx      fy      fz
   1     1    10000  10000  10000
   2     1    10000  10000  10000
   3     1    10000  10000  10000
   4     1    10000  10000  10000
```

FIGURE B.6: The file defining Carbonate.

tip3p.itp

```
[ moleculetype ]
; molname   nrexcl
SOL     2

[ atoms ]
; id    at type res nr  residu name at name     cg nr   charge
#ifdef _FF_OPLS
1     opls_111  1       SOL              OW             1       -0.834
2     opls_112  1       SOL             HW1             1        0.417
3     opls_112  1       SOL             HW2             1        0.417
#endif
#ifdef _FF_CHARMM
1       OT      1       SOL              OW             1       -0.834
2       HT      1       SOL             HW1             1        0.417
3       HT      1       SOL             HW2             1        0.417
#endif
#ifdef _FF_GROMACS
1       OWT3    1       SOL              OW             1       -0.834
2       HW      1       SOL             HW1             1        0.417
3       HW      1       SOL             HW2             1        0.417
#endif
#ifdef _FF_GROMOS96
1       OWT3    1       SOL              OW             1       -0.834
2       HW      1       SOL             HW1             1        0.417
3       HW      1       SOL             HW2             1        0.417
#endif
#ifdef _FF_AMBER94
;   nr    type  resnr residue  atom   cgnr     charge       mass
     1  amber94_42   1  SOL      OW      1      -0.834   16.00000
     2  amber94_27   1  SOL     HW1      1       0.417    1.00800
     3  amber94_27   1  SOL     HW2      1       0.417    1.00800
#endif
#ifdef _FF_AMBER99
     1  amber99_42   1  SOL      OW      1      -0.834   16.00000
     2  amber99_27   1  SOL     HW1      1       0.417    1.00800
     3  amber99_27   1  SOL     HW2      1       0.417    1.00800
#endif

#ifdef FLEXIBLE
#ifdef _FF_AMBER
[ bonds ]
; i j   funct   length  force.c.
1   2   1   0.09572   462750.4 0.09572   462750.4
1   3   1   0.09572   462750.4 0.09572   462750.4

[ angles ]
; i j   k   funct   angle   force.c.
2   1   3   1   104.520    836.800  104.520    836.800
#else
[ bonds ]
; i j   funct   length  force.c.
1   2   1   0.09572 502416.0 0.09572    502416.0
1   3   1   0.09572 502416.0 0.09572    502416.0

[ angles ]
; i j   k   funct   angle   force.c.
2   1   3   1   104.52  628.02  104.52  628.02
#endif
#else
[ settles ]
; i j   funct   length
1   1   0.09572 0.15139

[ exclusions ]
1   2   3
2   1   3
3   1   2
#endif
```

FIGURE B.7: The file defining the water model.

DODEC.itp

```
;       This is your topology file for definition of the Dodecane

;#############################################CO3#################
#########################
;#####################################################################
#########################

[ moleculetype ]
; name  nrexcl
AEG     3

[ atoms ]
;   nr  type    resnr   residu  atom    cgnr  charge     mass
#ifdef _FF_OPLS
        1  opls_136   1   AEG      C2    1   0.10800     12.011
        2  opls_140   1   AEG      H4    1   0.00000     1.008
        3  opls_140   1   AEG      H5    1   0.00000     1.008
        4  opls_135   1   AEG      C1    2   -0.30300     12.011
        5  opls_140   1   AEG      H1    2   0.06500     1.008
        6  opls_140   1   AEG      H2    2   0.06500     1.008
        7  opls_140   1   AEG      H3    2   0.06500     1.008
        8  opls_136   1   AEG      C3    3   -0.00200     12.011
        9  opls_140   1   AEG      H6    3   0.00100     1.008
       10  opls_140   1   AEG      H7    3   0.00100     1.008
       11  opls_136   1   AEG      C4    4   -0.00200     12.011
       12  opls_140   1   AEG      H8    4   0.00100     1.008
       13  opls_140   1   AEG      H9    4   0.00100     1.008
       14  opls_136   1   AEG      C5    5   -0.00200     12.011
       15  opls_140   1   AEG      H10    5   0.00100     1.008
       16  opls_140   1   AEG      H11    5   0.00100     1.008
       17  opls_136   1   AEG      C6    6   -0.00200     12.011
       18  opls_140   1   AEG      H12    6   0.00100     1.008
       19  opls_140   1   AEG      H13    6   0.00100     1.008
       20  opls_136   1   AEG      C7    7   -0.00200     12.011
       21  opls_140   1   AEG      H14    7   0.00100     1.008
       22  opls_140   1   AEG      H15    7   0.00100     1.008
       23  opls_136   1   AEG      C8    8   -0.00200     12.011
       24  opls_140   1   AEG      H16    8   0.00100     1.008
       25  opls_140   1   AEG      H17    8   0.00100     1.008
       26  opls_136   1   AEG      C9    9   -0.00200     12.011
       27  opls_140   1   AEG      H18    9   0.00100     1.008
       28  opls_140   1   AEG      H19    9   0.00100     1.008
       29  opls_136   1   AEG      C10    10   -0.00200     12.011
       30  opls_140   1   AEG      H20    10   0.00100     1.008
       31  opls_140   1   AEG      H21    10   0.00100     1.008
       32  opls_136   1   AEG      C11    11   0.10800     12.011
       33  opls_140   1   AEG      H22    11   0.00000     1.008
       34  opls_140   1   AEG      H23    11   0.00000     1.008
       35  opls_135   1   AEG      C12    12   -0.30300     12.011
       36  opls_140   1   AEG      H24    12   0.06500     1.008
       37  opls_140   1   AEG      H25    12   0.06500     1.008
       38  opls_140   1   AEG      H26    12   0.06500     1.008
#endif
```

```
[ bonds ]
; i      j  funct  length   force.c.
1        2   1    0.110  284512.0  0.110  284512.0
1        3   1    0.110  284512.0  0.110  284512.0
1        4   1    0.153  224262.4  0.153  224262.4
1        8   1    0.153  224262.4  0.153  224262.4
4        5   1    0.110  284512.0  0.110  284512.0
4        6   1    0.110  284512.0  0.110  284512.0
4        7   1    0.110  284512.0  0.110  284512.0
8        9   1    0.110  284512.0  0.110  284512.0
8        10  1    0.110  284512.0  0.110  284512.0
8        11  1    0.153  224262.4  0.153  224262.4
11       12  1    0.110  284512.0  0.110  284512.0
11       13  1    0.110  284512.0  0.110  284512.0
11       14  1    0.154  224262.4  0.154  224262.4
14       15  1    0.110  284512.0  0.110  284512.0
14       16  1    0.110  284512.0  0.110  284512.0
14       17  1    0.153  224262.4  0.153  224262.4
17       18  1    0.110  284512.0  0.110  284512.0
17       19  1    0.110  284512.0  0.110  284512.0
17       20  1    0.154  224262.4  0.154  224262.4
20       21  1    0.110  284512.0  0.110  284512.0
20       22  1    0.110  284512.0  0.110  284512.0
20       23  1    0.153  224262.4  0.153  224262.4
23       24  1    0.110  284512.0  0.110  284512.0
23       25  1    0.110  284512.0  0.110  284512.0
23       26  1    0.154  224262.4  0.154  224262.4
26       27  1    0.110  284512.0  0.110  284512.0
26       28  1    0.110  284512.0  0.110  284512.0
26       29  1    0.153  224262.4  0.153  224262.4
29       30  1    0.110  284512.0  0.110  284512.0
29       31  1    0.110  284512.0  0.110  284512.0
29       32  1    0.153  224262.4  0.153  224262.4
32       33  1    0.110  284512.0  0.110  284512.0
32       34  1    0.110  284512.0  0.110  284512.0
32       35  1    0.153  224262.4  0.153  224262.4
35       36  1    0.110  284512.0  0.110  284512.0
35       37  1    0.110  284512.0  0.110  284512.0
35       38  1    0.110  284512.0  0.110  284512.0

[ angles ]
;  ai    aj    ak     funct    theta0      k_theta
1 4 5 1  111.141  313.800
1 4 6 1  111.406  313.800
1 4 7 1  111.143  313.800
1 8 9 1  109.167  313.800
1 8 10 1  109.104  313.800
1 8 11 1  113.614  488.273
2 1 3 1  106.107  276.144
2 1 4 1  109.429  313.800
2 1 8 1  109.239  313.800
3 1 4 1  109.378  313.800
3 1 8 1  109.164  313.800
4 1 8 1  113.273  488.273
```

```
5 4 6 1  107.678  276.144
5 4 7 1  107.610  276.144
6 4 7 1  107.681  276.144
8 11 12 1  109.184  313.800
8 11 13 1  109.217  313.800
8 11 14 1  113.583  488.273
9 8 10 1  106.095  276.144
9 8 11 1  109.264  313.800
10 8 11 1  109.324  313.800
11 14 15 1  109.195  313.800
11 14 16 1  109.226  313.800
11 14 17 1  113.532  488.273
12 11 13 1  106.098  276.144
12 11 14 1  109.226  313.800
13 11 14 1  109.261  313.800
14 17 18 1  109.260  313.800
14 17 19 1  109.262  313.800
14 17 20 1  113.584  488.273
15 14 16 1  106.139  276.144
15 14 17 1  109.241  313.800
16 14 17 1  109.243  313.800
17 20 21 1  109.250  313.800
17 20 22 1  109.155  313.800
17 20 23 1  113.584  488.273
18 17 19 1  106.055  276.144
18 17 20 1  109.250  313.800
19 17 20 1  109.155  313.800
20 23 24 1  109.241  313.800
20 23 25 1  109.243  313.800
20 23 26 1  113.532  488.273
21 20 22 1  106.055  276.144
21 20 23 1  109.260  313.800
22 20 23 1  109.262  313.800
23 26 27 1  109.226  313.800
23 26 28 1  109.261  313.800
23 26 29 1  113.583  488.273
24 23 25 1  106.139  276.144
24 23 26 1  109.195  313.800
25 23 26 1  109.226  313.800
26 29 30 1  109.264  313.800
26 29 31 1  109.324  313.800
26 29 32 1  113.614  488.273
27 26 28 1  106.098  276.144
27 26 29 1  109.184  313.800
28 26 29 1  109.217  313.800
29 32 33 1  109.239  313.800
29 32 34 1  109.164  313.800
29 32 35 1  113.273  488.273
30 29 31 1  106.095  276.144
30 29 32 1  109.167  313.800
31 29 32 1  109.104  313.800
32 35 36 1  111.406  313.800
32 35 37 1  111.141  313.800
32 35 38 1  111.143  313.800
```

```
33 32 34 1  106.107  276.144
33 32 35 1  109.429  313.800
34 32 35 1  109.378  313.800
36 35 37 1  107.678  276.144
36 35 38 1  107.681  276.144
37 35 38 1  107.610  276.144


[ dihedrals ]
;  ai    aj    ak    al   funct       phi_s           k_phi
n
2 1 4 5 3
3 1 4 5 3
8 1 4 5 3
2 1 4 6 3
3 1 4 6 3
8 1 4 6 3
2 1 4 7 3
3 1 4 7 3
8 1 4 7 3
2 1 8 9 3
3 1 8 9 3
4 1 8 9 3
2 1 8 10 3
3 1 8 10 3
4 1 8 10 3
2 1 8 11 3
3 1 8 11 3
4 1 8 11 3
1 8 11 12 3
9 8 11 12 3
10 8 11 12 3
1 8 11 13 3
9 8 11 13 3
10 8 11 13 3
1 8 11 14 3
9 8 11 14 3
10 8 11 14 3
8 11 14 15 3
12 11 14 15 3
13 11 14 15 3
8 11 14 16 3
12 11 14 16 3
13 11 14 16 3
8 11 14 17 3
12 11 14 17 3
13 11 14 17 3
11 14 17 18 3
15 14 17 18 3
16 14 17 18 3
11 14 17 19 3
15 14 17 19 3
16 14 17 19 3
```

```
11 14 17 20 3
15 14 17 20 3
16 14 17 20 3
14 17 20 21 3
18 17 20 21 3
19 17 20 21 3
14 17 20 22 3
18 17 20 22 3
19 17 20 22 3
14 17 20 23 3
18 17 20 23 3
19 17 20 23 3
17 20 23 24 3
21 20 23 24 3
22 20 23 24 3
17 20 23 25 3
21 20 23 25 3
22 20 23 25 3
17 20 23 26 3
21 20 23 26 3
22 20 23 26 3
20 23 26 27 3
24 23 26 27 3
25 23 26 27 3
20 23 26 28 3
24 23 26 28 3
25 23 26 28 3
20 23 26 29 3
24 23 26 29 3
25 23 26 29 3
23 26 29 30 3
27 26 29 30 3
28 26 29 30 3
23 26 29 31 3
27 26 29 31 3
28 26 29 31 3
23 26 29 32 3
27 26 29 32 3
28 26 29 32 3
26 29 32 33 3
30 29 32 33 3
31 29 32 33 3
26 29 32 34 3
30 29 32 34 3
31 29 32 34 3
26 29 32 35 3
30 29 32 35 3
31 29 32 35 3
29 32 35 36 3
33 32 35 36 3
34 32 35 36 3
29 32 35 37 3
33 32 35 37 3
34 32 35 37 3
```

```
29 32 35 38 3
33 32 35 38 3
34 32 35 38 3

[ exclusions ]
5 2 1
5 3 1
5 8 1
6 2 1
6 3 1
6 8 1
7 2 1
7 3 1
7 8 1
9 2 1
9 3 1
9 4 1
10 2 1
10 3 1
10 4 1
11 2 1
11 3 1
11 4 1
12 1 1
12 9 1
12 10 1
13 1 1
13 9 1
13 10 1
14 1 1
14 9 1
14 10 1
15 8 1
15 12 1
15 13 1
16 8 1
16 12 1
16 13 1
17 8 1
17 12 1
17 13 1
18 11 1
18 15 1
18 16 1
19 11 1
19 15 1
19 16 1
20 11 1
20 15 1
20 16 1
21 14 1
21 18 1
21 19 1
22 14 1
```

```
22 18 1
22 19 1
23 14 1
23 18 1
23 19 1
24 17 1
24 21 1
24 22 1
25 17 1
25 21 1
25 22 1
26 17 1
26 21 1
26 22 1
27 20 1
27 24 1
27 25 1
28 20 1
28 24 1
28 25 1
29 20 1
29 24 1
29 25 1
30 23 1
30 27 1
30 28 1
31 23 1
31 27 1
31 28 1
32 23 1
32 27 1
32 28 1
33 26 1
33 30 1
33 31 1
34 26 1
34 30 1
34 31 1
35 26 1
35 30 1
35 31 1
36 29 1
36 33 1
36 34 1
37 29 1
37 33 1
37 34 1
38 29 1
38 33 1
38 34 1
```

FIGURE B.8: The file defining the dodecane model.

MDP Files

minim.mdp

```
; minim.mdp - used as input into grompp to generate em.tpr
; Parameters describing what to do, when to stop and what to save
integrator      = steep         ; Algorithm (steep = steepest descent minimization)
emtol           = 10.0          ; Stop minimization when the maximum force < 1000.0 kJ/mol/nm
emstep          = 0.001          ; Energy step size
nsteps          = 300000        ; Maximum number of (minimization) steps to perform

; Parameters describing how to find the neighbors of each atom and how to calculate the interactions
nstlist         = 1             ; Frequency to update the neighbor list and long range forces
ns_type         = grid          ; Method to determine neighbor list (simple, grid)
rlist           = 1.0           ; Cut-off for making neighbor list (short range forces)
coulombtype     = PME           ; Treatment of long range electrostatic interactions
rcoulomb        = 1.0           ; Short-range electrostatic cut-off
rvdw            = 1.0           ; Short-range Van der Waals cut-off
pbc             = xyz           ; Periodic Boundary Conditions (yes/no)
```

FIGURE B.9: The mdp file for the energy minimisation process.

calcite_water.mdp

```
;====================================================================
integrator              =  md
dt                      =  0.001
nsteps                  =  2500000
comm_mode               =  None
nstcomm                 =  100                  ; reset c.o.m. motion
nstxout                 =  10000                ; write coords
nstvout                 =  10000                ; write velocities
nstxtcout               =  1000                ; write coords to xtc-trajectory
nstlog                  =  1000                 ; print to logfile
nstlist                 =  10                   ; update pairlist
ns_type                 =  grid ;simple         ; pairlist method
freezegrps              =  AEG
freezedim               =  Y Y Y

;=================  Shake Specification  ==============================
continuation            =  no
constraint_algorithm    =  lincs        ; holonomic constraints
constraints             =  h-bonds
lincs_iter              =  1            ; accuracy of LINCS
lincs_order             =  4            ; also related to accuracy

;=================  Cutt off specification ============================
pbc                     =  xyz                  ; periodic boundary conditions
optimize_fft            =  yes                  ; perform FFT optimization at start
coulombtype             =  PME
rcoulomb                =  1.0                  ; cut-off for coulomb
rlist                   =  1.0                  ; cut-off for ns
vdw-type                =  cut-off
rvdw                    =  1.0                  ; cut-off for vdw
ewald_geometry          =  3dc
pme_order               =  6
fourierspacing          =  0.15
;====================================================================
Tcoupl                  =  v-rescale            ; berendsen;nose-hoover;
tc-grps                 =  THERMAL NONTHERMAL SOL     Srl1    AEG
ref_t                   =  298.15  298.15     298.15  298.15  298.15
tau_t                   =  0.1     10e+10     0.1     10e+10  10e+10
Pcoupl                  =  No
;Pcoupl                  =  berendsen
;tau_p                   =  5.0
;compressibility         =  3.0e-7
;ref_p                   =  1.01325
;====================================================================
gen_vel                 =  no                   ; generate initial velocities
gen_temp                =  300                  ; initial temperature
gen_seed                =  1903                 ; random seed
```

FIGURE B.10: The mdp file for the simulation process.

Files for the pulling simulation

pull_water.mdp

```
title       = Umbrella pulling simulation
; Run parameters
integrator  = md
dt          = 0.001
tinit       = 0
nsteps      = 250000    ; 250 ps
nstcomm     = 10
; Output parameters
nstxout     = 5000      ; every 10 ps
nstvout     = 5000
nstfout     = 500
nstxtcout   = 500       ; every 1 ps
nstenergy   = 500
; Bond parameters
constraint_algorithm    = lincs
constraints             = h-bonds
continuation            = no       ; continuing from NPT
lincs_iter              =  1            ; accuracy of LINCS
lincs_order             =  4            ; also related to accuracy
; Single-range cutoff scheme
nstlist     = 5
ns_type     = grid
; PME electrostatics parameters
optimize_fft            =  yes                  ; perform FFT optimization at start
coulombtype             =  PME
rcoulomb                =  1.0                  ; cut-off for coulomb
rlist                   =  1.0                  ; cut-off for ns
vdw-type                =  cut-off
rvdw                    =  1.0                  ; cut-off for vdw
ewald_geometry          =  3dc
pme_order               =  6
fourierspacing          =  0.15
; Berendsen temperature coupling is on in two groups
Tcoupl      = v-rescale
tc-grps         =  THERMAL NONTHERMAL SOL     Srl1    Dummy   Probe
ref_t           =  298.15  298.15     298.15  298.15  298.15  298.15
tau_t           =  0.1     10e+10     10e+10  10e+10  10e+10  10e+10
; Pressure coupling is on
Pcoupl          = No
;pcoupltype      = isotropic
;tau_p           = 1.0
;compressibility = 4.5e-5
;ref_p           = 1.0
;refcoord_scaling = com
; Generate velocities is off
gen_vel     = no
freezegrps  = Dummy
freezedim   = Y Y Y
; Periodic boundary conditions are on in all directions
pbc     = xyz
; Long-range dispersion correction
DispCorr    = EnerPres
; Pull code
pull            = constraint
pull_geometry   = distance  ; simple distance increase
pull_dim        = N N Y
pull_start      = yes       ; define initial COM distance > 0
pull_ngroups    = 1
pull_group0     = Dummy
pull_group1     = Probe
pull_rate1      = 0.01       ; 0.01 nm per ps = 10 nm per ns
pull_k1         = 500       ; kJ mol^-1 nm^-2
pull_vec1       = 0 0 1
```

FIGURE B.11: The mdp file for the pulling simulations used in the potential of mean force calculations.

Appendix C

MATLAB Scripts

This chapter contains the necessary files to replicate the graphs found in Chapter 3 using MATLAB.

C.1 Scripts

Partial Density

```
%  File:  partialdensity.m
%
%  A sample MATLAB script to plot averages and moving average and label the plot

x = (unnamed(:,1));         %  x axis
y1 = (unnamed(:,2));        %  y values
y2 = (unnamed(:,3));        %  moving average y values
y3 = (unnamed(:,4));        %  moving average y values
y4 = (unnamed(:,5));        %  moving average y values
y5 = (unnamed(:,6));        %  moving average y values
plot(x, y1,'k', 'LineWidth', 4)
hold on
plot(x, y2,'r', 'LineWidth', 4)
%plot(x, y2, 'Color',[0 .5 0],'LineWidth', 2)   %Green line
plot(x, y3, 'b','LineWidth', 4)
hold on
plot(x, y4, 'r-.', 'LineWidth', 2)
hold on
%plot(x, y5, 'Color',[0 .5 0],'LineStyle','-.', 'LineWidth', 2) %, x, y5, 'b-.',
'LineWidth', 2)   %   plot
plot(x, y5, 'b','LineStyle','-.', 'LineWidth', 2) %, x, y5, 'b-.', 'LineWidth', 2)
%   plot
%plot(x, y5, 'k','LineStyle','-.', 'LineWidth', 2) %, x, y5, 'b-.', 'LineWidth', 2)
%   plot
axis([3.5,5.5,0,4000]);
set(gca,'fontsize',28);
xlabel('Distance from Z=0 (nm)', 'FontSize', 32, 'FontWeight', 'bold');          %
label the x-axis
ylabel('Density (kg/m^{3})', 'FontSize', 32, 'FontWeight', 'bold'); %  label the y-
axis
title('Partial Densities of Water (Flat System)', 'FontSize', 40, 'FontWeight',
'bold');        %  put a title on the plot
hleg1 = legend('Initial Water Density','Final Water Density (298K)','Final Water
Density (353K)','Average Water Density (298K)','Average Water Density (353K)');
set(hleg1,'FontSize',32);
```

FIGURE C.1: The script to plot the partial density of water relative to the z dimension.

Interfacial Density

```
%  File:  interfacialdens.m
%
%  A sample MATLAB script to plot averages and moving average and label the plot

x = (unnamed(:,1));         %  x axis
y1 = (unnamed(:,2));        %  y values
y2 = (unnamed(:,3));        %  moving average y values
y3 = (unnamed(:,4));        %  moving average y values
y4 = (unnamed(:,5));        %  moving average y values
plot(x, y1,'k', 'LineWidth', 4)
hold on
%plot(x, y2,'r', 'LineWidth', 4)
plot(x, y2, 'Color',[0 .5 0],'LineWidth', 2)   %Green line
hold on
plot(x, y3, 'k-.', 'LineWidth', 2)
%hold on
plot(x, y4, 'Color',[0 .5 0],'LineStyle','-.', 'LineWidth', 2) %, x, y5, 'b-.',
'LineWidth', 2)   %   plot
%plot(x, y5, 'k','LineStyle','-.', 'LineWidth', 2) %, x, y5, 'b-.', 'LineWidth', 2)
%   plot
axis([3.5,7,0,5000]);
set(gca,'fontsize',28);
xlabel('Distance from Z=0 (nm)', 'FontSize', 32, 'FontWeight', 'bold');          %
label the x-axis
ylabel('Density (kg/m^{3})', 'FontSize', 32, 'FontWeight', 'bold'); %  label the y-
axis
title('Final Densities of Water and Dodecane  ', 'FontSize', 40, 'FontWeight',
'bold');        %  put a title on the plot
hleg1 = legend('Water Density (353K)','Dodecane Density (353K)','Average Water
Density (353K)','Average Dodecane Density (353K)');
set(hleg1,'FontSize',32);
```

FIGURE C.2: The script to plot the densities of water and dodecane relative to the z dimension.

Radial Distribution Function

```
%  File:  RDF.m
%
%  A sample MATLAB script to plot radial distribution function

x = (unnamed(:,1));          %  x axis
y1 = (unnamed(:,2));         %  y values
%plot(x, y1,'Color',[0 .5 0], 'LineWidth', 4)
%hold on
plot(x, y1, 'k', 'LineWidth', 4)
%%%%%%%
text(x(y1==max(y1)),max(y1),' \leftarrow  Distance = 2.38Å',
'FontSize', 30, 'FontWeight', 'bold')
axis([0,25,0,60]);
set(gca,'fontsize',28);
xlabel('Ca - O_{water} distance (Å)', 'FontSize', 32, 'FontWeight',
'bold');           %  label the x-axis
ylabel('g(r)', 'FontSize', 32, 'FontWeight', 'bold'); %  label the y-
axis
title('Radial Distribution Function of the Ca - O_{water} distance',
'FontSize', 40, 'FontWeight', 'bold');        %  put a title on the
plot
```

FIGURE C.3: The script to plot the radial distribution function.

Appendix D

PYTHON Scripts

This chapter contains the necessary files to replicate the contact angles found in Chapter 3 using Python.

D.1 Scripts

Contact Angle

Whilst the following pages contain only images of the script, it is available at the request of the author.

```
# -*- coding: utf-8 -*-

import numpy as np
import matplotlib.pyplot as plt
import sys
from scipy import stats
from mpl_toolkits.mplot3d import Axes3D


settings = {'number_of_grid_points' : 600,
            'grid_x_range' : (0., 30.6),
            'grid_y_range' : (0., 30.6),
            'margin' : .2}

z_slices = [(0., 5)]


def set_plt_parameters():
    rcdef = plt.rcParams.copy()

    newparams = {'axes.labelsize': 14, 'axes.linewidth': 1, 'savefig.dpi': 300,
                 'lines.linewidth': 1.5, 'figure.figsize': (8, 5),
                 'figure.subplot.wspace': 0.4,
                 'ytick.labelsize': 12, 'xtick.labelsize': 12,
                 'ytick.major.pad': 5, 'xtick.major.pad': 5,
                 'legend.fontsize': 12, 'legend.frameon': False,
                 'legend.handlelength': 1.5}

    plt.rcParams.update(rcdef)
    plt.rcParams.update(newparams)


def load_data(path_to_gro_file):
    """Returns normalized in z numpy coordinates"""
    f = open(path_to_gro_file, 'rb')
    coord_list = []

    for line in f:
      pieces = line.split()
      name = pieces[0]
      if name.endswith('SOL') and not pieces[1].startswith('HW'):
        line = line[21:]
        numbers = line.split()
        assert len(numbers) == 6
        point = numbers[0:3]
        coord_list.append(map(float, point))


    coords = np.array(coord_list)
    coords[:, 2] -= min(coords[:, 2])
    print_ranges(coords)
    return coords


def write_scatter3d(name, data, dot_size=.1, x_range=(0, 30), y_range=(0, 30),
                    z_range=(0, 30)):
    """Data should be N x 3 nympy array"""
    fig = plt.figure()
    ax = fig.add_subplot(111, projection='3d')
    ax.scatter3D(data[:, 0], data[:, 1], data[:, 2], s=dot_size)
    ax.set_zlim(z_range)
    ax.set_xlim(x_range)
    ax.set_ylim(y_range)
    fig.savefig('{}.png'.format(name))
```

```
def write_scatter_plot_and_regression_line(name, x, y, slope, intercept):
    fig = plt.figure()
    plt.plot(x, y, 'x')
    xs = np.arange(min(x), max(x), 1)
    ys = slope*xs + intercept
    pred = np.vstack((xs, ys)).T
    plt.plot(pred[:, 0], pred[:, 1])
    fig.savefig('{}.png'.format(name))


def print_ranges(numpy_array):
    """Prints minimum and maximum values of first, second, and third column.
    They are assumed to me x, y, z variables."""
    x_max = max(numpy_array[:, 0])
    x_min = min(numpy_array[:, 0])

    y_max = max(numpy_array[:, 1])
    y_min = min(numpy_array[:, 1])

    z_max = max(numpy_array[:, 2])
    z_min = min(numpy_array[:, 2])

    print 'X range: ({} {})'.format(x_min, x_max)
    print 'Y range: ({} {})'.format(y_min, y_max)
    print 'Z range: ({} {})'.format(z_min, z_max)


def find_grid_point_index(coord, coord_range, number_of_grid_points):
    """returns index of grid point"""
    return round(coord/coord_range*(number_of_grid_points-1))


def create_coarse_grid(settings):
    """returns numpy array of size N x 2 containing coordinates of all
    grid points as well as x and y vecotrs"""
    x_min_grid, x_max_grid = settings['grid_x_range']
    y_min_grid, y_max_grid = settings['grid_y_range']
    number_of_grid_points = settings['number_of_grid_points']
    x = np.linspace(x_min_grid, x_max_grid, number_of_grid_points)   # Allowed x coordinates
    y = np.linspace(y_min_grid, y_max_grid, number_of_grid_points)   # y coords
    return x, y


def distribute_hights_into_grid_dictionary(coords, settings):
    """Distriubtes points between coarse grid.
    Returns dictionary in which keys are point coordinates on coarse grid
    and values are list of hights of points associated with this particular
    grid point"""
    h_dic = {}
    x, y = create_coarse_grid(settings)
    x_range = settings['grid_x_range'][1] - settings['grid_x_range'][0]
    y_range = settings['grid_y_range'][1] - settings['grid_y_range'][0]
    number_of_grid_points = settings['number_of_grid_points']

    for point in coords:
        x_index = find_grid_point_index(point[0], x_range, number_of_grid_points)
        y_index = find_grid_point_index(point[1], y_range, number_of_grid_points)
        coordinate = (x[x_index], y[y_index])
        try:
            h_dic[coordinate].append(point[2])
        except KeyError:
            h_dic[coordinate] = [point[2]]
    return h_dic
```

```
def highest_point(l, margin):
    l.sort()
    while len(l) > 1 and l[-1] - l[-2] > margin:
        l.pop()
    return l[-1]


def find_highest_points(name, coords, settings):
    """Returns N x 3 numpy array which has coordinates of highest point
    in each coarse grid point. To decrease noise highest point is defined
    as point which has second highest point within amrgin."""
    h_dic = distribute_hights_into_grid_dictionary(coords, settings)
    highest_points_dic = {}
    margin = settings['margin']
    h_dic_size = len(h_dic)

    for key, value in h_dic.iteritems():
        highest_p = highest_point(value, margin)
        highest_points_dic[key] = highest_p

    # Create matrix of highest points
    highest_points = np.empty((h_dic_size, 3), dtype=float)

    row = 0
    for key, value in highest_points_dic.iteritems():
        point = np.append(key, value)
        highest_points[row, :] = point
        row += 1

    np.savetxt(name, highest_points, delimiter=",")
    return highest_points


def remove_lower_and_higher_points_than_range(z_slice, highest_points):
    """returns highest_points which fall into given z range"""
    z_low_boundary, z_high_boundary = z_slice
    highest_points_sliced = highest_points[highest_points[:, 2] >= z_low_boundary]
    return highest_points_sliced[highest_points_sliced[:, 2] <= z_high_boundary]


def Cylindrical(highest_points_sliced):
    """Converts to highest_points to cylindrical coordinates."""
    CM = highest_points_sliced.sum(0)/highest_points_sliced.shape[0]
    CM[2] = 0
    centered = highest_points_sliced - CM

    ro = np.sqrt(centered[:,0]**2 + centered[:,1]**2)
    fi = np.arctan2(centered[:,0], centered[:,1]) + np.pi
    ptsnew = np.vstack((ro, fi, centered[:,2])).T
    return ptsnew


def find_contact_angle_fit(name, highest_points_sliced):
    cyl = Cylindrical(highest_points_sliced)
    x = cyl[:, 0]
    y = cyl[:, 2]

    stacked = np.vstack((x, y)).T
    np.savetxt(name, stacked, delimiter=',')

    slope, intercept, r_value, p_value, std_err = stats.linregress(x, y)

    mx = x.mean()
    er_squared = ((y - x*slope - intercept)**2).sum()

    sd_slope = np.sqrt(er_squared/(len(x) - 2)/((x - mx)**2).sum())

    return x, y, slope, intercept, r_value, sd_slope
```

```
def sectors(cyl):
    """Not used"""
    number_of_sectors = 4
    circ_grid = np.linspace(0, 2*np.pi, number_of_sectors + 1)
    number_of_grid_points = len(circ_grid)

    def find_sector_index(coord, number_of_sectors):
        """returns sector of point"""
        idx = round(coord/2/np.pi*number_of_sectors)
        if idx == number_of_grid_points:
            idx = 0
        return idx

    # Dictionary of sectors
    sec_dic = {}

    # Distribuiton of angles into dictionary

    index_of_r_and_height = np.array([0, 2])

    for point in cyl:
        sector_index = find_sector_index(point[1], number_of_sectors)
        try:
            sec_dic[sector_index].append(point[index_of_r_and_height])
        except KeyError:
            sec_dic[sector_index] = [point[index_of_r_and_height]]
    sec_dic[0].extend(sec_dic[number_of_sectors])
    sec_dic.pop(number_of_sectors)

    for i in sec_dic:
        slope, intercept, r_value, p_value, std_err = stats.linregress(sec_dic[i])
        print i
        print slope
        print intercept
        print 'r2_value',r_value**2
        print 'Contact angle: {}'.format(-np.arctan(slope)/np.pi*180)
        print ''
        xy = np.array(sec_dic[i])
        plt.figure(i+1)
        plt.plot(xy[:, 0], xy[:, 1], 'x')

        xs = np.arange(min(xy[:, 0])-1, max(xy[:, 0])+1, 1)
        ys = slope*xs + intercept

        pred = np.vstack((xs, ys)).T


        plt.plot(pred[:, 0], pred[:, 1])


def main(gro_file):
    set_plt_parameters()
    #load all data
    all_data = load_data(gro_file)
    #find surface (highest) points
    highest_points = find_highest_points('{}_surface.csv'.format(gro_file),
                                         all_data, settings)
    #find contact angle for given z slice
    for z_slice in z_slices:
        name = '{}_{}_{}_regression.csv'.format(gro_file, z_slice[0], z_slice[1])
        highest_points_sliced = remove_lower_and_higher_points_than_range(z_slice, highest_points)
        x, y, slope, intercept, r_value, slope_err = find_contact_angle_fit(name,
                                                                            highest_points_sliced)
        name = '{}_{}_{}_projection'.format(gro_file, z_slice[0], z_slice[1])
        write_scatter_plot_and_regression_line(name, x, y, slope, intercept)
        print '\n{}'.format(z_slice)
        print 'Contact angle: {}'.format(-np.arctan(slope)/np.pi*180)
        print 'R value: {}'.format(r_value)
        print 'Regression error: {}'.format(slope_err)









if __name__ == '__main__':
    main(sys.argv[1])
```

Bibliography

[1] B. Coto, C. Martos, J. L. Peña, R. Rodríguez, and G. Pastor. Effects in the solubility of CaCO3: experimental study and model description. *Fluid Phase Equilibria*, 324:1–7, June 2012.

[2] William L. Leffler. *Petroleum Refining for the Non-Technical Person*. PennWell Corporation, 1985.

[3] National Foreign Assessment Center. *The World Factbook*. Central Intelligence Agency., Washington, D.C., 1981.

[4] John W. Harbaugh. Chapter 7 carbonate oil reservoir rocks. In Harold J. Bissell George V. Chilingar and Rhodes W. Fairbridge, editors, *Developments in Sedimentology*, volume 9, Part A of *Carbonate Rocks Origin, Occurrence and Classification*, pages 349–398. Elsevier, 1967.

[5] N. Mungan. Enhanced oil recovery using water as a driving fluid. *World Oil*, 193:2, August 1981.

[6] Charles R. Stahl, Michael A. Gibson, and Christian W. Knudsen. Thermally-enhanced oil recovery method and apparatus, September 1987.

[7] Maria Ricci, Peter Spijker, Francesco Stellacci, Jean-Francois Molinari, and Kislon Voïtchovsky. Direct visualization of single ions in the stern layer of calcite. *Langmuir*, 29(7):2207–2216, February 2013.

[8] James W. McCauley. Calcite group in encyclopedia of mineralogy. In Keith Frye, editor, *Encyclopedia of Mineralogy*, Encyclopedia of Earth Science, pages 56–61. Springer US, January 1981.

[9] F. González-García, V. Romero-Acosta, G. García-Ramos, and M. González-Rodríguez. Firing transformations of mixtures of clays containing illite, kaolinite and calcium carbonate used by ornamental tile industries. *Appl. Clay Sci.*, 5(4):361–375, December 1990.

[10] Werner Kogler. Pigment mixture for the paper industry consisting of calcium carbonate ..., June 1992.

[11] J. P. Gattuso, M. Frankignoulle, I. Bourge, S. Romaine, and R. W. Buddemeier. Effect of calcium carbonate saturation of seawater on coral calcification. *Global Planet. Change*, 18(1–2): 37–46, July 1998.

[12] Eduardo Slatopolsky, Carol Weerts, Silvia Lopez-Hilker, Kathryn Norwood, Mary Zink, David Windus, and James Delmez. Calcium carbonate as a phosphate binder in patients with chronic renal failure undergoing dialysis. *New. Engl. J. Med.*, 315(3):157–161, July 1986.

[13] Herbert A Lieberman, Leon , Lachman, and Joseph B Schwartz. *Pharmaceutical dosage forms–tablets*. Dekker, New York, 1989.

[14] Ilan Gabriely, James P. Leu, and Uriel S. Barzel. Back to basics. *New. Engl. J. Med.*, 358(18):1952–1956, 2008.

[15] J. W. Morse and F. T. Mackenzie. *Geochemistry of Sedimentary Carbonates*. Elsevier, August 1990.

[16] Carl W. Turner and David W. Smith. Calcium carbonate scaling kinetics determined from radiotracer experiments with calcium-47. *Ind. Eng. Chem. Res.*, 37(2):439–448, February 1998.

[17] Arthur N. Palmer. Origin and morphology of limestone caves. *Geol. Soc. Am. Bull.*, 103(1):1–21, January 1991.

[18] Sean O'Connor. *Molecular Mechanisms of Biological Adaptation to Extreme Ionic Environments*. BSc hons mathematics and physics, University of Strathclyde, 2013.

[19] Andrew R. Leach. *Molecular Modelling: Principles and Applications*. Pearson Education, 2001.

[20] Sebastien Kerisit, Chongxuan Liu, and Eugene S. Ilton. Molecular dynamics simulations of the orthoclase (0 0 1)- and (0 1 0)-water interfaces. *Geochim. Cosmochim. Act.*, 72(6):1481–1497, March 2008.

[21] A. A. Skelton, P. Fenter, J. D. Kubicki, D. J. Wesolowski, and P. T. Cummings. Simulations of the quartz(101?1)/Water interface: A comparison of classical force fields, ab initio molecular

dynamics, and x-ray reflectivity experiments. *J. Phys. Chem. C*, 115(5):2076–2088, February 2011.

[22] Jacob N. Israelachvili and Richard M. Pashley. Molecular layering of water at surfaces and origin of repulsive hydration forces. *Nature*, 306(5940):249–250, November 1983.

[23] Yingxi Zhu and Steve Granick. Rate-dependent slip of newtonian liquid at smooth surfaces. *Phys. Rev. Lett.*, 87(9):096105, August 2001.

[24] M. Heuberger, M. Zäch, and N. D. Spencer. Density fluctuations under confinement: When is a fluid not a fluid? *Science*, 292 (5518):905–908, May 2001.

[25] Maxim V. Fedorov and Alexei A. Kornyshev. Ionic liquid near a charged wall: Structure and capacitance of electrical double layer. *J. Phys. Chem. B*, 112(38):11868–11872, 2008.

[26] C. H. Bridgeman and N. T. Skipper. A monte carlo study of water at an uncharged clay surface. *J. Phys.: Condens. Matter*, 9(20):4081, May 1997.

[27] Sung-Ho Park and Garrison Sposito. Structure of water adsorbed on a mica surface. *Phys. Rev. Lett.*, 89(8):085501, August 2002.

[28] Y. Liang, A. S. Lea, D. R. Baer, and M. H. Engelhard. Structure of the cleaved CaCO3(1014) surface in an aqueous environment. *Surf. Sci.*, 351(1–3):172–182, May 1996.

[29] D.L. Blanchard, D. L. Lessor, J.P. LaFemina, D.R. Baer, W.K. Ford, and T. Guo. A low-energy electron diffraction study of the MgO(001) surface structure. *J. Vac. Sci. Technol., A*, 9(3): 1814–1819, May 1991.

[30] Susan L. Stipp and Michael F. Hochella Jr. Structure and bonding environments at the calcite surface as observed with x-ray photoelectron spectroscopy (XPS) and low energy electron diffraction (LEED). *Geochim. Cosmochim. Act.*, 55(6):1723–1736, June 1991.

[31] P. Fenter, P. Geissbühler, E. DiMasi, G. Srajer, L. B. Sorensen, and N. C. Sturchio. Surface speciation of calcite observed in situ by high-resolution x-ray reflectivity. *Geochim. Cosmochim. Act.*, 64(7):1221–1228, April 2000.

[32] P. Fenter and N. C. Sturchio. Calcite (1 0 4)–water interface structure, revisited. *Geochim. Cosmochim. Act.*, 97:58–69, November 2012.

[33] James A. Fay. Physical processes in the spread of oil on a water surface. *Int. Oil Spill Conf. Proc.*, 1971(1):463–467, June 1971.

[34] P. G. De Gennes and C. Taupin. Microemulsions and the flexibility of oil/water interfaces. *J. Phys. Chem.*, 86(13):2294–2304, June 1982.

[35] J.J. Taber. Dynamic and static forces required to remove a discontinuous oil phase from porous media containing both oil and water. *Soc. Petrol. Eng*, 9(01):3–12, March 1969.

[36] Milton J. Rosen, Hongzhuang Wang, Pingping Shen, and Youyi Zhu. Ultralow interfacial tension for enhanced oil recovery at very low surfactant concentrations. *Langmuir*, 21(9):3749–3756, April 2005.

[37] W.R. Foster. A low-tension waterflooding process. *J. Pet. Technol.*, 25(02):205–210, February 1973.

[38] J.C. Melrose. Role of capillary forces in detennining microscopic displacement efficiency for oil recovery by waterflooding. *J. Can. Pet. Technol.*, 13(04), October 1974.

[39] W. G. Anderson. Wettability literature survey - part 1: Rock-/Oil/Brine interactions and the effects of core handling on wettability. *J. Pet. Technol.*, 38:11, October 1986.

[40] W. Abdallah, J. S. Buckley, A. Carnegie, J. Edwards, B. Herold, E. Fordham, A. Graue, T. Habashy, N. Seleznev, C. Signer, H. Hussain, B. Montaron, and M. Ziauddin. Fundamentals of wettability. *Oilfield Rev.*, 2007.

[41] Heinrich Kayser. Ueber die verdichtung von gasen an oberflächen in ihrer abhängigkeit von druck und temperatur. *Ann. Phys.*, 248(4):526–537, 1881.

[42] Trevor M. Letcher. *Developments and Applications in Solubility.* Royal Society of Chemistry, 2007.

[43] F. Hirata, editor. *Molecular theory of solvation.* Kluwer Academic Publishers, Dordrecht, Netherlands, 2003.

[44] Shankar Kumar, John M. Rosenberg, Djamal Bouzida, Robert H. Swendsen, and Peter A. Kollman. THE weighted histogram analysis method for free-energy calculations on biomolecules. i. the method. *J. Comput. Chem.*, 13(8):1011–1021, October 1992.

[45] B. Hess, C. Kutzner, D. van der Spoel, and E. Lindahl. GROMACS 4: Algorithms for highly efficient, load-balanced, and scalable molecular simulation. *J. Chem. Theory Comput.*, 4(3): 435–447, 2008.

[46] Sander Pronk, Szilárd Páll, Roland Schulz, Per Larsson, Pär Bjelkmar, Rossen Apostolov, Michael R. Shirts, Jeremy C. Smith, Peter M. Kasson, David van der Spoel, Berk Hess, and Erik Lindahl. GROMACS 4.5: a high-throughput and highly parallel open source molecular simulation toolkit. *Bioinformatics*, 29(7):845–854, April 2013.

[47] G. Bussi, D. Donadio, and M. Parrinello. Canonical sampling through velocity rescaling. *J. Chem. Phys.*, 126(1):014101–7, 2007.

[48] T. Darden, D. York, and L. Pedersen. Particle mesh ewald: An n log (n) method for ewald sums in large systems. *J. Chem. Phys.*, 98:10089–10092, 1993.

[49] P. S. Crozier, R. L. Rowley, D. Henderson, and D. Boda. A corrected 3D ewald calculation of the low effective temperature

properties of the electrochemical interface. *Chem. Phys. Lett.*, 325(5-6):675–677, August 2000.

[50] P. S. Crozier, R. L. Rowley, E. Spohr, and D. Henderson. Comparison of charged sheets and corrected 3D ewald calculations of long-range forces in slab geometry electrolyte systems with solvent molecules. *J. Chem. Phys.*, 112(21):9253–9257, June 2000.

[51] David Bostick and Max L. Berkowitz. The implementation of slab geometry for membrane-channel molecular dynamics simulations. *Biophys J*, 85(1):97–107, July 2003.

[52] W. L. Jorgensen, D. S. Maxwell, and J. Tirado-Rives. Development and testing of the OPLS all-atom force field on conformational energetics and properties of organic liquids. *J. Am. Chem. Soc.*, 118(45):11225–11236, November 1996.

[53] G. A. Kaminski, R. A. Friesner, J. Tirado-Rives, and W. L. Jorgensen. Evaluation and reparametrization of the OPLS-AA force field for proteins via comparison with accurate quantum chemical calculations on peptides. *J. Phys. Chem. B*, 105(28): 6474–6487, July 2001.

[54] William L. Jorgensen, Jayaraman Chandrasekhar, Jeffry D. Madura, Roger W. Impey, and Michael L. Klein. Comparison of simple potential functions for simulating liquid water. *J. Chem. Phys.*, 79(2):926–935, July 1983.

[55] Michael Friendly. Milestones in the history of thematic cartography, statistical graphics, and data visualization. In *13TH INTERNATIONAL CONFERENCE ON DATABASE AND EXPERT SYSTEMS APPLICATIONS (DEXA 2002), AIX EN PROVENCE*, page 59–66. Press, 1995.

[56] W Humphrey, A Dalke, and K Schulten. VMD: visual molecular dynamics. *J Mol Graph*, 14(1):33–38, 27–28, February 1996.

[57] K. Kirchner and M. Fedorov. NaRIBaS, 2013.

[58] MATLAB. *Simulink Student Version R2013a (8.1.0.604)*. The MathWorks Inc., Natick, Massachusetts, 2013.

[59] Stephen C. Harvey, Robert K.-Z. Tan, and Thomas E. Cheatham. The flying ice cube: Velocity rescaling in molecular dynamics leads to violation of energy equipartition. *J. Comput. Chem.*, 19(7):726–740, 1998.

[60] J. S. Lardge, D. M. Duffy, and M. J. Gillan. Investigation of the interaction of water with the calcite (10.4) surface using ab initio simulation. *J. Phys. Chem. C*, 113(17):7207–7212, April 2009.

[61] Shuichi Miyamoto and Peter A. Kollman. Settle: An analytical version of the SHAKE and RATTLE algorithm for rigid water models. *J. Comput. Chem.*, 13(8):952–962, October 1992.

[62] Susana Zeppieri, Jhosgre Rodríguez, and A. L. López de Ramos. Interfacial tension of alkane + water systems†. *J. Chem. Eng. Data*, 46(5):1086–1088, September 2001.

[63] A. Goebel and K. Lunkenheimer. Interfacial tension of the water/n-alkane interface. *Langmuir*, 13(2):369–372, January 1997.

[64] HongYan Xiao, Zhen Zhen, HuanQuan Sun, XuLong Cao, Zhen-Quan Li, XinWang Song, XiaoHong Cui, and XinHou Liu. Molecular dynamics study of the water/n-alkane interface. *Sci. China Chem.*, 53(4):945–949, April 2010.

[65] Tori Z. Forbes, A. V. Radha, and Alexandra Navrotsky. The energetics of nanophase calcite. *Geochimica et Cosmochimica Acta*, 75(24):7893–7905, December 2011.

[66] Phan van Cuong, Tatiana Kuznetsova, Bjørn Kvamme, and Bjørnar Jensen. Adsorption energy and stability of H2O and CO2 on calcite effect by short-range force field parameters and temperature. *Int. J. Energy Environ.*, 2012.

[67] D. V. Okhrimenko, J. Nissenbaum, M. P. Andersson, M. H. M. Olsson, and S. L. S. Stipp. Energies of the adsorption of functional groups to calcium carbonate polymorphs: The importance of -OH and -COOH groups. *Langmuir*, 29(35):11062–11073, September 2013.

[68] T.G. Cooper and N.H. de Leeuw. Adsorption of methanoic acid onto the low-index surfaces of calcite and aragonite. *Mol. Simulat.*, 28(6-7):539–556, 2002.

[69] Kate Wright, Randall T. Cygan, and Ben Slater. Structure of the (104) surfaces of calcite, dolomite and magnesite under wet

and dry conditions. *Phys. Chem. Chem. Phys.*, 3(5):839–844, January 2001.

[70] Asif Rahaman, Vicki H. Grassian, and Claudio J. Margulis. Dynamics of water adsorption onto a calcite surface as a function of relative humidity. *J. Phys. Chem. C*, 112(6):2109–2115, February 2008.

[71] S. Kerisit and S. C. Parker. Free energy of adsorption of water and metal ions on the 1014 calcite surface. *J. Am. Chem. Soc.*, 126(32):10152–10161, August 2004.

[72] Sebastien Kerisit, Stephen C. Parker, and John H. Harding. Atomistic simulation of the dissociative adsorption of water on calcite surfaces. *J. Phys. Chem. B*, 107(31):7676–7682, August 2003.

[73] Nora H. de Leeuw and Stephen C. Parker. Surface structure and morphology of calcium carbonate polymorphs calcite, aragonite, and vaterite: An atomistic approach. *J. Phys. Chem. B*, 102(16): 2914–2922, April 1998.

[74] Dandina N. Rao. Wettability effects in thermal recovery operations. *SPE Reserv. Eval. & Eng.*, 2(05):420–430, October 1999.

[75] Shirley W. I. Siu, Kristyna Pluhackova, and Rainer A. Böckmann. Optimization of the OPLS-AA force field for long hydrocarbons. *J. Chem. Theory Comput.*, 8(4):1459–1470, April 2012.

[76] H. J. C. Berendsen, D. van der Spoel, and R. van Drunen. GROMACS: a message-passing parallel molecular dynamics implementation. *Comput. Phys. Comm.*, 91:43–56, 1995.

[77] Erik Lindahl, Berk Hess, and David Van Der Spoel. GROMACS 3.0: a package for molecular simulation and trajectory analysis. *J. Mol. Model.*, 7(8):306–317, 2001.

[78] D. van der Spoel, E. Lindahl, B. Hess, G. Groenhof, A. E. Mark, and H. J. C. Berendsen. GROMACS: fast, flexible, and free. *J. Comput. Chem.*, 26(16):1701–1718, December 2005.

[79] M. W. Mahoney and W. L. Jorgensen. A five-site model for liquid water and the reproduction of the density anomaly by rigid, nonpolarizable potential functions. *J. Chem. Phys.*, 112 (20):8910–8922, May 2000.

[80] Guillaume Lamoureux, Edward Harder, Igor V. Vorobyov, Benoît Roux, and Alexander D. MacKerell Jr. A polarizable model of water for molecular dynamics simulations of biomolecules. *Chem. Phys. Lett.*, 418(1–3):245–249, January 2006.

[81] H. J. C. Berendsen, J. P. M. Postma, W. F. van Gunsteren, A. Dinola, and J. R. Haak. Molecular dynamics with coupling to an external bath. *J. Chem. Phys.*, 81(8):3684–3690, 1984.

Figure References

Figure 2.6

http://www.archie-west.ac.uk/

cited 10th April, 2014

Please note: if any figures appear in the thesis yet are not listed above they may have been referenced in the previous section, or were created by the author.